Technical University of Munich
Physics Department

Bachelor Thesis

Symmetry-Plane Correlations in Flow Analyses

Author: Marcel Lesch

Supervisor: Dr. Ante Bilandzic

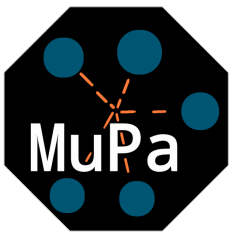

July 2019

"Sometimes science is more art than science"
- Rick

Abstract

Multi-particle correlations built from azimuthal angles whose distributions were parametrized with the Fourier series expansion, depend generically on two distinct degrees of freedom: flow amplitudes v_n and symmetry-planes Ψ_n. While analyses techniques for flow amplitudes v_n have advanced over the past years, robust and unbiased techniques for analyzing symmetry-planes Ψ_n still need to be developed.
Previous analyses of symmetry-plane correlations neglect any correlation between the flow amplitudes. Such an assumption is leading to a biased result as recent analyses in the direction of Symmetric Cumulants have shown that flow amplitudes are correlated [1]. Thus a new, bias-free method has to be used to avoid such a wrong contribution.
In this thesis, different approaches for symmetry-plane correlations in the final state are being presented and their behaviour investigated. Furthermore, results from initial state studies of symmetry-plane correlations with the Monte Carlo-Glauber model will be shown and discussed. Lastly, a first look at experimental analyses of different symmetry-plane correlations will be presented and shortly discussed.

Contents

Chapter 1

Introduction

1.1 Quantum Chromodynamics

[1]Interactions between quarks can - according to the Standard Model - be described via the strong nuclear force which is carried by elementary particles called gluons. The corresponding "charge" of the strong nuclear force is the *color*, a quantity with three possibilities: red, blue and green as well as negative colors anti-red, anti-blue and anti-green. Quarks carry only a single positive (or negative for anti-quarks) unit of color. Gluons, on the other hand, carry a positive and negative color at the same time, they are bicolored. As gluons do not carry any further electromagnetic charge, flavour or mass, interactions between quarks, which is transmitted via gluons, can only change the color of the participating particles (in a discrete way). Therefore, the underlying theory of the strong nuclear force is called Quantum Chromodynamics (QCD).
Regarding QCD, three fundamental phenomena have to be mentioned. The first being *confinement*, which describes that quarks (or anti-quarks) cannot exist freely as independent elementary particles but can only be found in bounded systems like baryons (system consisting of three quarks) or mesons (systems consisting of a quark and an anti-quark). The phenomenon of *asymptotic freedom* states the strength of interaction between quarks depending on their energy: At large energies (equivalent to short distances), quarks interact weakly while their interaction (and therefore their interaction energy) becomes greater with increasing relative distance. Therefore, quarks are prevented from separation: if their relative distance (and their interaction energy) becomes too large, new quark -anti-quark pairs will be produced which create new bounded systems with the now separated initial quarks. At last, the phenomenon of *chiral symmetry restoration* is to be named. Only in the case of massless quarks, the chiral symmetry is an exact symmetry. However, it is restored approximately at sufficiently high temperatures and energy densities as in these regimes the quark masses are reduced from the large effective values (found in hadronic matter) to the smaller bare ones.
Furthermore, the Lagrangian of QCD reads

$$\mathcal{L} = \bar{\psi}_i \left(i\gamma_\mu \mathcal{D}^\mu_{ij} - m\delta_{ij} \right) \psi_j - \frac{1}{4} \mathcal{F}_{\mu\nu\alpha} \mathcal{F}^{\mu\nu\alpha} \,. \tag{1.1}$$

In Eq. (1.1), ψ_i denotes a quark field, γ_μ the Dirac matrices, $\mathcal{D}^\mu$ a covariant derivative, m the quark mass, δ the Kronecker symbol and $\mathcal{F}^{\mu\nu}_\alpha$ the field strength of gluons. In this representation of the Lagrangian, natural units ($\hbar = c = k_B = 1$) and the Minkowski metric ($g^{\mu\nu} = \mathrm{diag}(1, -1, -1, -1)$) have been used. It has to be mentioned that, in QCD, interactions between gluons themselves are possible.

[1]Section based on [2] and references therein.

1.2 Quark Gluon Plasma

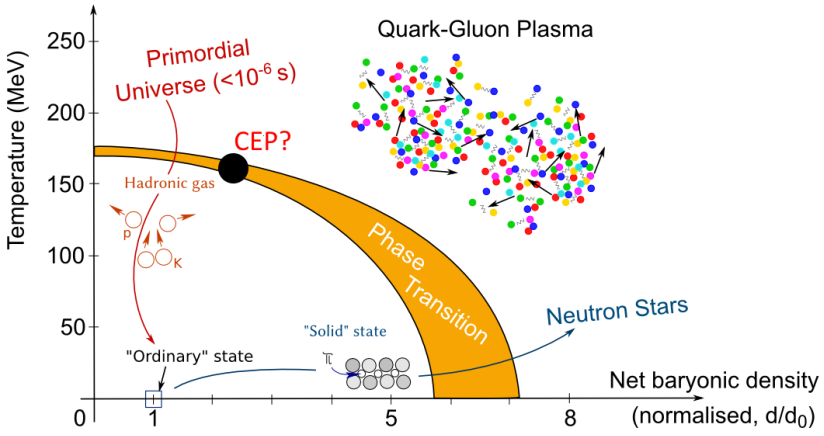

Figure 1.1: Schematic QCD phase-diagram, taken from [3].

Firstly suggested by Edward Shuryak in 1978 [4], the Quark Gluon Plasma (QGP) is a state of matter in which the quarks and gluons are deconfined. This deconfinement can be linked to the asymptotic freedom described before, leading to the production of QGP in laboratories at high temperatures and/or high energy densities. Previously, it had been theorized that such a state of matter would behave like a weakly interacting gas. However, such behaviour would contradict experimental studies of heavy ion collisions. In such collision systems - if they are non-central - the initial geometric shape of the interacting matter (i.e. the QGP) has an anisotropic shape. The transfer of this anisotropy in coordinate space via the thermalized medium into an anisotropy in momentum space (which is experimentally accessible) is called *anisotropic flow*. A more detailed explanation of anisotropic flow will follow in the corresponding Sec. 1.4.1. If QGP would behave like a weakly interacting gas, the anisotropic flow would be small and therefore only a small - if any - anisotropy in momentum space could be observed. Results from e.g. the STAR Collaboration at Relativist Heavy Ion Collider (RHIC) [5] or the ALICE Collaboration at the Large Hadron Collider (LHC) [6] have shown that anisotropic flow is not negligible. As such QGP is found to behave more like a strongly coupled fluid [7], not like a weakly interacting gas. Furthermore, experimental results at RHIC and LHC show that QGP has a shear-viscosity over entropy density (η/s) close to the theorized lower universal boundary of $\hbar/4\pi k_B$ [8]. Thus QGP can be described as a "perfect fluid". However, many questions about the phase-diagram of the QCD (Fig. 1.1) and about properties of QGP still remain open:

- When does the phase transition occur?
- Does the critical point exist, and if so, where is its placement in the phase diagram?
- Does the phase transition behave like a cross over or perhaps like a first order phase transition?

As it is theorized that the QGP existed in the early stage of the universe, the understanding of its behaviour can lead to new insights into the evolution of our universe. Furthermore, QGP is hypothesized to make up the cores of extremely dense neutron stars [9]. Therefore, also in this regard more knowledge about QGP is needed.

1.3 Heavy Ion Collisions

1.3.1 Time Evolution

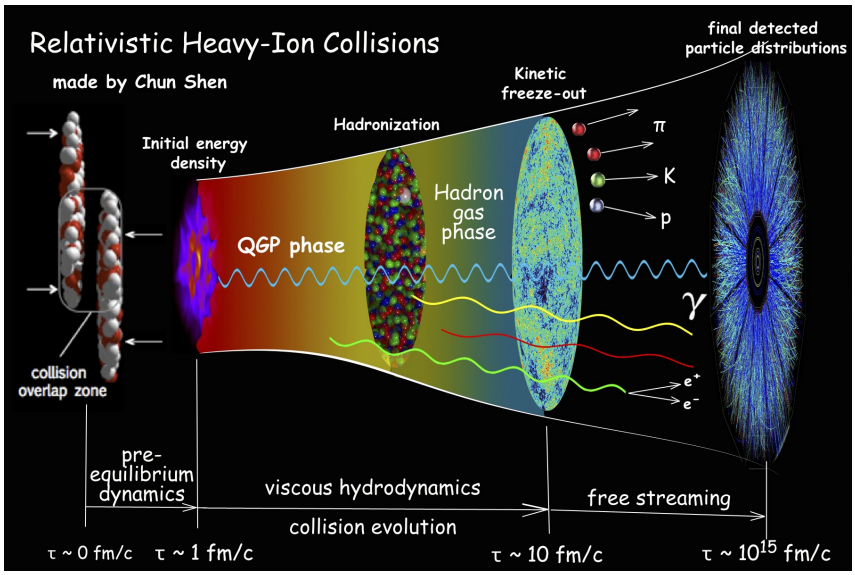

Figure 1.2: Time evolution of a heavy ion collision, taken from [10].

[2]In ultra-relativistic heavy ion collisions (Fig. 1.2) the colliding nuclei are extremely Lorentz-contracted. The collisions can be described as the shattering of colour-glass-condensate plates [12]. During this shattering a significant amount of kinetic energy is stored in the overlapping region, leading to a fireball with a high energy density. This non-equilibrate state is called glasma [12]. As the number of collisions between partons increase, the glasma starts to thermalize locally at a time of about 1 fm/c. This state of local glasma thermalization is the QGP. Further processes can be described by relativistic hydrodynamics. The system will expand, cool and it will become dilute. Finally, hadronization will start, forming hadrons which will interact elastically and inelastically. These last stages starting from the hadronization are described by relativistic kinetic theories. As soon as inelastic processes cease, the system reaches the chemical freeze-out. With the end of elastic processes, the kinetic freeze-out is reached. At a time of about 10-15 fm/c after the collision occurred, hadrons leave the system and travel towards the detectors.

1.3.2 Geometric Description

Taking the beam axis as the z-axis, the geometric quantities of a heavy ion collision (see Fig. 1.3) can be described as follows. As the collision occurs, the colliding/interacting nucleons are called *participants* and the nucleons which do not interact directly in the collision process are called *spectators*. The distance between the centres of mass between the colliding nuclei is the *impact parameter* b. The corresponding vector of the impact parameter $\mathbf{b}$ with respect to the fixed laboratory system has a randomly fluctuating orientation per event. The plane spanned by the beam axis z and the impact parameter vector is called *reaction plane*, its orientation in the fixed laboratory system characterised by Ψ_{RP}. The transverse plane is spanned perpendicular to the beam axis, intersecting

[2]This section is based on [11].

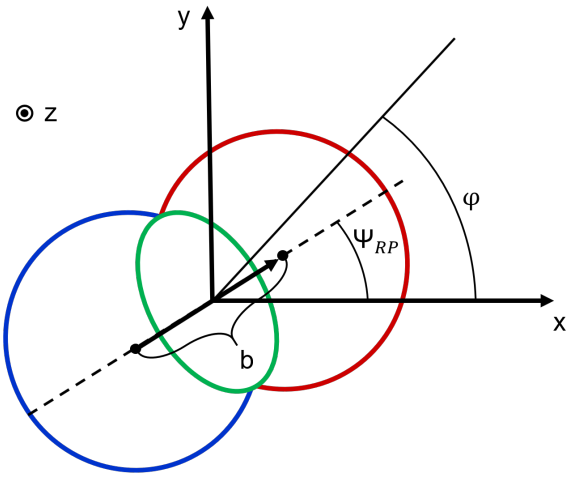

Figure 1.3: Schematic geometry of a heavy ion collision. The green region contains the participants.

the beam axis at the interaction point. Due to fluctuations (e.g. due to fluctuating density profiles of the colliding nuclei) additional planes, the so-called *symmetry-planes* (characterized by Ψ_n) are introduced. They are spanned by the beam axis z and the minor axis of the $n^{th} - order$ shape of the participant-region, where the 2^{nd} order is an ellipsoid, the 3^{rd} order a triangle and so on (see Fig. 1.4). A further explanation of the symmetry-planes and their use-case will be presented in Sec. 1.4.1. At this point, it has to be mentioned that in the absence of fluctuations, all symmetry-planes Ψ_n would be consistent with the reaction plane Ψ_{RP}.

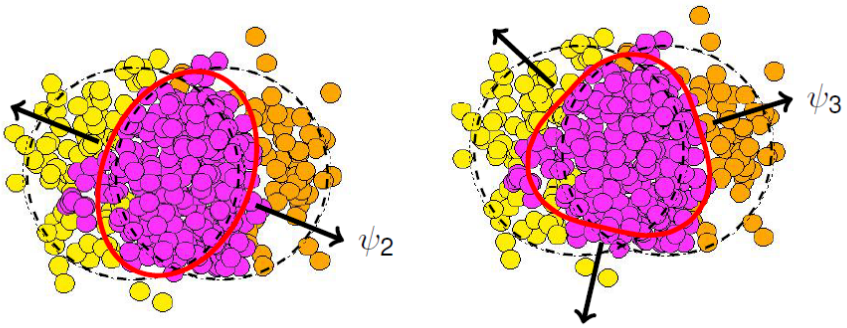

Figure 1.4: Orientations of the symmetry-planes Ψ_2 and Ψ_3 in the initial distribution of the participants, taken from [13].

1.4 Flow

1.4.1 Anisotropic Flow

[3]Properties of the QGP produced in high-energy heavy ion collisions can be studied by the investigation of azimuthal anisotropies (with azimuthal angle φ measured in the transverse plane perpendicular to the beam axis, see Fig. 1.3). Such phenomena can only occur as collective effects of strongly interacting matter, not if the collision consists of

[3]Information of the section taken from [11], [14], [15].

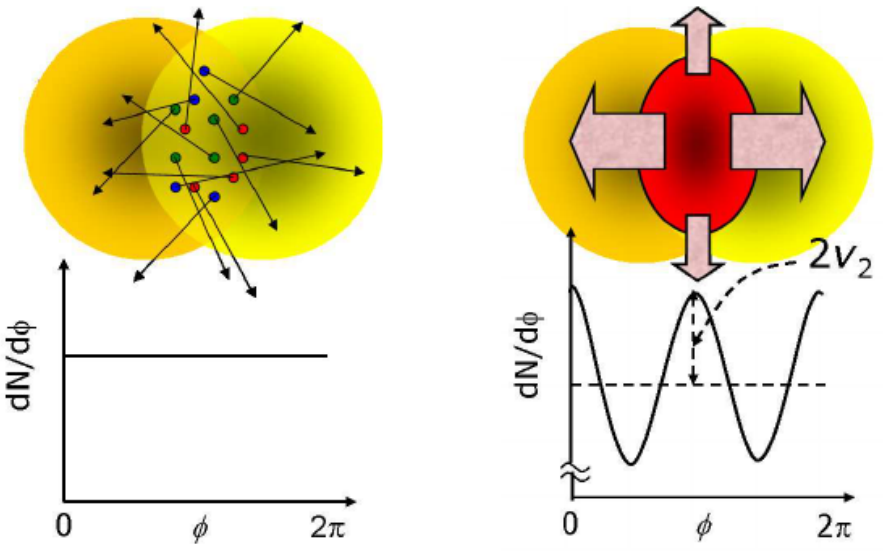

(a) Large mean free path (b) Small mean free path

Figure 1.5: Particle distribution in case that anisotropic flow did not (a) and did (b) develop, taken from [2].

pure nucleon-nucleon interactions.
In non-central heavy ion collisions, the geometry of the interacting matter is anisotropic in the initial state (so-called *anisotropy in coordinate space*). If the medium thermalizes, pressure gradients in the hot and dense matter develop, transferring the initial coordinate anisotropy into an anisotropy in momentum space. This transfer is called *anisotropic flow*. The anisotropy in momentum space can be observed as an anisotropic azimuthal distribution of the emitted particles, which originate from the interacting matter (see Fig. 1.5).
The *flow principle* is an assumption that if only flow as a collective effect is present, the anisotropically emitted particles are solely correlated to the geometry of the emitting source (i.e. emitted independently from the strongly interacting matter). Therefore, the trajectories of emitted particles are the same, whether the particles are emitted simultaneously, or one by one. As the underlying distribution of particles per azimuthal angle φ is 2π-periodic around the beam axis it can be described by a Fourier series [16]:

$$E\frac{\mathrm{d}^3N}{\mathrm{d}^3\mathbf{p}} = \frac{\mathrm{d}^3N}{p_T\mathrm{d}p_T\mathrm{d}\eta\mathrm{d}\varphi} = \frac{1}{2\pi}\frac{\mathrm{d}^2N}{p_T\mathrm{d}p_T\mathrm{d}\eta}\left[1 + 2\sum_{n=1}^{\infty} v_n(p_T,\eta)\cos\left[n\left(\varphi - \Psi_n\right)\right]\right] . \tag{1.2}$$

In Eq. (1.2), φ describes the azimuthal angle of a particle, E its energy and $\mathbf{p}$ its 3-momentum vector. Furthermore, the transverse momentum is represented by p_T and the pseudorapidity by η. The symmetry-planes Ψ_n have been described in Sec. 1.3.2, but again it has to be stressed that they are non-trivial as collisions have event-by-event fluctuations (e.g. due to fluctuating density profiles of the colliding nuclei).
The v_n are the so-called flow amplitudes, with v_1 for the directed flow, v_2 for the elliptic flow, v_3 for the triangular and so on. As it is shown in Appendix A.1, the flow amplitudes can be related to

$$v_n(p_T,\eta) = \langle\cos[n(\varphi - \Psi_n)]\rangle . \tag{1.3}$$

As v_n in general depends on the transverse momentum p_T and pseudorapidity η, it is referred to as the n^{th} *harmonic differential flow*. Averaging over p_T and η leads to the *integrated flow*

$$\langle v_n(p_T,\eta)\rangle = \langle\langle\cos[n(\varphi-\Psi_n)]\rangle\rangle \ . \tag{1.4}$$

where $\langle\cdot\rangle$ denotes the single-event average and $\langle\langle\cdot\rangle\rangle$ the all-event average in a corresponding p_T, η bin. This notation will be kept throughout this thesis.
Therefore, the number of particle N per azimuthal angle φ can be written as

$$\frac{\mathrm{d}N}{\mathrm{d}\varphi} = \frac{\langle N\rangle}{2\pi}\left[1+2\sum_{n=1}^{\infty}\langle v_n(p_T,\eta)\rangle\cos\left[n\left(\varphi-\Psi_n\right)\right]\right] , \tag{1.5}$$

which links the anisotropic distribution of emitted particles per azimuthal angle φ to the flow amplitudes v_n and the symmetry-planes Ψ_n.

1.4.2 Flow vs Non-Flow

In general two kind of phenomena have to be taken into account when using correlation techniques to estimate anisotropic flow in heavy ion collisions: *flow* as a collective effect and *non-flow*. Flow affects all emitted particles where each particle is emitted independently from the source (i.e. the hot and strongly interaction matter). Anisotropic flow as a genuine multi-particle phenomenon is such a collective effect, i.e. flow. Therefore, the underlying probability density function (p.d.f.) of a collision with M emitted particles (and only flow) can be factorised into the marginal Fourier like p.d.f.'s (Eq. (1.2)):

$$f(\varphi_1,\varphi_2,...\varphi_M) = f_{\varphi_1}(\varphi_1)f_{\varphi_2}(\varphi_2)...f_{\varphi_M}(\varphi_M)\,. \tag{1.6}$$

In contrast to that, non-flow typically involves only few particles. Non-flow can be any kind of correlation that is present between particles and which is not directly linked to the emitting source geometry. Phenomena that can be accounted to non-flow are momentum conservation, jet fragmentation, final state interaction (e.g. Coulomb-interactions), resonance decays, etc. All these effects break the factorization in Eq. (1.6) and bias flow measurements.

1.5 Multi-Particle Correlation Techniques

1.5.1 Basics of Multi-Particle Correlation and Notations

As stated before, $\langle\cdot\rangle$ denotes the single-event average and $\langle\langle\cdot\rangle\rangle$ the all-event average. Presented in [17], the general k-particle correlation for one event can be written as

$$\begin{aligned}\langle k\rangle_{n_1,n_2,...,n_k} &\equiv \left\langle e^{i\left(n_1\varphi_{l_1}+n_2\varphi_{l_2}+...+n_k\varphi_{l_k}\right)}\right\rangle \\ &\equiv \frac{\sum\limits_{\substack{l_1,l_2,...l_k=1\\ l_1\neq l_2\neq...\neq l_k}}^{M} w_{l_1}w_{l_2}\cdots w_{l_k}e^{i\left(n_1\varphi_{l_1}+n_2\varphi_{l_2}+...+n_k\varphi_{l_k}\right)}}{\sum\limits_{\substack{l_1,l_2,...l_k=1\\ l_1\neq l_2\neq...\neq l_k}}^{M} w_{l_1}w_{l_2}\cdots w_{l_k}} .\end{aligned} \tag{1.7}$$

In Eq. (1.7), M is the multiplicity, $\{n_1,n_2,...,n_k\}$ the set of harmonics and $\{\varphi_1,\varphi_2,...,\varphi_k\}$ the azimuthal angles. The weights $\{w_1,w_2,...,w_k\}$ are the so-called particle weights and can be the most general function i.e.

$$w_i = w_i\left(\varphi,p_T,\eta,...\right) \ . \tag{1.8}$$

They can depend on the transverse momentum p_T, the pseudorapidity η as well as the azimuthal angle φ (and much more). They, for example, can be used to correct for various detector inefficiencies. Furthermore, event weights have to be used, where each single-event average of azimuthal correlators is weighted individually in the process of building the all-event average. Throughout this thesis for any kind of k-particle correlation multiplicity weights

$$w_{\langle k \rangle} = \binom{M}{k} k! \tag{1.9}$$

will be used as event weights. In Eq. (1.9) M is the multiplicity of the given event. These weights represent the number of combinations of the event and correct for fluctuating multiplicity between events.
Additionally, the set of correlators $\{n_1, n_2, ..., n_k\}$ of the k-particle correlation have to satisfy the so-called isotropy condition i.e.

$$\sum_{i=1}^{k} n_i = 0\,. \tag{1.10}$$

If this condition is not satisfied, the result of the given multi-particle correlation will trivially lead to 0 when the single-event averages are extended to the all-event averages. This can be linked to the angle of the impact parameter vector which fluctuates randomly each event [18]. It has to be noted that this effect only occurs in detectors which cover the full azimuth (which is given for the ALICE main detector, more details in the corresponding Sec. 2.2).
Furthermore, the condition $l_1 \neq l_2 \neq ... \neq l_k$ in Eq. 1.7 has to be applied. It removes exactly all autocorrelations which would otherwise bias the result of the multi-particle correlation. This can be further understood if one takes a 2-particle correlation in harmonics n and $-n$ as an example (setting the particle-weights to 1 for simplicity):

$$\begin{aligned} \langle 2 \rangle_{n,-n} &\equiv \left\langle e^{i\left(n(\varphi_{l_1} - \varphi_{l_2})\right)} \right\rangle \\ &\equiv \sum_{\substack{l_1, l_2 = 1 \\ l_1 \neq l_2}}^{M} e^{i\left(n(\varphi_{l_1} - \varphi_{l_2})\right)}\,. \end{aligned} \tag{1.11}$$

The neglect of $l_1 \neq l_2$ in Eq. (1.11) would lead to the addition of a 1 for the real part (i.e. $\cos\left(n(\varphi_{l_1} - \varphi_{l_2})\right)$) for each case where $\varphi_{l_1} = \varphi_{l_2}$. The real part is the part one is mostly interested in due to its link to the Fourier series (Eq. (1.2)) and the flow observables, (see Sec. 1.5.2). This addition of a 1, which is the maximum value for the cosine, will occur M times for a event consisting of M particles. Thus the final result will be biased strongly, demonstrating the importance of the removal of autocorrelations.

1.5.2 Link to Flow

As it is shown in [18] a k-particle correlation with correlators $\{n_1, n_2, ..., n_k\}$ and azimuthal angles $\{\varphi_1, \varphi_2, ..., \varphi_k\}$ can be linked to the flow observables as

$$\langle \cos\left(n_1\varphi_1 + n_2\varphi_2 + ... + n_k\varphi_k\right) \rangle = v_{n_1} v_{n_2} ... v_{n_k} \cos(n_1\Psi_{n_1} + n_2\Psi_{n_2} + ... + n_k\Psi_{n_k})\,. \tag{1.12}$$

In Eq. (1.12), v_n are the flow amplitudes and Ψ_n the symmetry-planes. This link between the flow observables and the k-particle correlation is made with the real part of the multi-particle correlation (Eq. (1.7)), i.e. $\Re\left(\langle k_{n_1,n_2,...,n_k} \rangle\right)$ due to its connection to the Fourier series (Eq. (1.2)).

1.5.3 Q-vectors

As stated before, for any k-particle correlation, autocorrelations must be prevented. One way to compute Eq. (1.7) is the usage of nested loops with the condition to remove autocorrelations applied. This leads to precise results, though for a k-particle correlation in total k nested loops have to be used. As such, this approach would computationally not be feasible within reasonable time for higher order correlators and the high multiplicities in heavy ion events. Therefore, a different, more efficient approach in the calculation of multi-particle correlations has to be used.
The so-called Q-vector can be defined as

$$Q_n = \sum_{k=1}^{M} e^{in\varphi_k} \tag{1.13}$$

where M is the multiplicity of the event and n the harmonic. The advantage of using the Q-vector becomes clear if one takes a look at the 2-particle correlation as an example. Now one can write analytically the single-event average of the 2-particle correlation in harmonics n and $-n$ ($\langle 2 \rangle_{n,-n}$) as

$$\langle 2 \rangle_{n,-n} \equiv \left\langle e^{in(\varphi_1 - \varphi_2)} \right\rangle \tag{1.14}$$

$$= \frac{1}{\binom{M}{2} 2!} \sum_{\substack{j,k=1 \\ (j \neq k)}}^{M} e^{in(\varphi_j - \varphi_k)} \tag{1.15}$$

$$= \frac{1}{\binom{M}{2} 2!} \times \left[|Q_n|^2 - M \right]. \tag{1.16}$$

The derivation of this example can be found in Appendix A.2. Instead of two nested loops, the Q-vector can be built "in one go" over all azimuthal angles and the 2-particle correlation of the given event can be calculated. Such an expression for the single-event average can be written for any kind of k-particle correlation, when on the RHS only Q-vectors evaluated (in general) in different harmonics and multiplicity M appear, all of which can be calculated in a single pass over azimuthal angles. For more details see [17].

1.6 Glauber Model

1.6.1 Monte Carlo-Glauber

The Monte Carlo-Glauber (MC-Glauber) approach is a model that allows calculations of initial geometric properties in heavy ion collisions. In preparation for this thesis, a new version of the MC-Glauber has been coded in ROOT [19] (code in Appendix H) with the concepts taken from [20]. The basic steps of this approach per "event" are:

1. Sampling of two nuclei A and B by using the Woods-Saxon distribution

$$\rho(r) = \rho_0 \frac{1 + w \left(\frac{r}{R}\right)^2}{1 + \exp\left(\frac{r-R}{a}\right)} \tag{1.17}$$

where ρ_0 is the nucleon density in the centre of the nucleus and R the nuclear radius. The "sphere-parameter" w describes deviations from a spherical shape, a the "skin depth" of the nucleus. The radial component of a nucleon is drawn from $\propto \rho(r)\, r^2$.

The angle φ is uniformly distributed in the interval $[0, 2\pi)$, the angle θ is sampled from p.d.f. $\sin(\theta)$ within the interval $[0, \pi)$. No difference between protons and neutrons is taken into account for the nucleon sampling. Furthermore, the code provides two options for the sampling:

Default: No minimal distance between the nucleons is taken into account.

Minimal Distance: A minimal distance between the nucleons of the same nucleus is being set. The default value of this minimal distance is 0.8 fm between the centres of the nucleons, where a nucleon hard core radius of $R_n = 0.4$ fm is assumed (as it is in [20], with recent experimental results [21] suggesting a similar regime for R_n).

Commonly used values for the parameters in Eq. (1.17) can be found in Appendix Tab. B.1 (taken from [22]).

2. Projection of both nuclei into the x-y-plane and shift of the x-coordinate of nucleus A by $-b/2$ and x-coordinate of nucleus B by $b/2$. Here b represents the impact parameter, i. e. the distance between the centre of masses of the two nuclei (in the x-y-projection-plane). The impact parameter b is taken as an input for this MC-Glauber model, therefore no link to the collisions cross-section is made. Due to this last fact, the implemented MC-Glauber code is not used for centrality estimation, yet later versions will be updated to achieve this.

3. Check that the centres of mass of the projections (x,y) are set correctly: nucleus A at ($-b/2$,0) and nucleus B at ($b/2$,0).

4. "Collision" of the nuclei: If a nucleon experiences an interaction, it is a so-called participant. It is assumed that a nucleon can interact multiple times with different nucleons while remaining on a straight trajectory after a collision. Additionally, it is assumed that nucleon-nucleon cross-sections remain constant and are independent from the number of collisions a nucleon experienced. The total number of participants within the collisions of two nuclei is referred as N_{Part}, the total number of binary collisions of the participating nucleons as N_{Coll}. Two options are available for this step:

   Black-Disc: Probability of interaction between two nucleons is given as

   $$p_{BD}(b) = \Theta(R - b) \tag{1.18}$$

   where b is their distance in the transverse plane and R is a parameter which is linked with the total inelastic nucleon-nucleon cross-section σ_{inel}^{NN} (see Appendix B.3).

   Gaussian Nucleon-Nucleon Overlap: The probability of two nucleons interacting is given by

   $$p(b) = 1 - \left[1 - \alpha \exp\left(-\gamma b^2\right)\right]^2 \tag{1.19}$$

   where b describes the distance of the two nucleons in the transverse plane (taken from [23]). The parameter α and γ can be related to the total inelastic nucleon-nucleon cross-section σ_{inel}^{NN} and the total nucleon-nucleon cross-section σ_{tot}^{NN} (see Appendix B.4). It has to be mentioned that these nucleon-nucleon cross-section are measured independently and used as an experimental input to the Glauber model.

5. By using the coordinates of the participants, one can calculate eccentricities ϵ_n and symmetry-planes in the initial state Φ_n as

   $$\epsilon_n = \frac{\sqrt{\langle r^n \cdot \cos(n \cdot \varphi)\rangle^2 + \langle r^n \cdot \sin(n \cdot \varphi)\rangle^2}}{\langle r^n \rangle} \tag{1.20}$$

and

$$\Phi_n = \frac{1}{n} \cdot \left[\text{atan2}\left(\langle r^n \cdot \sin\left(n \cdot \varphi\right)\rangle, \langle r^n \cdot \cos\left(n \cdot \varphi\right)\rangle\right) + \pi\right] . \tag{1.21}$$

Anisotropies in coordinate space are quantified with ϵ_n and Φ_n, while in the momentum space they are quantified by v_n and Ψ_n. Therefore, it is very interesting to study the relation between ϵ_n and Φ_n.
Equation (1.20) and (1.21) have been taken from [24]. In the calculation of the eccentricities ϵ_n and symmetry-planes in the initial state Φ_n two options are available:

Default: The positions of the nucleons are being taken as delta functions.

Gaussian Smearing: The nucleons are smeared around their initial position (x_i, y_i).

1.6.2 Validation

To validate the Monte Carlo-Glauber code a simulation of Gold-Gold (Au-Au) collisions at $\sqrt{s_{NN}} = 200$ GeV has been carried out (Fig. 1.6, left). For this, the MC-Glauber code has been set up to the following properties: Black Disc - NN overlap, Minimal Distance between nucleons and no Gaussian-Smearing. The obtained result of eccentricities ϵ_1 to ϵ_6 vs. number of participants N_{Part} has been compared to Fig. 1.6 right, taken from [25]. The results obtained with the simple, self-written version of the MC-Glauber model are in good agreement with the published ones.

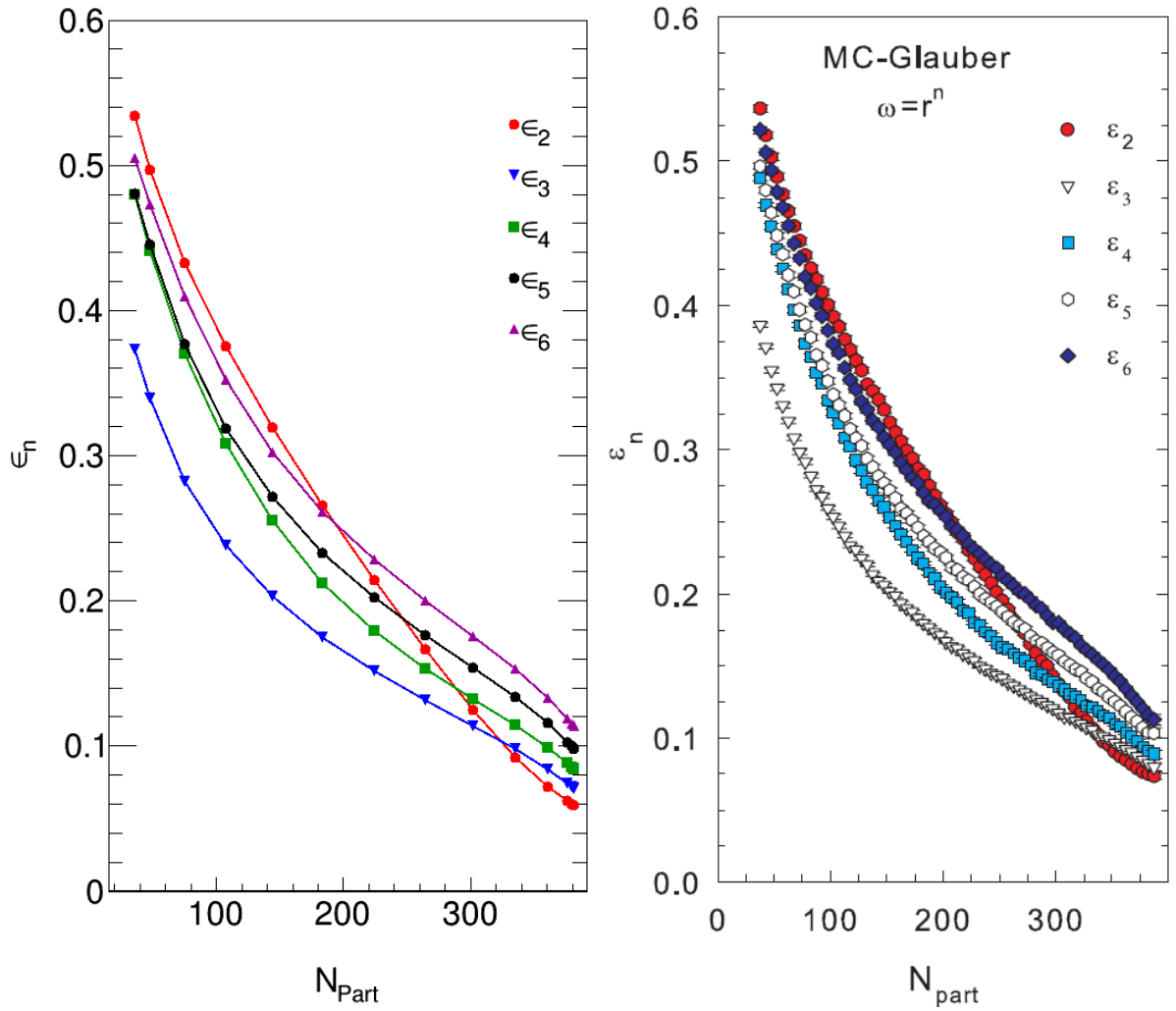

Figure 1.6: Eccentricities ϵ_n for Au-Au Collisions with $\sqrt{s_{NN}} = 200$ GeV. Results by the self-written MC-Glauber code (left) and results of the MC-Glauber code used in [25] (right).

Chapter 2

Experimental Setup

2.1 Large Hadron Collider (LHC)

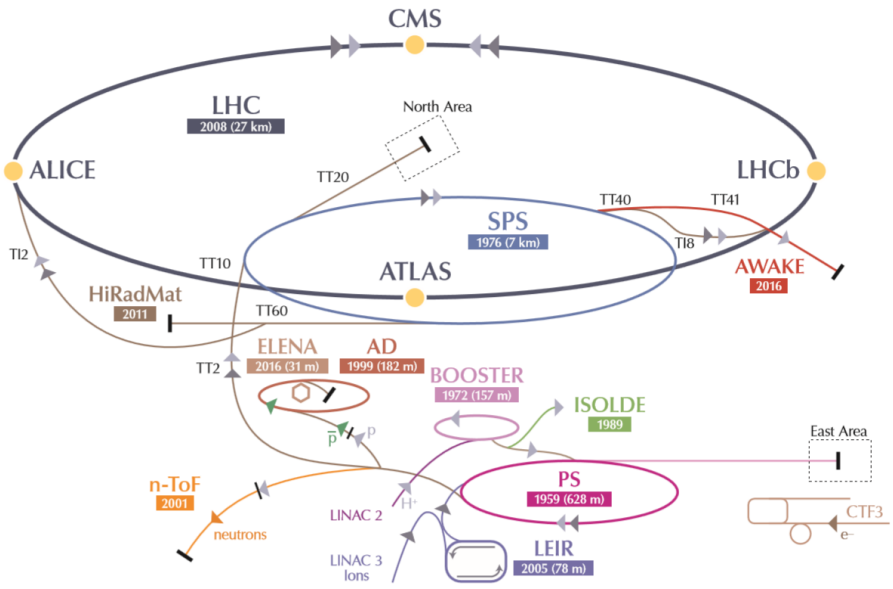

Figure 2.1: The LHC and its pre-accelerators, taken from [26].

[1]Located at the European Organization for Nuclear Research (*Conseil Européen pour la Recherche Nucléaire* - CERN), the *Large Hadron Collider* (LHC) (Fig. 2.1) is the biggest particle collider in the world. The LHC is a synchrotron-type accelerator with a circumference of its main storage ring of 27 km, placed 100 m underground. It has 8 radio-frequency cavities per beam for particle acceleration. In total, about 9600 superconducting magnets (cooled to 1.9 K) with maximum magnetic fields of 8.33 T guide the particles through the vacuum tube which has a vacuum pressure of about 10^{-13} atm.
The first collection of data at LHC (so-called "Run 1") reached centre of mass energies per nucleon pairs of $\sqrt{s} = 7$ TeV for proton-proton (p-p) collisions and $\sqrt{s_{NN}} = 2.76$ TeV for lead-lead (Pb-Pb) collisions. After the 2015 upgrade the LHC provides "Run 2" data with $\sqrt{s} = 13$ TeV for p-p collisions and $\sqrt{s_{NN}} = 5.02$ TeV Pb-Pb collisions. At the moment LHC undergoes an additional upgrade to increase its current luminosity to about 50 kHz in Pb-Pb collisions [29], thus preparing the accelerator for "Run 3".

[1]Section based on [2], [26], [27] and [28].

Stationed at LHC are seven detector experiments: ALICE (A Large Ion Collider Experiment), ATLAS (A Toroidal LHC Apparatus), CMS (Compact Muon Solenoid), LHCb (Large Hadron Collider beauty), LHCf (Large Hadron Collider forward), TOTEM (TOTal Elastic and diffractive cross section Measurement) and Monopole and Exotics Detector at the LHC (MoEDAL). Some of the main goals of these experiments is the research about:

- Existence and properties of the Higgs boson ([30], [31])
- Asymmetry between matter and anti-matter
- Dark matter and Dark energy
- Properties of QGP
- Search for the existence of supersymmetric particles

2.2 A Large Ion Collider Experiment (ALICE)

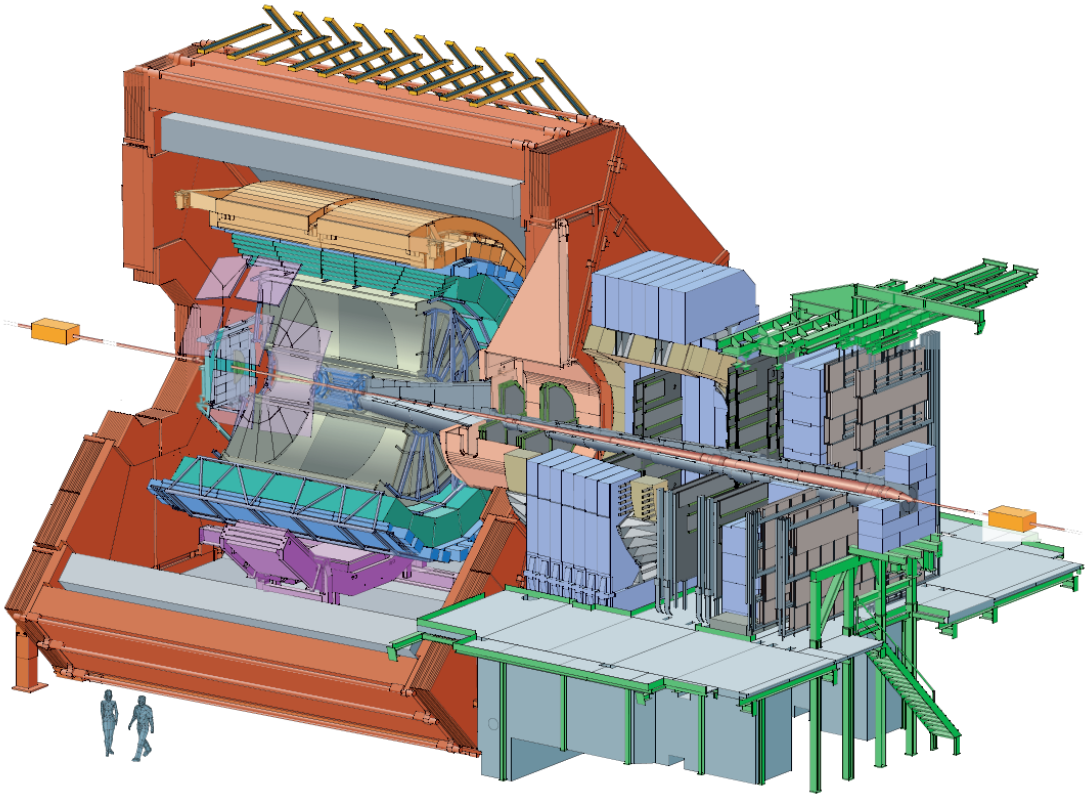

Figure 2.2: Schematic of ALICE, taken from [32].

[2]Designed for the study of strongly interacting QCD matter, the main purpose of ALICE is the investigation of properties of the QGP. ALICE, which is the only dedicated heavy ion experiment at LHC, can provide information of the colliding events with high-momentum resolution and good particle identification (PID). At the same time, the experiment is able to cope with the extreme amount of particles that are produced in Pb-Pb collisions at LHC energies. The barrel-shaped experiment (see Fig. 2.2) consists of multiple layers of different detectors, starting with the *Inner Tracking System (ITS)*

[2]The information of this part are taken from [32].

as the most inner one. The ITS consists of six layers of Silicon detectors (detailed description in the ITS section). Following the ITS is the cylinder-shaped *Time Projection Chamber (TPC)* and three arrays for particle identification: *Time of Flight (TOF)*, *High Momentum Particle Identification (HMPID)* - a Ring Imaging Cherenkov Detector, finally followed by two *Electromagnetic Calorimeters (EMCal)*.
Placed directly around the beam pipe, the ITS is used in the determination of the primary vertex and secondary vertices of fast decaying heavy flavour and strange particles. It allows the tracking of low momentum particles (which do not reach TPC). Furthermore, it has the highest spatial resolution in comparison with the other ALICE detectors which is necessary due to its close placement to the beam pipe.
The TPC is a gas detector used for tracking and high resolution PID (further details in the corresponding section of TPC).
Momentum resolution in the regime of high momenta can be further improved by the *Transition Radiation Detector (TRD)*, the identification of charged hadrons can be further done with TOF. The HMPID provides information in PID for high momentum particles. EMCal as an electromagnetic calorimeter is used in the energy measurement of charged particles, as a trigger for high momentum particles as well as in the improvement of jet measurements. Photons and neutral mesons are identified by the *Photon Spectrometer (PHOS)*. All of these detectors are surrounded by a solenoid magnet with a magnetic field of $B = 0.5$ T. Besides the previously described detectors, ALICE has detectors in forward and backward direction which are located close to the beam pipe. Acting as a trigger and estimator for longitudinal vertex positions the *V0* detector is to be named, consisting of *Photo Multiplier Tubes (PMT)*. The *Forward Multiplicity Detector (FMD)* is used in the multiplicity measurement of charged particles. Similarly, the *Photon Multiplicity Detector (PMD)* provides information of photon multiplicities. The *Zero Degree Calorimeters (ZDC)* are located 116 m away from the beam time and used in the centrality determination as they provide information about spectator nucleons. Furthermore, muon spectrometers for the detection of muon pairs can be found.
Currently, ALICE is undergoing an upgrade, preparing the experiment for the high luminosities which are aimed with LHC "Run 3".

2.2.1 Time Projection Chamber

[3] Having a fine track reconstruction with a large amount of points per track while being able to cope with collisions at a rate of 10 kHz, the TPC (Fig. 2.3) has been chosen as the primary detector of ALICE. The cylindrical detector is filled with 90 m^3 of gas which consists of 90 % Ne and 10 % CO_2. Its dimensions are 5 m along the beam axis, an inner radius of 85 cm and an outer radius of 2.5 m while being separated by a cathode in the middle. TPC as a gas detector is able to recognize charged particles traversing as those particles ionize the gas along their path. The electrons released in such ionisation processes are accelerated in a uniform electric field towards end plates. These end plates create the electric field as a potential is applied to them. As the electrons reach the end plates they will be registered by *Multi-Wire Proportional Chambers (MWPC)* which amplify the incoming signal of primary electrons. The r and ϕ coordinate of the electron can be reconstructed directly by the MWPC's, the z coordinate can be extracted from the time of flight that the electron needs to reach the end plate. From these three coordinates, the origin of the electron and therefore the place of its creating particle can be reconstructed. Thus a full three-dimensional track of charged particles can be obtained.

[3] Information of this subsection have been taken from [32], [33], [34].

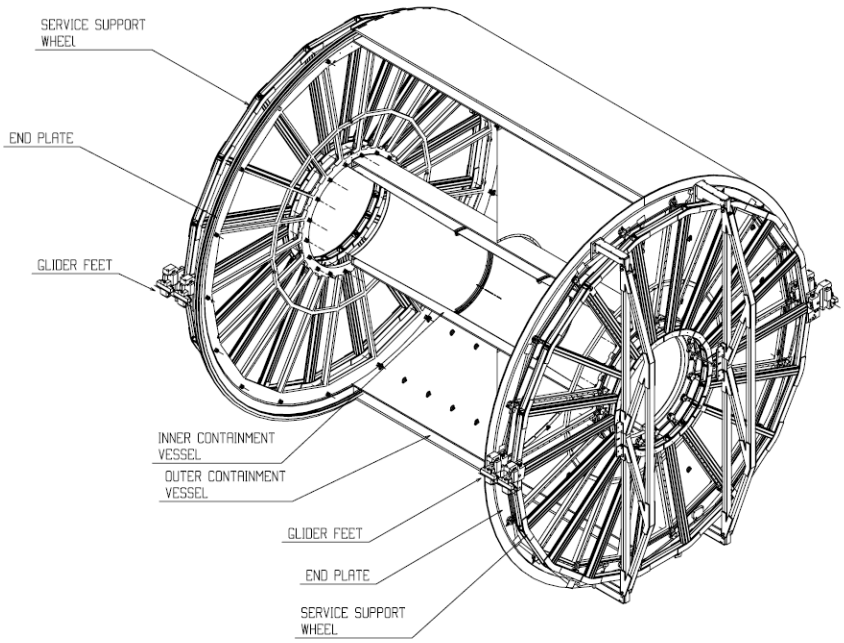

Figure 2.3: Schematic of TPC, taken from [32].

TPC covers a transverse momentum range of $0.1\,\mathrm{GeV}/c < p_T < 100\,\mathrm{GeV}/c$. It has a resolution of 6 % for $p_T < 20\,\mathrm{GeV}/c$ in central Pb-Pb collisions and a track finding efficiency of about 90 % for $p_T > 1\,\mathrm{GeV}/c$. Over the whole p_T range TPC provides a azimuthal resolution of $\Delta\varphi = 0.7$ mrad and although a full coverage of azimuthal angles is provided, the detector has dead zones in between neighbouring sectors, thus leading to a loss in efficiency. Concerning the pseudorapidity range, TPC provides a uniform azimuthal coverage for $|\eta| < 0.9$.
Furthermore, TPC can be used for particle identification: The measured amplitude in the MWPC provides information about $\mathrm{d}E/\mathrm{d}x$. In combination with the momentum of the charged particle (radius of its track within the magnetic field) the particle identification can be processed. Additionally, TPC can be used for the centrality estimation of the collisions.

2.2.2 Inner Tracking System

[4]The ITS (Fig. 2.4) is built of six layers of silicon detectors. In total, three different types of these silicon detectors are used, with the two innermost layers being *Silicon Pixel Detector (SPD)*, followed by two layers of *Silicon Drift Detectors (SDD)* and the two outermost layers of *Silicon Strip Detectors (SSD)*.
The SPD have the highest spatial resolution, necessary as they are the closest to the beam pipe. Each of the SPD layers is made out of 9.8×10^6 binary readout cells. Thus SPD can still well separate two tracks in the region of 50 tracks per cm^2 while providing a pseudorapidity coverage of $|\eta| < 2.0$. Additionally, SPD can be used as a centrality estimator.
The two middle layers of SSD have, due to their greater distance to the beam pipe, a track density of 1 track per cm^2. Therefore, the spatial resolutions of these detectors can be smaller.

[4]Information of this subsection have been taken from [32], [34], [35] and [36].

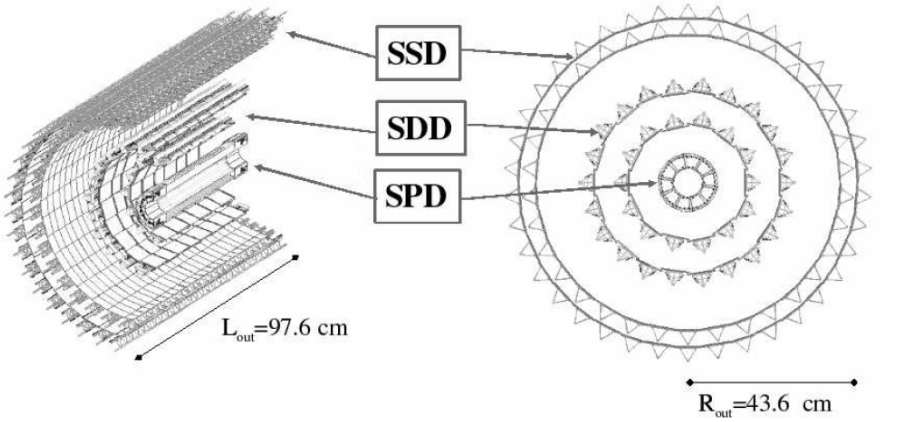

Figure 2.4: Schematic of ITS, taken from [32].

Combining all layers of ITS the primary vertex can be located within 100 μm. The coverage for transverse momentum is $0.1\,\mathrm{GeV}/c < p_T < 3\,\mathrm{GeV}/c$ with a resolution of 2 % for pions.
ITS provides a pseudorapidity coverage of $|\eta| < 0.9$ and is used in the determination of the main interaction vertex as well as secondary vertices. ITS can provide information about fast decaying heavy flavour and strange particles and allows tracking of low momentum particles.

Chapter 3

Theoretical SPC

As shown in Sec. 1.4.1, the phenomenon of anisotropic flow can be described by a Fourier series (Eq. (1.2)), parametrized by the flow amplitudes v_n and the symmetry-planes Ψ_n. The goal is the measurement of symmetry-plane correlations (SPC) in the form $\cos\left[\alpha(\Psi_m - \Psi_n)\right]$ (with α a correlator dependent pre-factor). Such new observables allow a better understanding of correlations between the phases themselves and, as the main purpose, enable additional constraints and independent information about properties of the QGP.
Previous attempts [37] to measure these kind of observables were based on building ratios in the form of

$$\begin{aligned} &\langle\cos\left(c_1\Psi_1 + 2c_2\Psi_2 + ... + lc_l\Psi_l\right)\rangle \\ &= \frac{\langle v_1^{c_1} v_2^{c_2} ... v_l^{c_l} \cos\left(c_1\Psi_1 + 2c_2\Psi_2 + ... + lc_l\Psi_l\right)\rangle}{\sqrt{\left\langle v_1^{2c_1}\right\rangle \left\langle v_2^{2c_2}\right\rangle ... \left\langle v_l^{2c_l}\right\rangle}} \,. \end{aligned} \tag{3.1}$$

In Eq. (3.1) the isotropy of the correlators has to be ensured, i.e.

$$\sum_{j=1}^{l} j c_j = 0 \,. \tag{3.2}$$

As it is shown in [1], correlations between flow amplitudes v_n themselves can be observed. This result leads to

$$\langle v_n v_m\rangle \neq \langle v_n\rangle \langle v_m\rangle \,. \tag{3.3}$$

Therefore, the cancelling of flow amplitudes v_n in the numerator by factorised v_n in the denominator as done in [37] will lead to a biased result.
This statement holds true even if one assumes no correlation between flow amplitudes v_n and $\cos(n_1\Psi_{n_1} + n_2\Psi_{n_2} + ... + n_k\Psi_{n_k})$ (for a k-particle correlation). This will be demonstrated in Sec. 3.3.1. The goal of this thesis is the examination of new approaches to measure SPC without neglecting correlations between flow amplitudes v_n themselves. The basic concept lies in building ratios where the denominator is not factorised. Two main approaches and their properties will be investigated:

- All-Event-Approach (AE)
- Event-by-Event-Approach (EbE)

Furthermore, the concepts of two additional approaches

- Expansion-Approach
- Tan-Approach

will be presented. The details of each approach will be explained later. Again it has to be stressed that all of these four approaches are based on the removal of flow-amplitudes v_n "in one go".

3.1 General (m,n)-SPC

For the derivation of the general SPC, it does not matter which approach is used (AE, EbE or Expansion), as for all of them the sets of correlators have to fulfil the same constraints (removal of flow amplitudes with non-factorised denominator). The azimuthal angles φ are taken as an input. The aim is to provide an output correlator of symmetry-planes Ψ_m, Ψ_n without any contribution from flow amplitudes.
The general approach for the SPC presented here is the usage of ratios between two sets of correlators. In this derivation, the EbE-Approach will be used to build the ratio per event (the sets of correlators stay the same in the other approaches, their results will be presented in their corresponding section). In the most general case, this ratio can be written as:

$$\begin{aligned} &\frac{\langle \cos\left(n_1 \cdot \varphi_1 + ... + n_k \cdot \varphi_k\right)\rangle}{\langle \cos\left(p_1 \cdot \varphi_1 + ... + p_l \cdot \varphi_l\right)\rangle} \\ &= \frac{v_{n_1} \cdot ... \cdot v_{n_k} \cos\left(n_1 \cdot \Psi_{n_1} + ... + n_k \cdot \Psi_{n_k}\right)}{v_{p_1} \cdot ... \cdot v_{p_l} \cos\left(p_1 \cdot \Psi_{p_1} + ... + p_l \cdot \Psi_{p_l}\right)} . \end{aligned} \tag{3.4}$$

This can be written in a more compact way

$$\begin{aligned} &\frac{\left\langle \cos\left(\sum_{j=1}^{k} n_j \cdot \varphi_j\right)\right\rangle}{\left\langle \cos\left(\sum_{j=1}^{l} p_j \cdot \varphi_j\right)\right\rangle} \\ &= \frac{\prod_{i=1}^{k} v_{n_i} \cos\left(\sum_{j=1}^{k} n_j \cdot \Psi_{n_j}\right)}{\prod_{i=1}^{l} v_{p_i} \cos\left(\sum_{j=1}^{l} p_j \cdot \Psi_{p_j}\right)} , \end{aligned} \tag{3.5}$$

where $\{n_1, n_2, ..., n_k\}$ is the set of harmonics of the numerator, $\{p_1, p_2, ..., p_l\}$ the harmonics of the denominator, φ the azimuthal angles, v_n (v_p) the flow amplitudes and Ψ_n (Ψ_p) the symmetry-planes. Now $\{n_1, n_2, ..., n_k\}$ and $\{p_1, p_2, ..., p_l\}$ have to be chosen in such a way that the flow amplitudes will cancel while at the same time any contribution of symmetry-planes stays only in the numerator. These constraints will be presented in the following section.

3.1.1 Constraints

The first constraint in SPC is the isotropy of the correlators both in numerator and denominator. This constraint must hold true for any multi-particle correlator. Therefore

$$\sum_{j=1}^{k} n_j = 0 , \tag{3.6}$$

$$\sum_{j=1}^{l} p_j = 0 . \tag{3.7}$$

Furthermore, the sum of symmetry-planes appearing in the numerator must not be equal to 0 whereas the one in the denominator has to i.e.

$$\sum_{j=1}^{k} n_j \cdot \Psi_{n_j} \neq 0\,, \tag{3.8}$$

$$\sum_{j=1}^{l} p_j \cdot \Psi_{p_j} = 0\,. \tag{3.9}$$

The flow amplitudes v_n of the numerator and denominator have to cancel each other, so that one is left only with the correlator of symmetry-planes in the numerator. Therefore, their product has to be the same i.e.

$$\prod_{i=1}^{k} v_{n_i} = \prod_{i=1}^{l} v_{p_i}\,. \tag{3.10}$$

From Eq. (3.10):

$$\Rightarrow k = l\,, \tag{3.11}$$

which means that the multi-particle correlators in the numerator and the denominator have to be of the same order.
Furthermore, the sets of "absolute values" have to be equal as $v_{-n} = v_n$:

$$\{|n_1|\,, |n_2|\,, ..., |n_k|\} = \{|p_1|\,, |p_2|\,, ..., |p_k|\}\ . \tag{3.12}$$

As presented in the following section, it is possible to construct sets of correlators for a (m,n)-SPC in such a way that the previously presented constraints Eq. (3.6) to Eq. (3.10) are satisfied.

3.1.2 Generalisation

Given the constraints Eq. (3.8) to Eq. (3.10) to measure a Ψ_m-Ψ_n SPC, the general sets of correlators in harmonics m and n (where $m \neq n$) can be set up for

- the numerator as: $\left\{\underbrace{m, ..., m}_{a_m\ times}, \underbrace{-n, ..., -n}_{a_n\ times}\right\}$
- and the denominator as: $\left\{\underbrace{m, -m..., m, -m}_{a_m\ times}, \underbrace{n, -n, ..., n, -n}_{a_n\ times}\right\}$

where $a_m, a_n \in \mathbb{N}$. Given the constraints Eq. (3.6) and Eq. (3.7) the following constraints for a_m and a_n appear as

$$\sum_{j=1}^{a_m} m + \sum_{k=1}^{a_n} (-n) \equiv a_m \cdot m - a_n \cdot n = 0 \implies \frac{a_m}{n} = \frac{a_n}{m}\,, \tag{3.13}$$

$$\sum_{j=1}^{a_m} (-1)^j \cdot m + \sum_{k=1}^{a_n} (-1)^k \cdot n = 0 \implies a_m \wedge a_n \text{ even}\,, \tag{3.14}$$

where $\wedge$ is the logical "and". This way, the constraints from Eq. (3.8) and Eq. (3.9) are satisfied as well. Possible choices for a_m and a_n are

1. Direct Method $\begin{cases} a_m = n \text{ and } a_n = m & \text{for } m \wedge n \text{ even} \\ a_m = 2n \text{ and } a_n = 2m & \text{for } m \vee n \text{ odd} \end{cases}$

2. LCM-Method: $a_m = \frac{2 \cdot LCM(m,n)}{m}$ and $a_n = \frac{2 \cdot LCM(m,n)}{n}$

where $LCM(m,n)$ denotes the least common multiple of m and n, $\wedge$ the logical "and" and $\vee$ the logical "or" (this notation will be kept through this thesis).
It has to be noted that for the LCM-Method the pre-factor 2 has to be used to ensure that a_m and a_n are both even as

$$\nexists\, m,n \in \mathbb{N}: \ \frac{LCM(m,n)}{m} = 2j \wedge \frac{LCM(m,n)}{n} = 2k \text{ with } j,k \in \mathbb{N}\,. \tag{3.15}$$

The proof of this statement can be found in Appendix C.1.

The order of the multi-particle correlators used in both approaches are

1. Direct Method $\begin{cases} n+m & \text{for } m \wedge n \text{ even} \\ 2\,(n+m) & \text{for } m \vee n \text{ odd} \end{cases}$

2. LCM-Method: $2 \cdot LCM(m,n)\left(\frac{1}{m} + \frac{1}{n}\right)$

As it is shown in Appendix C.2 for any integers m and n the order of the correlators in the LCM-Method is always smaller equal compared to the Direct Method. This is favourable as SPC deal with high order of correlators in general. To reach feasibility, the order of the correlators has to be reduced as much as possible.
As a conclusion, the LCM-Method will be used for any further (m,n)-SPC approaches. Therefore, the sets of correlators for any (m,n)-SPC are given for

- the numerator as: $\left\{ \underbrace{m,...,m}_{a_m \text{ times}}, \underbrace{-n,...,-n}_{a_n \text{ times}} \right\}$
- and the denominator as: $\left\{ \underbrace{m,-m...,m,-m}_{a_m \text{ times}}, \underbrace{n,-n,...,n,-n}_{a_n \text{ times}} \right\}$

with

$$a_m = 2\ \frac{LCM(m,n)}{m} \tag{3.16}$$

and

$$a_n = 2\ \frac{LCM(m,n)}{n}\,. \tag{3.17}$$

These sets of correlators satisfy the constraints Eq. (3.6) to Eq. (3.10) while minimizing the order of the correlators (compared to the "Direct-Method" shown before).

Therefore, the SPC between ψ_m and ψ_n in the EbE-method is given by

$$\frac{\left\langle \cos\left(\sum_{j=1}^{a_m} m\cdot\varphi_j - \sum_{k=1}^{a_n} n\cdot\varphi_{a_m+k}\right)\right\rangle}{\left\langle \cos\left(\sum_{j=1}^{a_m}(-1)^j\cdot m\cdot\varphi_j + \sum_{k=1}^{a_n}(-1)^k\cdot n\cdot\varphi_{a_m+k}\right)\right\rangle}$$

$$= \frac{\left(\prod_{i=1}^{a_m} v_m\right)\left(\prod_{j=1}^{a_n} v_n\right)\cos\left(\sum_{j=1}^{a_m} m\cdot\Psi_m - \sum_{k=1}^{a_n} n\cdot\Psi_n\right)}{\left(\prod_{i=1}^{a_m} v_m\right)\left(\prod_{j=1}^{a_n} v_n\right)\cos\left(\sum_{j=1}^{a_m}(-1)^j\cdot m\cdot\Psi_m + \sum_{k=1}^{a_n}(-1)^k\cdot n\cdot\Psi_n\right)} \tag{3.18}$$

$$= \cos\left[2\cdot LCM(m,n)\cdot(\Psi_m - \Psi_n)\right] .$$

The transition from the first to the second line in Eq. (3.18) has been obtained with Eq. (1.12). Furthermore, the order of the particle correlators used in the numerator and denominator in Eq. (3.18) is the size of $2\cdot LCM(m,n)\left(\frac{1}{m}+\frac{1}{n}\right)$.

It has to be stressed that the previous formula for a (kn,n)-SPC [38] given by

$$\cos\left[2kn\left(\Psi_{kn} - \Psi_n\right)\right] = \frac{\left\langle \cos\left[n\left(k\varphi_1 + k\varphi_2 - \sum_{j=3}^{2k+2}\varphi_j\right)\right]\right\rangle}{\left\langle \cos\left[n\left(k\varphi_1 - k\varphi_2 - \sum_{j=3}^{2k+2}(-1)^j\varphi_j\right)\right]\right\rangle} \tag{3.19}$$

can be obtained by Eq. (3.18) as a special case for $m = kn$ as in this case $LCM(kn,n) = kn$.

3.2 Preliminary (m,n,q)-SPC

A general (m,n,q)-SPC has to satisfy the previously presented constraints Eq. (3.6) to Eq. (3.10).
Having the constraints Eq. (3.8) to Eq. (3.10) in mind, the general sets of correlators in harmonics m, n and q (where $m \neq n \neq q$) can be set up for

- the numerator as: $\left\{\underbrace{m,...,m}_{a_m\ times},\underbrace{-n,...,-n}_{a_n\ times},\underbrace{-q,...,-q}_{a_q\ times}\right\}$
- and the denominator as: $\left\{\underbrace{m,-m...,m,-m}_{a_m\ times},\underbrace{n,-n,...,n,-n}_{a_n\ times},\underbrace{q,-q,...,q,-q}_{a_q\ times}\right\}$

where a_m, a_n, $a_q \in \mathbb{N}$. Given the constraints Eq. (3.6) and Eq. (3.7) the following constraints for a_m, a_n and a_a are given by

$$\sum_{j=1}^{a_m} m + \sum_{k=1}^{a_n}(-n) + \sum_{k=1}^{a_q}(-q) \equiv a_m\cdot m - a_n\cdot n - a_q\cdot q = 0\,, \tag{3.20}$$

$$\sum_{j=1}^{a_m}(-1)^j\cdot m + \sum_{k=1}^{a_n}(-1)^k\cdot n + \sum_{k=1}^{a_q}(-1)^k\cdot q = 0 \implies a_m \wedge a_n \wedge a_q \text{ even}\,. \tag{3.21}$$

In such a way, the constraints from Eq. (3.8) and Eq. (3.9) are satisfied as well. Choices that come up for a_m, a_n and a_q are

1. Direct Method $\begin{cases} a_m = 2nq,\ a_n = mq \text{ and } a_q = mn & \text{for all even or 1 odd} \\ a_m = 4nq,\ a_n = 2mq \text{ and } a_q = 2mn & \text{for all odd or 1 even} \end{cases}$

2. LCM-Method: $\begin{cases} a_m = 2m',\ a_n = n' \text{ and } a_q = q' & \text{for } n' \wedge q' \text{ even} \\ a_m = 3m',\ a_n = n' \text{ and } a_q = 2q' & \text{for } (m' \wedge n' \text{ even}) \wedge q' \text{ odd} \\ a_m = 3m',\ a_n = 2n' \text{ and } a_q = q' & \text{for } (m' \wedge q' \text{ even}) \wedge n' \text{ odd} \\ a_m = 4m',\ a_n = 2n' \text{ and } a_q = 2q' & \text{for } [m' \text{ odd} \wedge (n' \vee q' \text{ odd})] \\ & \quad \vee [m' \text{ even} \wedge (n' \wedge q' \text{ odd})] \end{cases}$.

The following abbreviations have been used:

$$m' = \frac{LCM(m,n,q)}{m}$$
$$n' = \frac{LCM(m,n,q)}{n}$$
$$q' = \frac{LCM(m,n,q)}{q}$$

where $LCM(m,n,q)$ denotes the least common multiple of m, n and q.
For the LCM of two integers m and n it has been shown (Appendix C.1) that

$$\nexists\, m,n \in \mathbb{N}: \ \frac{LCM(m,n)}{m} = 2j \wedge \frac{LCM(m,n)}{n} = 2k \text{ with } j,k \in \mathbb{N}. \tag{3.22}$$

This limited the ways of building a_m and a_n for two numbers as at least one ratio of $LCM(m,n)/m$ or $LCM(m,n)/n$ is odd. This statement can be extended for three integers:

$$\nexists\, m,n,q \in \mathbb{N}: \frac{LCM(m,n,q)}{m} = 2i \wedge \frac{LCM(m,n,q)}{n} = 2j \wedge \frac{LCM(m,n,q)}{q} = 2k \quad \text{with } i,j,k \in \mathbb{N}. \tag{3.23}$$

A proof of this can be found in Appendix C.3.
The order of the correlators is

1. Direct Method $\begin{cases} 2nq + mq + mn & \text{for all even or 1 odd} \\ 4nq + 2mq + 2mn & \text{for all odd or 1 even} \end{cases}$

2. LCM-Method: $\begin{cases} LCM(m,n,q)\left(\frac{2}{m} + \frac{1}{n} + \frac{1}{q}\right) & \text{for } n' \wedge q' \text{ even} \\ LCM(m,n,q)\left(\frac{3}{m} + \frac{1}{n} + \frac{2}{q}\right) & \text{for } (m' \wedge n' \text{ even}) \wedge q' \text{ odd} \\ LCM(m,n,q)\left(\frac{3}{m} + \frac{2}{n} + \frac{1}{q}\right) & \text{for } (m' \wedge q' \text{ even}) \wedge n' \text{ odd} \\ LCM(m,n,q)\left(\frac{4}{m} + \frac{2}{n} + \frac{2}{q}\right) & \text{for } [m' \text{ odd} \wedge (n' \vee q' \text{ odd})] \\ & \quad \vee [m' \text{ even} \wedge (n' \wedge q' \text{ odd})] \end{cases}$

with

$$m' = \frac{LCM(m,n,q)}{m}$$
$$n' = \frac{LCM(m,n,q)}{n}$$
$$q' = \frac{LCM(m,n,q)}{q}\,.$$

In cases of m, n and q all being odd or at maximum one even, the order of correlators in the LCM-Method is smaller than or equal to the ones in the Direct-Method, as $LCM(m,n,q) \leq mnq$.
A proof that the LCM-Method reduces the order of the correlators in case of all integers being even or one odd is left open at this point.

It has to be mentioned that in the special case of a (kn, mn, n)-SPC (without loss of generality $k > m$), the SPC given by [38]

$$\begin{aligned}&\cos\left[2n(k\Psi_{kn} - m\Psi_{mn} - (k-m)\Psi_n)\right]\\ &= \frac{\left\langle \cos\left[n(k\varphi_1 + k\varphi_2 - m\varphi_3 - m\varphi_4 - \sum_{j=5}^{2(k-m)+4}\varphi_j)\right]\right\rangle}{\left\langle \cos\left[n(k\varphi_1 - k\varphi_2 + m\varphi_3 - m\varphi_4 - \sum_{j=5}^{2(k-m)+4}(-1)^j\varphi_j)\right]\right\rangle}\end{aligned} \tag{3.24}$$

is leading to a smaller correlator.

3.3 All-Event SPC

The All-Event SPC (AE-SPC) is using the general sets of correlators presented in Sec. 3.1 in such a way that the averages over all events of numerator and denominator are calculated individually. Afterwards, the ratio between the averaged numerator and averaged denominator is built. This approach assumes no correlation between flow amplitudes and $\cos\left[2 \cdot LCM(m,n) \cdot (\Psi_m - \Psi_n)\right]$. Based on this idea, one can write the general AE-SPC as

$$\begin{aligned}&\frac{\left\langle\left\langle \cos\left(\sum_{j=1}^{a_m} m\cdot\varphi_j - \sum_{k=1}^{a_n} n\cdot\varphi_{a_m+k}\right)\right\rangle\right\rangle}{\left\langle\left\langle \cos\left(\sum_{j=1}^{a_m}(-1)^j\cdot m\cdot\varphi_j + \sum_{k=1}^{a_n}(-1)^k\cdot n\cdot\varphi_{a_m+k}\right)\right\rangle\right\rangle}\\ &= \frac{\left\langle \left(\prod_{i=1}^{a_m} v_m\right)\left(\prod_{j=1}^{a_n} v_n\right)\cos\left(\sum_{j=1}^{a_m} m\cdot\Psi_m - \sum_{k=1}^{a_n} n\cdot\Psi_n\right)\right\rangle}{\left\langle \left(\prod_{i=1}^{a_m} v_m\right)\left(\prod_{j=1}^{a_n} v_n\right)\cos\left(\sum_{j=1}^{a_m}(-1)^j\cdot m\cdot\Psi_m + \sum_{k=1}^{a_n}(-1)^k\cdot n\cdot\Psi_n\right)\right\rangle}\\ &= \left\langle\cos\left[2\cdot LCM(m,n)\cdot(\Psi_m - \Psi_n)\right]\right\rangle\,.\end{aligned} \tag{3.25}$$

To validate that the AE-SPC is leading to an unbiased result in case of correlated flow amplitudes v_n, two sets of Toy Monte Carlo studies (TMC) have been carried out. In these studies, the Fourier series Eq. (1.5) is given as an input. It serves as a probability density function to sample the azimuthal angles φ. These angles are then passed to the analysis framework, whose output is stored. Lastly, the averaged output of the analysis framework is compared to the theoretical expected value given by the parameters plugged into the Fourier series.

3.3.1 TMC: Correlation Study

To verify the AE-SPC in different cases of correlations between flow amplitudes v_n, a Toy Monte Carlo study has been carried out. In this study, no correlation between flow amplitudes v_n and symmetry-planes Ψ_n has been implemented.
A ratio with factorised denominator (similar to the approach in [37]) is being compared with the AE-SPC for four different cases

1. Fixed flow amplitudes $v_1 = 0.05$ and $v_2 = 0.08$, else $v_n = 0$

2. Fluctuating but not correlated flow amplitudes $v_1 \in [0.05,0.08]$ (uniformly distributed) and $v_2 \in [0.05,0.08]$ (uniformly distributed) , else $v_n = 0$

3. Fluctuating and correlated flow amplitudes: $v_1 \in [0.03,0.06]$ (uniformly distributed) and $v_2 = v_1 + 0.03$, else $v_n = 0$

4. Fluctuating and anti-correlated flow amplitudes: $v_1 \in [0.03,0.06]$ (uniformly distributed) and $v_2 = 0.12 - v_1$, else $v_n = 0$.

The symmetry-planes Ψ_1 and Ψ_2 are correlated by

$$\Psi_2 = \Psi_1 + \frac{\pi}{12}\,. \tag{3.26}$$

Therefore, the theoretically expected value is

$$\langle \cos\left[4\left(\Psi_2 - \Psi_1\right)\right]\rangle_{theo} = \frac{1}{2}\,. \tag{3.27}$$

For each case and each approach $4.5 \cdot 10^6$ events have been sampled with 50000 "particles" per event. This unrealistically large amount of particles per event has been chosen to easily suppress statistical errors. The error has been obtained with error propagation under the neglect of any covariance terms (see G.1).
In Fig. 3.1 the statistical error bars are so small that the markers are covering them. A closer representation of the relevant data points can be seen in Fig. 3.2. It becomes obvious that in the case of correlated flow amplitudes the approach with a factorised denominator leads to a biased result. A non-factorised denominator as used in the proposed AE-SPC leads to results which are in good agreement with the theoretical input value. It is therefore, that any approaches using factorised denominators (as proposed in [37]) have to be rejected since correlated flow fluctuations are unavoidable in reality.

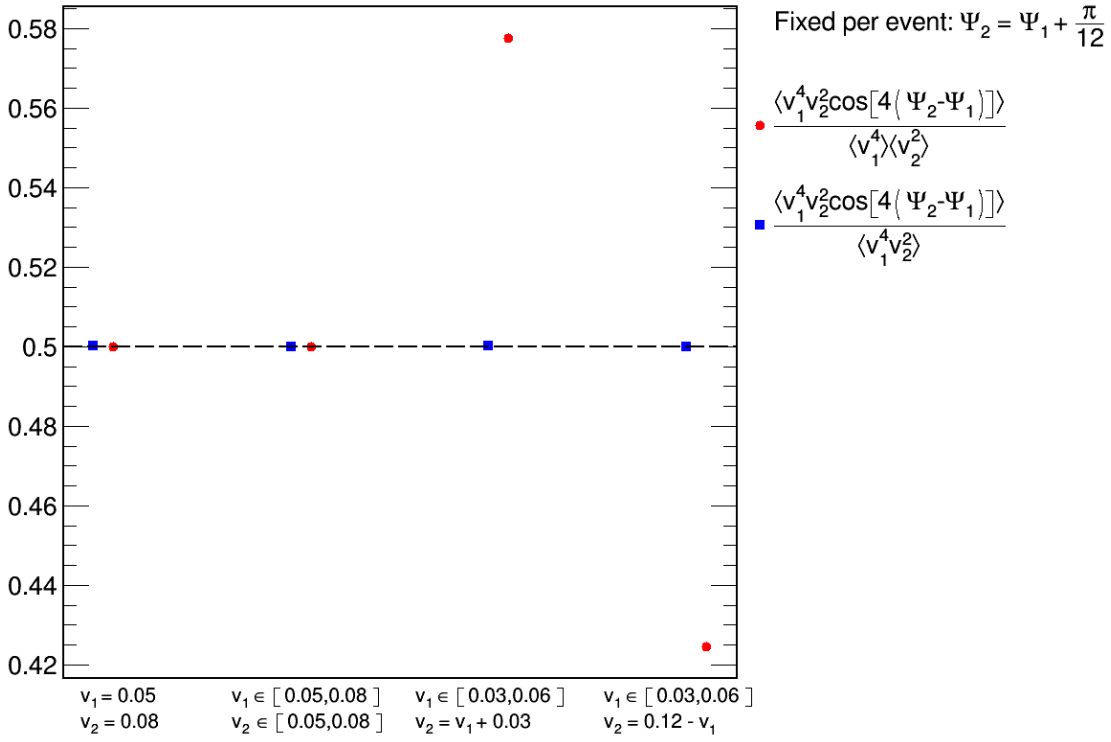

Figure 3.1: Study of the AE-approach for constant, uncorrelated, correlated and anti-correlated flow amplitudes. Comparison made to an approach with factorised flow amplitudes in the denominator. The dashed line indicates the theoretical expected value $\langle \cos[4(\Psi_2 - \Psi_1)]\rangle_{theo} = \frac{1}{2}$.

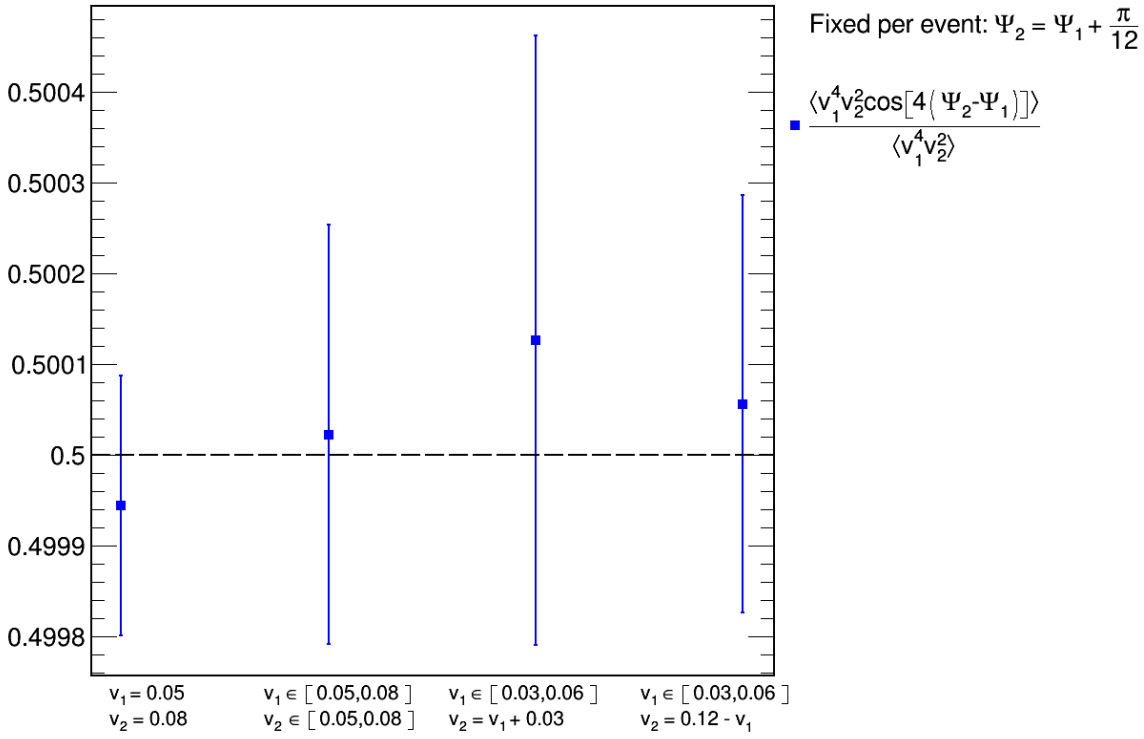

Figure 3.2: Zoom on case-study for constant, uncorrelated, correlated and anti-correlated flow amplitudes. The dashed line indicates the theoretical expected value $\langle \cos[4(\Psi_2 - \Psi_1)]\rangle_{theo} = \frac{1}{2}$.

3.3.2 TMC: Multiplicity Study

The second type of Toy Monte Carlo study looks at the behaviour of the AE-SPC with different amounts of particles per event. The following input values of the Fourier series have been used: Fluctuating and correlated flow amplitudes: $v_1 \in [0.03,0.06]$ (uniformly distributed) and $v_2 = v_1 + 0.03$, else $v_n = 0$.
The symmetry planes Ψ_1 and Ψ_2 are correlated by

$$\Psi_2 = \Psi_1 + \frac{\pi}{12} \tag{3.28}$$

and the theoretically expected value is

$$\langle \cos\left[4\left(\Psi_2 - \Psi_1\right)\right]\rangle_{theo} = \frac{1}{2}\,. \tag{3.29}$$

The study has been carried out for multiplicities 250 to 50000, each with $4.5 \cdot 10^6$ events. The result is shown in Fig. 3.3, a zoomed version for high multiplicities in Fig. 3.4. The statistical error has been obtained by error propagation under the neglect of any covariance terms (see G.1).
Again, biased results of the approach with the factorised denominator can be observed. The AE-SPC (non-factorised denominator) is in good agreement with the theoretical expected value. It has to be stressed that this is also true for multiplicities up to 5000 which represent the multiplicity range of heavy ion collisions at LHC energies.

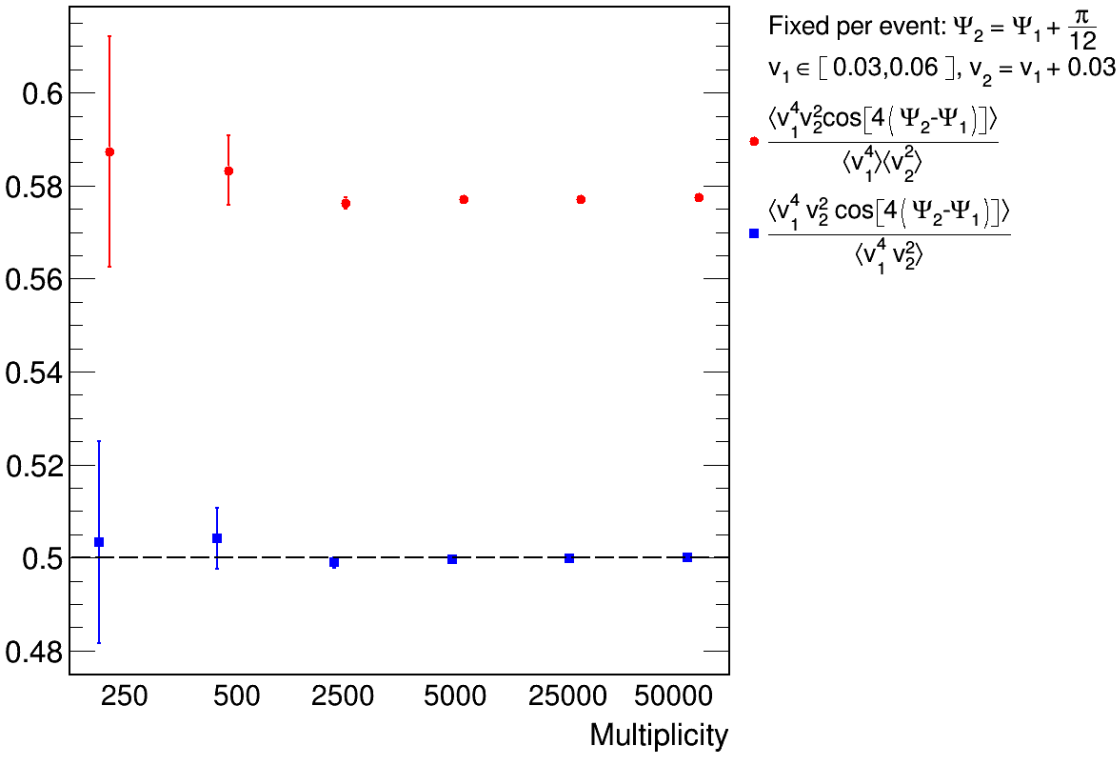

Figure 3.3: Multiplicity study for the AE-SPC in case of correlation $v_2 = v_1 + 0.03$. The dashed line indicates the theoretical expected value $\langle \cos\left[4\left(\Psi_2 - \Psi_1\right)\right]\rangle_{theo} = \frac{1}{2}$.

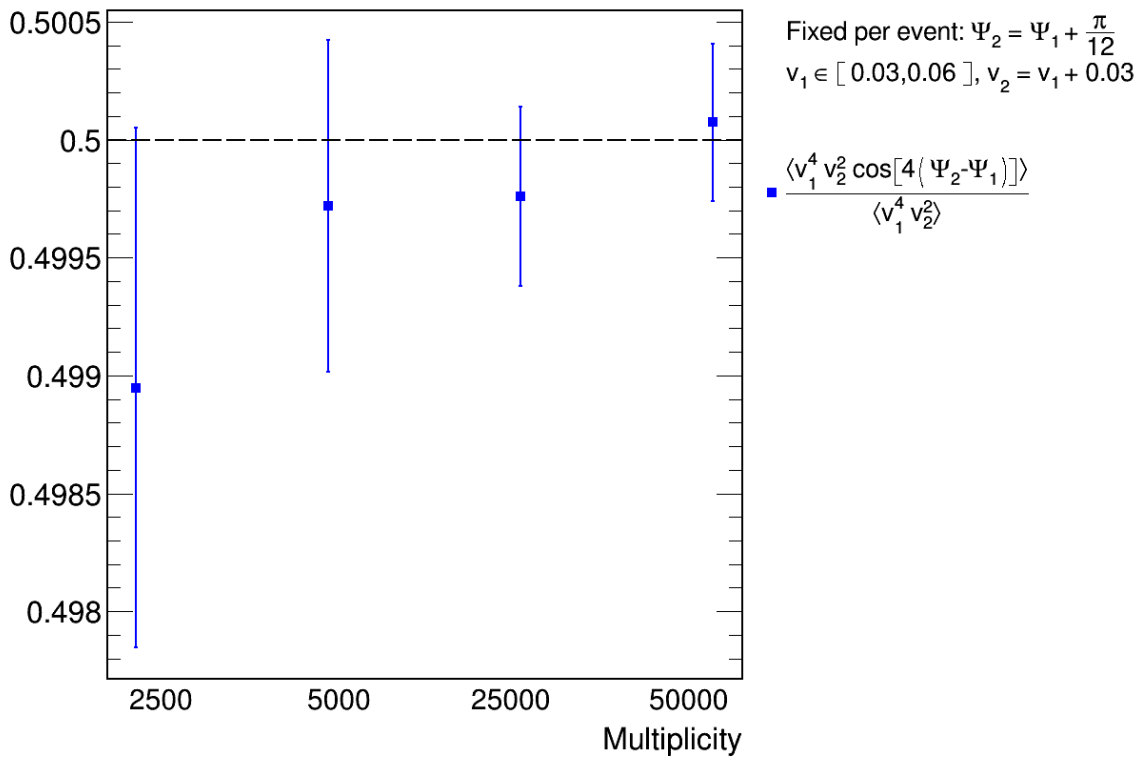

Figure 3.4: Zoom in multiplicity study for the AE-SPC in case of correlation $v_2 = v_1 + 0.03$. The dashed line indicates the theoretical expected value $\langle \cos[4(\Psi_2 - \Psi_1)]\rangle_{theo} = \frac{1}{2}$.

3.3.3 TMC: Signature of Correlations

To study the signature of a SPC in the context of the AE-approach, a TMC with the following input values of the Fourier series has been set up: Fluctuating and correlated flow amplitudes $v_1 \in [0.03,0.06]$ (uniformly distributed) and $v_2 = v_1 + 0.03$, else $v_n = 0$. The correlations between the symmetry-planes Ψ_1 and Ψ_2 differ between the following five cases

1. Fixed symmetry-planes: $\Psi_1 = 0$ and $\Psi_2 = \frac{\pi}{12}$
2. Fluctuating, but equal symmetry-planes: $\Psi_1 \in [0, 2\pi]$ (uniformly distributed) and $\Psi_2 = \Psi_1$
3. Fluctuating and uncorrelated symmetry-planes: $\Psi_1 \in [0, 2\pi]$ (uniformly distributed) and $\Psi_2 \in [0, \pi]$ (uniformly distributed)
4. Fluctuating and correlated symmetry-planes: $\Psi_1 \in [0, 2\pi]$ (uniformly distributed) and $\Psi_2 = \Psi_1 + \frac{\pi}{12}$
5. Fluctuating and anti-correlated symmetry-planes: $\Psi_1 \in [0,2\pi]$ (uniformly distributed) and $\Psi_2 = \Psi_1 - \frac{\pi}{12}$.

For each set-up $4.5 \cdot 10^6$ events have been sampled with 50000 "particles" per event. This unrealistically large amount of particles per event has been chosen to easily suppress statistical error. The error has been obtained with error propagation under neglect of any covariance terms (see G.1).

The results of this study can be seen in Fig. 3.5, a zoomed version of the most upper

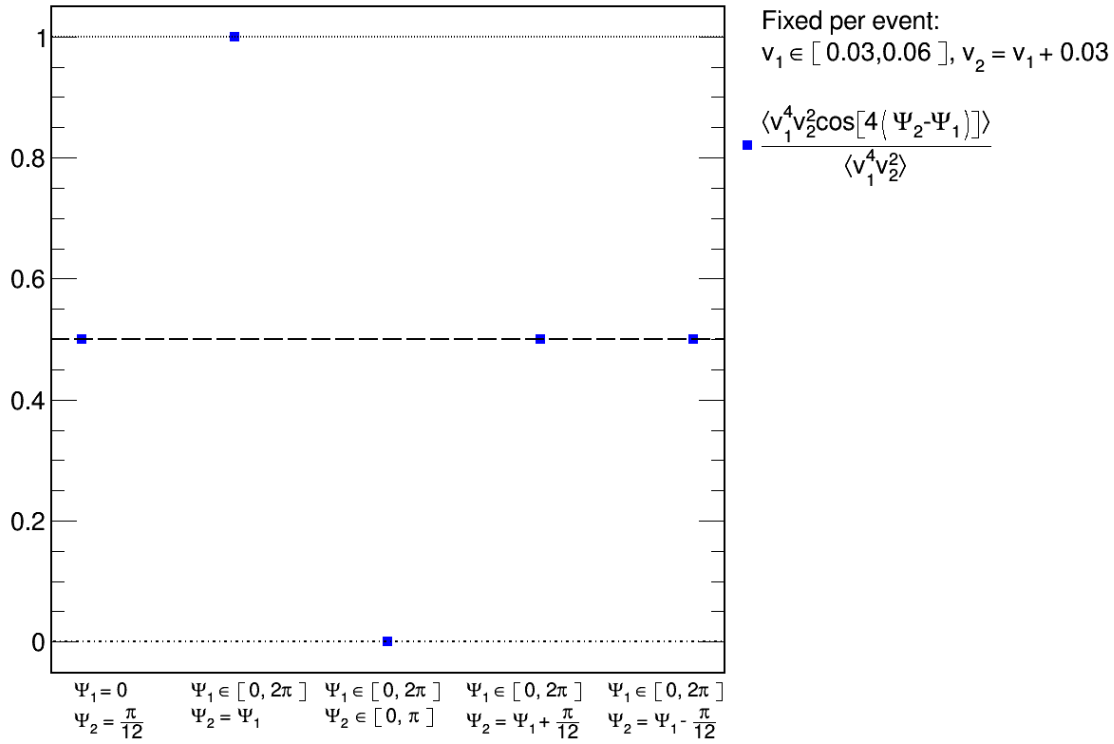

Figure 3.5: Signature study for the AE-SPC in case of correlation $v_2 = v_1 + 0.03$.

and most lower point in Fig. 3.6 and Fig. 3.7. A zoomed version in the cases of fixed symmetry-planes and correlated/anti-correlated symmetry-planes is not presented, their results are still consistent with their theoretical expected value of 0.5, as it has been in the previous studies which covered these cases. As one can see, in case of uncorrelated symmetry-planes, the AE-approach will lead to 0. This result stems from the fact, that in absence of correlation between the symmetry-planes, the cosine will fluctuate uniformly between -1 and 1, therefore its average will lead to 0. This study, especially the case of uncorrelated symmetry-planes, raises the following question: How can one distinguish uncorrelated symmetry-planes (leading to 0 in the AE-approach) and symmetry-planes with such a correlation, that the AE-approach will also lead to 0?

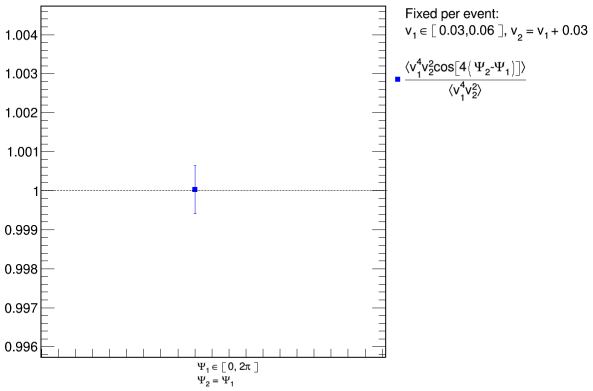

Figure 3.6: Zoom on upper line of the signature study, case $\Psi_2 = \Psi_1$.

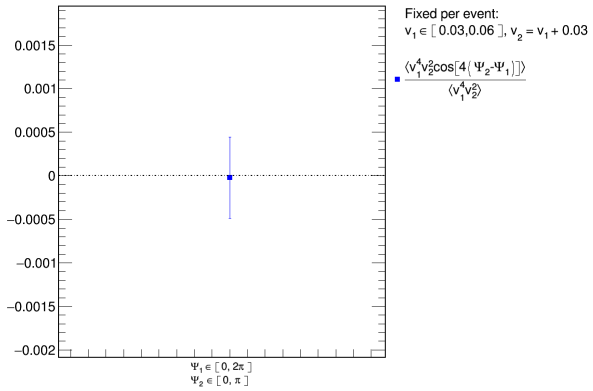

Figure 3.7: Zoom on lower line of the signature study, case Ψ_2 and Ψ_1 are uncorrelated.

Such a differentiation can be made by a parallel measurement of the SPC built from the sine. In case of uncorrelated symmetry-planes, also the sine will fluctuate uniformly between -1 and 1, leading again in its average of the AE-approach to 0. However, in cases that the symmetry-planes are correlated and the cosine term will lead to 0 in the AE-approach, the sine term should lead to a 1 in the AE-approach.
To demonstrate this, a TMC with the following input values of the Fourier series has been set up: Fluctuating and correlated flow amplitudes $v_1 \in [0.03,0.06]$ (uniformly distributed) and $v_2 = v_1 + 0.03$, else $v_n = 0$.
Two cases for the correlations between the symmetry-planes Ψ_1 and Ψ_2 have been chosen

1. Fluctuating and uncorrelated symmetry-planes: $\Psi_1 \in [0,\, 2\pi]$ (uniformly distributed) and $\Psi_2 \in [0,\, \pi]$

2. Fluctuating and correlated symmetry-planes: $\Psi_1 \in [0,\, 2\pi]$ (uniformly distributed) and $\Psi_2 = \Psi_1 + \frac{\pi}{8}$.

For both cases, the AE-SPC consisting of the cosine term and of the sine term have been measured separately. Per case, in total $4.5 \cdot 10^6$ events have been sampled with 50000 "particles" per event. Again the error has been obtained by error propagation under the neglect of any covariance terms (see G.1).
The results can be seen in Fig. 3.8 , zoomed versions in Fig. 3.9 and Fig. 3.10. This study proves that in absence of any correlation between the symmetry-planes, the SPC built from cosine terms and sine terms will lead to 0, in case of a correlation their results in the AE-approach will differ. It has to be noted that this interpretation of the signature of SPC by differing between the SPC built from cosine terms and sine terms can be in principle extended to other approaches (e.g. EbE, Expansion). It is therefore, that hereby a new observable

$$DOC\left[2 \cdot LCM(m,n)\left(\Psi_m - \Psi_n\right)\right] \tag{3.30}$$

$$:= \sqrt{\left\langle \cos\left[2 \cdot LCM(m,n)\left(\Psi_m - \Psi_n\right)\right]\right\rangle^2 + \left\langle \sin\left[2 \cdot LCM(m,n)\left(\Psi_m - \Psi_n\right)\right]\right\rangle^2}, \tag{3.31}$$

called "Degree of correlation between Ψ_m and Ψ_n", is being introduced. This observable should lead to 0 if the symmetry-planes are not correlated because in this case, the SPC for both the cosine and the sine will lead to 0 (as demonstrated before). In

case of a "perfect correlation" (i.e. a correlation that is constant for all events), the $DOC\left[2 \cdot LCM(m,n)\left(\Psi_m - \Psi_n\right)\right]$ should lead to a 1. Therefore, this new observable should indicate "how strong" the symmetry-planes are correlated.

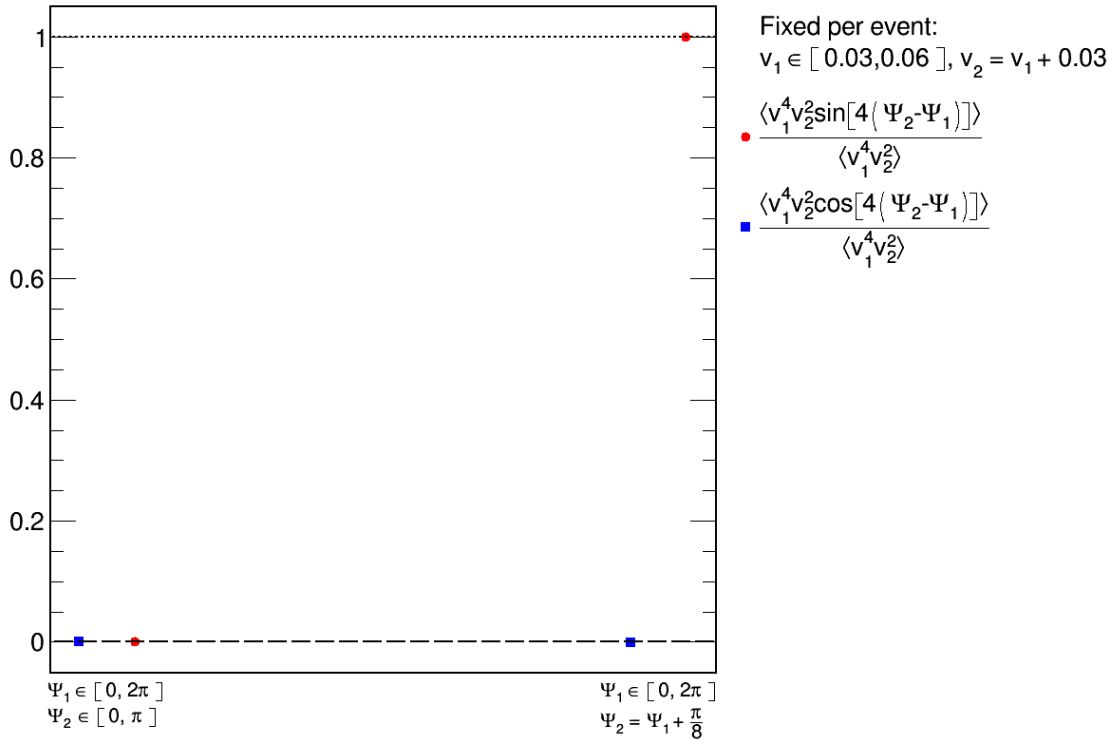

Figure 3.8: Comparison of the signature of the SPC obtained by cosine and by sine terms for uncorrelated and correlated symmetry-planes.

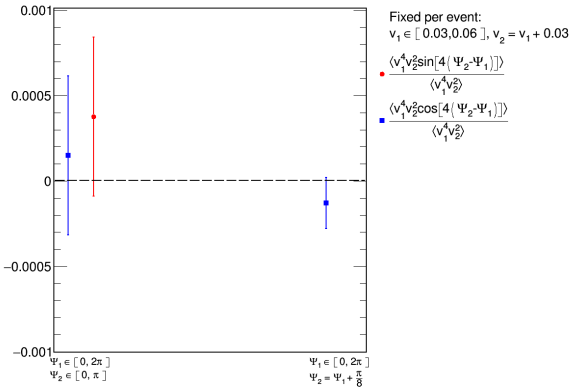

Figure 3.9: Zoom on Fig. 3.8, lower line.

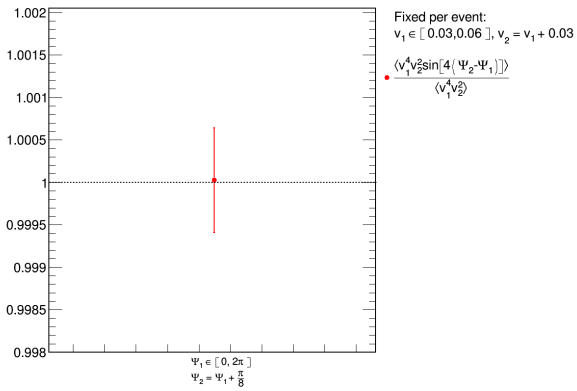

Figure 3.10: Zoom on Fig. 3.8, upper line.

3.3.4 Correlations between Eccentricities ϵ_n and Symmetry-Planes in the Initial State Φ_n

A key question is whether there is a correlation between flow amplitudes v_n and symmetry-planes Ψ_n. Such correlation has to be taken into account - especially as this would lead to biased results in the AE-SPC approach. Since these kind of correlations cannot be studied directly, correlations between eccentricities ϵ_n and symmetry-planes in the initial state Φ_n have been examined as they can be used as an indicator for similar correlations between v_n and Ψ_n. For this three MC-Glauber studies have been carried out, all with the following set-up: Pb-Pb collisions at $\sqrt{s_{NN}} = 2.76$ TeV, minimal distance between the nucleons, Gaussian nucleon-nucleon overlap function and Gaussian smearing. For each study, in total 50000 events have been carried out, however events with no interaction have not been taken into account which leads to a smaller number of events for very peripheral collisions.
The first study shows correlation plots between ϵ_2 and Φ_2 for selected impact parameters b (Fig. 3.11).

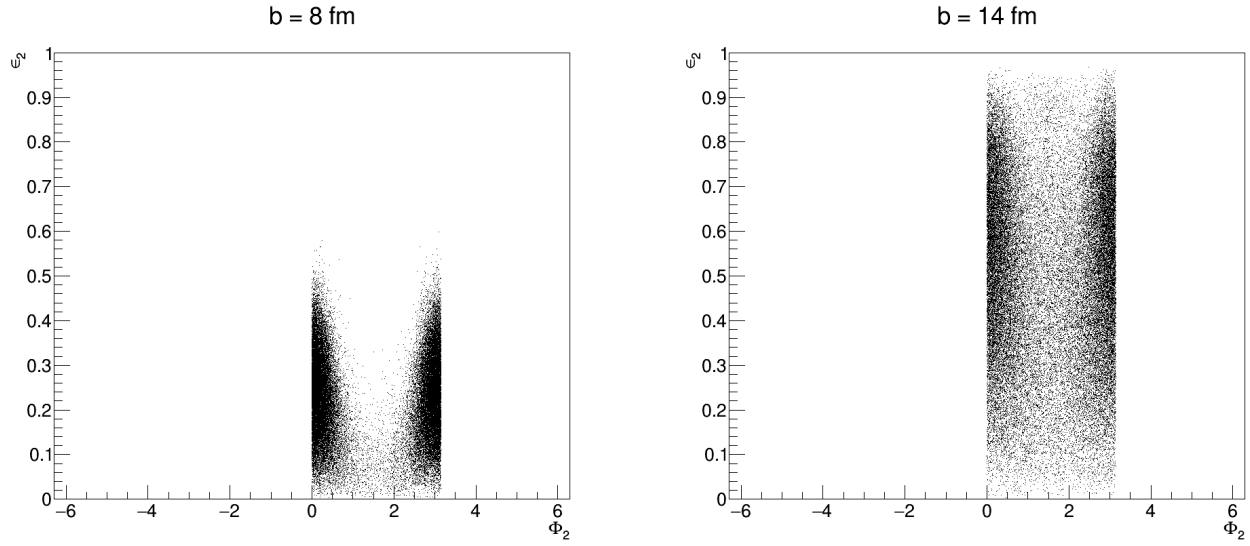

Figure 3.11: Correlation plots between ϵ_2 and Φ_2 for impact parameters $b = 8\,\text{fm}$ and $b = 14\,\text{fm}$.

More plots of this study are presented in Appendix D, Fig. D.1. Figure 3.11 shows that for rising impact parameter b, non trivial structures appear in the correlation plot. Such a result would indicate a correlation between ϵ_2 and Φ_2. This result however is not correct as it is an artefact of the fixed frame of the MC-Glauber implementation.

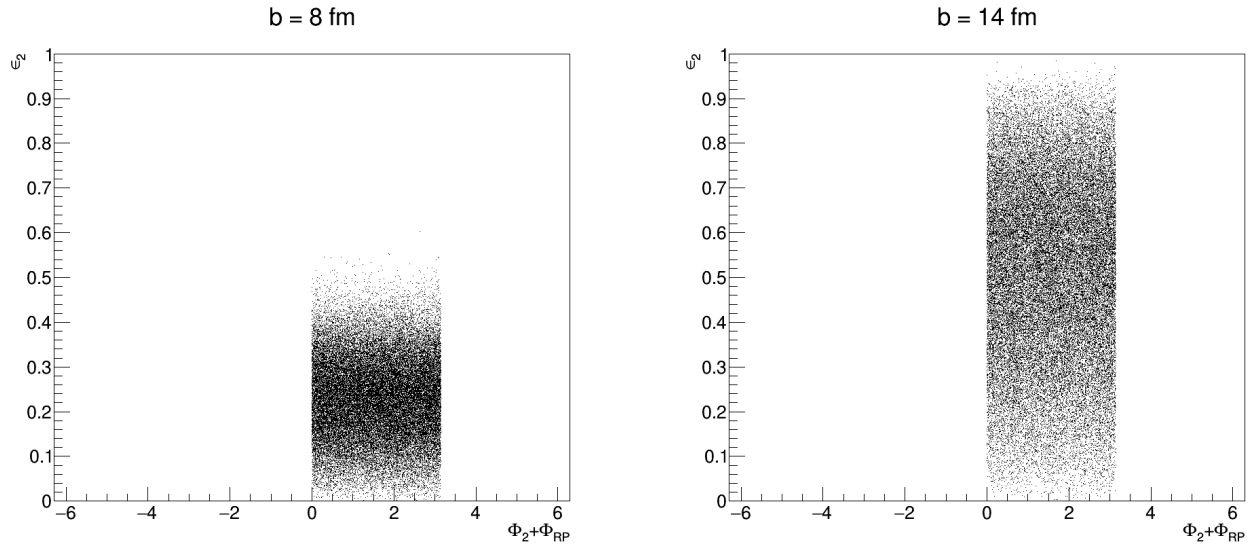

Figure 3.12: Correlation plots between ϵ_2 and $\Phi_2 + \Phi_{RP}$ for impact parameters $b = 8\,\text{fm}$ and $b = 14\,\text{fm}$.

In real heavy ion collisions, a random reaction plane Ψ_{RP} occurs each event which shifts all symmetry-planes of a fixed frame to $\tilde{\Psi}_n = \Psi_n + \Psi_{RP}$. This random shift should remove any correlation between phases and amplitudes. To demonstrate this, a second MC-Glauber study has been set up. In each event, a random $\Phi_{RP} \in [0, \pi)$ has been generated to simulate the reaction plane. After this the measured symmetry-plane in the initial state Φ_n has been shifted to $\tilde{\Phi}_n = \Phi_n + \Phi_{RP}$ and brought back to the interval $\tilde{\Phi}_n \in [0, \pi)$. Figure 3.12 shows the correlation plot between ϵ_2 and $\Phi_n + \Phi_{RP}$ for some selected impact parameters b. More plots of this study can be found in Appendix D, Fig. D.2. It is shown that there is no correlation between ϵ_2 and $\Phi_n + \Phi_{RP}$.

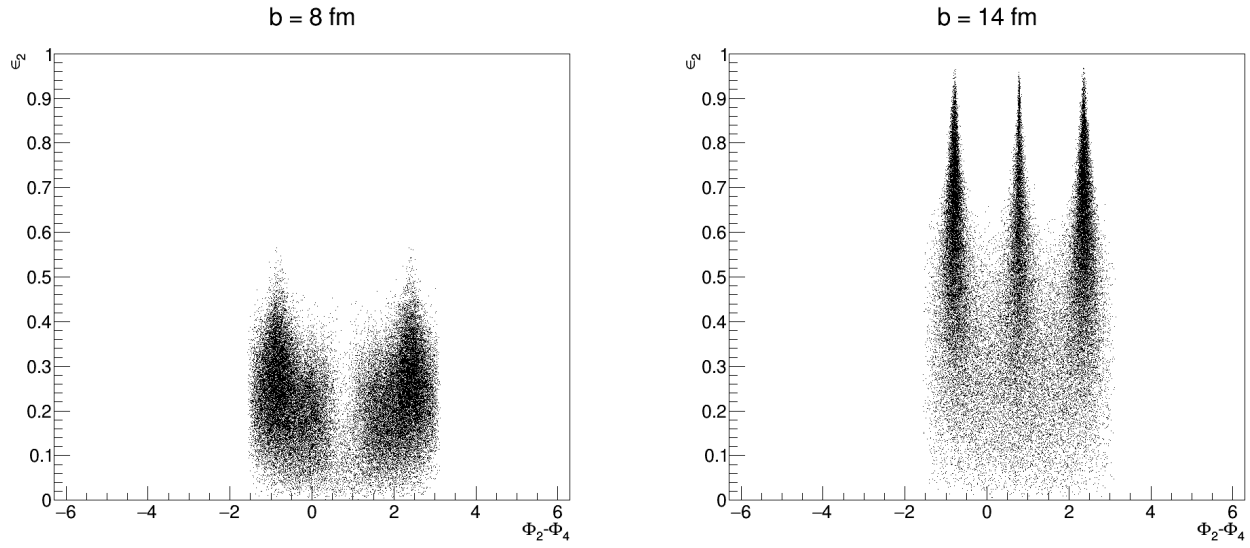

Figure 3.13: Correlation plots between ϵ_2 and $\Phi_2 - \Phi_4$ for impact parameters $b = 8\,\text{fm}$ and $b = 14\,\text{fm}$.

However, this argument of shifted symmetry-planes does not hold true if one looks at any sum of symmetry-planes with isotropic correlators (for example the difference of

two symmetry-planes). For such sums the added reaction planes cancel themselves. In the third MC-Glauber study of this kind, the correlation plot between $\Phi_2 - \Phi_4$ and ϵ_2 is shown in Fig. 3.13 . It is shown that for rising impact parameter b, non trivial structures appear which indicate a non-trivial correlation between ϵ_2 and $\Phi_2 - \Phi_4$. More plots of this study are presented in Appendix D Fig. D.3. The distance between the peaks for high impact parameter b (e.g. Fig. 3.13, right) can be calculated as every symmetry-planes Φ_n has a underlying periodicity of

$$\Phi_n = \Phi_n + \frac{2\pi}{n} \,. \tag{3.32}$$

Therefore, the distance of the peaks in Fig. 3.13 (right) can be computed as

$$\Phi_2 - \Phi_4 = \left(\Phi_2 + \frac{2\pi}{2}\right) - \left(\Phi_4 + \frac{2\pi}{4}\right) = \Phi_2 - \Phi_4 + \underbrace{\frac{\pi}{2}}_{\text{peak distance}} \,. \tag{3.33}$$

Further properties of the structures in Fig. 3.13 (right) still have to be studied in more detail.
These results clearly show that there is a possible correlation between v_n and $\Psi_n - \Psi_m$. Therefore, the factorisation as it is performed in the AE-SPC will lead to a biased result. As a consequence, the AE-SPC approach is rejected as a candidate for a complete bias-free SPC observable, even though this approach can correct for the bias caused by correlations among the flow amplitudes themselves. It has to be mentioned that the approach of building SPC with a factorised denominator [37] is not solely biased through the correlated flow amplitudes themselves, but additionally through this correlation between flow amplitudes and the (difference of) symmetry-planes.

3.4 Event-by-Event SPC

The AE-SPC approach is only feasible if (and only if) flow amplitudes v_n and symmetry-planes Ψ_n are not correlated. Otherwise, the result will be biased. However, as it is shown in Sec. 3.3.4, such an assumption of no correlation cannot be made (at least based on the Monte Carlo-Glauber model). To overcome this, the Event-by-Event SPC (EbE-SPC) approach has been developed.

The EbE-SPC approach is the computation of the ratio between the correlators per event where each event has a unit weight in absence of multiplicity fluctuations. In the real data analysis, multiplicity weights have to be used. The EbE-SPC is therefore given as

$$\begin{aligned} &\frac{\left\langle \cos\left(\sum_{j=1}^{a_m} m\cdot\varphi_j - \sum_{k=1}^{a_n} n\cdot\varphi_{a_m+k}\right)\right\rangle}{\left\langle \cos\left(\sum_{j=1}^{a_m}(-1)^j\cdot m\cdot\varphi_j + \sum_{k=1}^{a_n}(-1)^k\cdot n\cdot\varphi_{a_m+k}\right)\right\rangle} \\ &= \frac{\left(\prod_{i=1}^{a_m} v_m\right)\left(\prod_{j=1}^{a_n} v_n\right)\cos\left(\sum_{j=1}^{a_m} m\cdot\Psi_m - \sum_{k=1}^{a_n} n\cdot\Psi_n\right)}{\left(\prod_{i=1}^{a_m} v_m\right)\left(\prod_{j=1}^{a_n} v_n\right)\cos\left(\sum_{j=1}^{a_m}(-1)^j\cdot m\cdot\Psi_m + \sum_{k=1}^{a_n}(-1)^k\cdot n\cdot\Psi_n\right)} \\ &= \cos\left[2\cdot LCM(m,n)\cdot(\Psi_m - \Psi_n)\right] \,. \end{aligned} \tag{3.34}$$

To study the behaviour of this approach in the context of the analysis framework, a Toy Monte Carlo study has been set up with the following input values of the Fourier series Eq. (1.5): Fluctuating and correlated flow amplitudes $v_1 \in [0.03,0.06]$ (uniformly distributed) and $v_2 = v_1 + 0.03$, else $v_n = 0$.
The study has been carried out for multiplicities 250 to 50000, each with $4.5 \cdot 10^6$ events. The result is shown in Fig. 3.14 and zoomed in for higher multiplicities in Fig. 3.15.

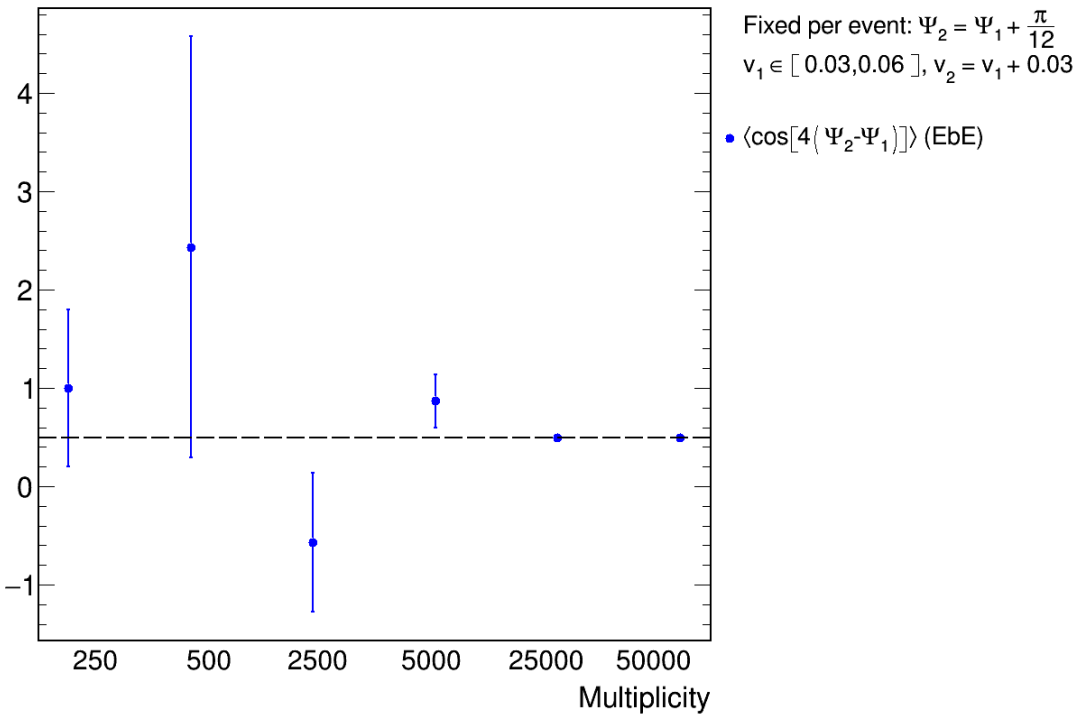

Figure 3.14: Multiplicity study for the EbE-SPC in case of correlation $v_2 = v_1 + 0.03$. The dashed line indicates the theoretical expected value $\langle \cos[4(\Psi_2 - \Psi_1)] \rangle_{theo} = \frac{1}{2}$.

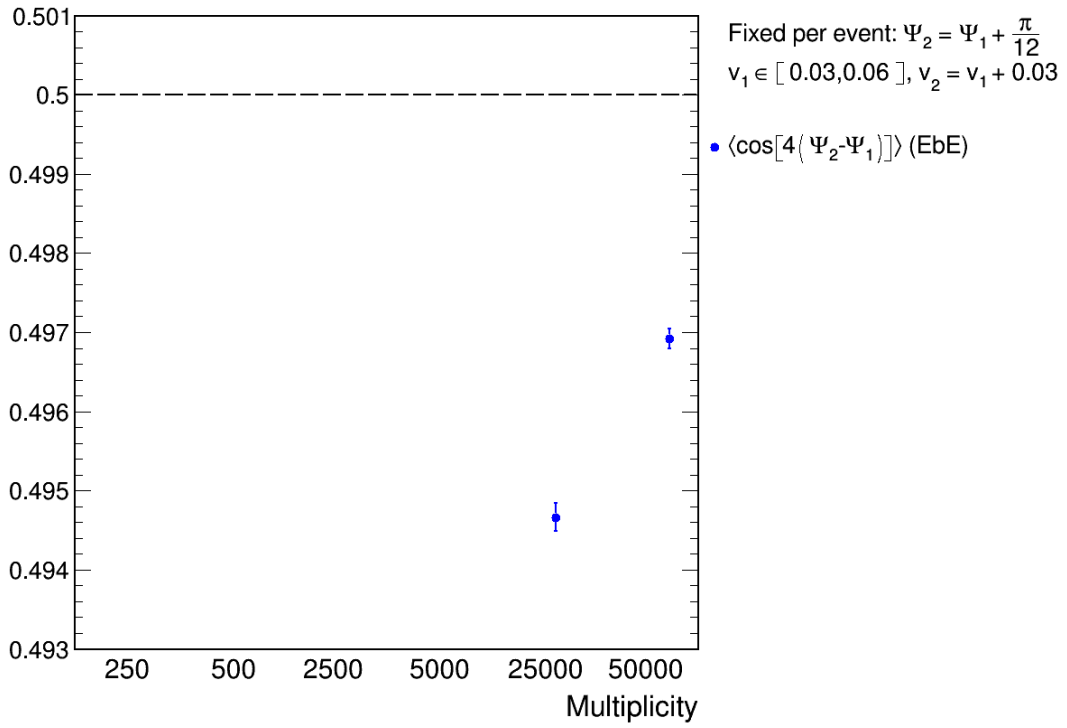

Figure 3.15: Zoom on the multiplicity study for the EbE-SPC in case of correlation $v_2 = v_1 + 0.03$. The dashed line indicates the theoretical expected value $\langle \cos[4(\Psi_2 - \Psi_1)] \rangle_{theo} = \frac{1}{2}$.

This result shows a huge statistical error for multiplicities up to 5000, even for a relatively large number of events. This statistical instability can be explained by "outlier events" which have an unusually small denominator. This leads to an abnormally large value in the ratio of this event which biases the whole average. It is therefore necessary to get rid of the "outliers". Regarding the unrealistically large multiplicities (i.e. 25000 and 50000), the results do not align with the expected value of 0.5, even though the error bars are small.
This statistically instability and the offset, which both are believed to be caused by the outlier events, lead to the result that a direct use of the EbE-approach is not feasible at the moment and more work has to be done in this direction. However, it again has to be stressed that this approach holds the potential to measure SPC without any bias caused by correlations between flow amplitudes v_n themselves and by correlations between flow amplitudes and the (difference) of symmetry-planes.

3.5 Expansion-Approach

As presented above, the AE-Approach is rejected due to possible correlation between the flow amplitudes and $\cos[2 \cdot LCM(m,n) \cdot (\Psi_m - \Psi_n)]$. The EbE-Approach, which would not be biased by such a correlation, is statistically not stable. It is therefore that in this section the "Expansion-Approach" is being presented. The main idea of this approach is the approximation of the unbiased EbE-Approach so that this approximation itself is only linked to statistically stable observables.

Consider two observables X and Y with mean $\mathrm{E}(X)$, $\mathrm{E}(Y)$. As shown in Appendix E, the second order expansion of the mean of the ration distribution $\frac{X}{Y}$ can be derived as

$$\mathrm{E}\left(\frac{X}{Y}\right) \approx \frac{\mathrm{E}(X)}{\mathrm{E}(Y)} \cdot \left(1 + \frac{\mathrm{E}(Y^2)}{\mathrm{E}(Y)^2}\right) - \frac{\mathrm{E}(XY)}{\mathrm{E}(Y)^2}\,. \tag{3.35}$$

In Eq. (3.35) it assumed that $\mathrm{E}(Y) \neq 0$, $\mathrm{E}(XY)$ is the mean of the product of X and Y. The third order expansion (derivation see Appendix E) reads

$$\mathrm{E}\left(\frac{X}{Y}\right) \approx \frac{\mathrm{E}(X)}{\mathrm{E}(Y)}\left[1 + 3\frac{\mathrm{E}(Y^2)}{\mathrm{E}(Y)^2} - \frac{\mathrm{E}(Y^3)}{\mathrm{E}(Y)^3}\right] - 3\frac{\mathrm{E}(XY)}{\mathrm{E}(Y)^2} + \frac{\mathrm{E}(XY^2)}{\mathrm{E}(Y)^3}\,. \tag{3.36}$$

For both cases (second and third order expansion), the first order error propagation is applied

$$\mathrm{Var}\left(\frac{X}{Y}\right) = \frac{\mathrm{E}(X)^2}{\mathrm{E}(Y)^2} \cdot \left(\frac{\mathrm{Var}(X)}{\mathrm{E}(X)^2} + \frac{\mathrm{Var}(Y)}{\mathrm{E}(Y)^2} - 2\frac{\mathrm{Cov}(X,Y)}{\mathrm{E}(X)\,\mathrm{E}(Y)}\right) \tag{3.37}$$

where $\mathrm{Cov}(X,Y)$ is the covariance of X and Y, $\mathrm{Var}(X)$ the variance of X and $\mathrm{Var}(Y)$ the variance of Y (as shown in [39]).

Considering the SPC in flow analyses, the variables X and Y will be chosen as

$$\begin{aligned}
X &= \left\langle \cos\left(\sum_{j=1}^{a_m} m\cdot\varphi_j - \sum_{k=1}^{a_n} n\cdot\varphi_{a_m+k}\right)\right\rangle \\
&\equiv \left(\prod_{i=1}^{a_m} v_m\right)\left(\prod_{j=1}^{a_n} v_n\right)\cos\left(\sum_{j=1}^{a_m} m\cdot\Psi_m - \sum_{k=1}^{a_n} n\cdot\Psi_n\right) \\
Y &= \left\langle \cos\left(\sum_{j=1}^{a_m}(-1)^j\cdot m\cdot\varphi_j + \sum_{k=1}^{a_n}(-1)^k\cdot n\cdot\varphi_{a_m+k}\right)\right\rangle \\
&\equiv \left(\prod_{i=1}^{a_m} v_m\right)\left(\prod_{j=1}^{a_n} v_n\right)\cos\left(\sum_{j=1}^{a_m}(-1)^j\cdot m\cdot\Psi_m + \sum_{k=1}^{a_n}(-1)^k\cdot n\cdot\Psi_n\right)
\end{aligned} \tag{3.38}$$

with

$$a_m = 2\,\frac{LCM(m,n)}{m} \tag{3.39}$$

and

$$a_n = 2\,\frac{LCM(m,n)}{n}\,. \tag{3.40}$$

Properties of this approach have to be investigated further.

3.6 Tan-Approach

As stated in [38], SPC can be extracted from a k-particle correlation by taking advantage of fundamental properties of complex numbers, i.e.

$$n_1\Psi_1 + ... + n_k\Psi_k \tag{3.41}$$
$$= \arg\left[\left\langle e^{-i(n_1\varphi_1+...+n_k\varphi_k)}\right\rangle\right] \tag{3.42}$$
$$= \mathrm{atan2}\left(\Im\left\langle e^{-i(n_1\varphi_1+...+n_k\varphi_k)}\right\rangle, \Re\left\langle e^{-i(n_1\varphi_1+...+n_k\varphi_k)}\right\rangle\right) \tag{3.43}$$

In this approach, only one set of correlators $\{n_1, n_2, ..., n_k\}$ has to be used, which has to fulfil

$$\sum_{j=1}^{k} n_j = 0 \tag{3.44}$$

and

$$\sum_{j=1}^{k} n_j \cdot \Psi_{n_j} \neq 0\,. \tag{3.45}$$

Though, as also stated in [38], the phase is limited to $[0, 2\pi)$, thus unfolding problems arise.
This can be improved by introducing the cosine to this approach

$$\cos\left(n_1\Psi_1 + ... + n_k\Psi_k\right) \tag{3.46}$$
$$= \cos\left(\arg\left[\left\langle e^{-i(n_1\varphi_1+...+n_k\varphi_k)}\right\rangle\right]\right) \tag{3.47}$$
$$= \cos\left(\operatorname{atan2}\left(\Im\left\langle e^{-i(n_1\varphi_1+...+n_k\varphi_k)}\right\rangle, \Re\left\langle e^{-i(n_1\varphi_1+...+n_k\varphi_k)}\right\rangle\right)\right) \tag{3.48}$$

as the 2π-periodicity of the cosine will overcome the limited phase. Further investigations of the approach still have to be done.

Chapter 4

First Look at Experimental SPC

4.1 Data Selection and Quality Assurance

The data used in this first look at experimental SPC have been recorded by ALICE at LHC. For this analysis, "Run 1" data of Pb-Pb collisions at $\sqrt{s_{NN}} = 2.76$ TeV (taken in 2010) have been used (a list of the used runs can be found in Appendix F.1). In this analysis, TPC and ITS have been used as the main detectors. The azimuthal angles provided by TPC have full azimuth coverage (Fig. 4.1), therefore no particle weights will be applied. Regarding event weights, the previously introduced (Sec. 1.5.1) multiplicity weights have been used to correct for fluctuating multiplicities between the events. The centrality of the given events has been estimated by SPD. Overall, minimum bias data have been used. The used tracks are hybrid tracks (filter 768).
As a global quality assurance, events that do not satisfy a z-Vertex of -10 cm $< z <$ 10 cm are rejected (Fig. 4.2). Furthermore, a cut to remove high multiplicity outliers (see Appendix F.2) has been applied.
The track selection of the kinematic variables (transverse momentum p_T and pseudorapidity η) was applied as follows: 0.2 GeV/c $< p_T <$ 5.0 GeV/c and $-0.8 < \eta < 0.8$. Distributions of p_T (Fig. 4.3), η (Fig. 4.4) and multiplicity (Fig. 4.5) after the track selection are presented below.

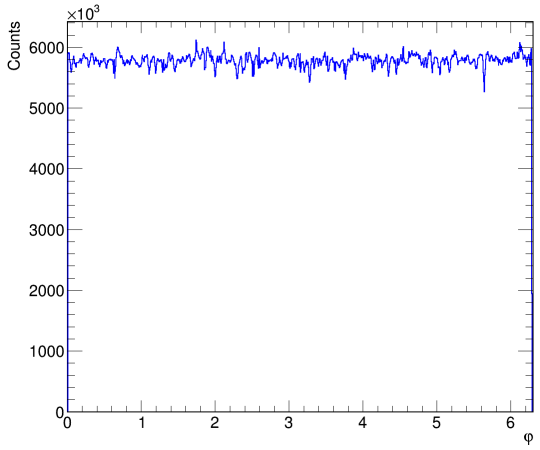

Figure 4.1: Distribution of azimuthal angle φ of all used runs after track selection.

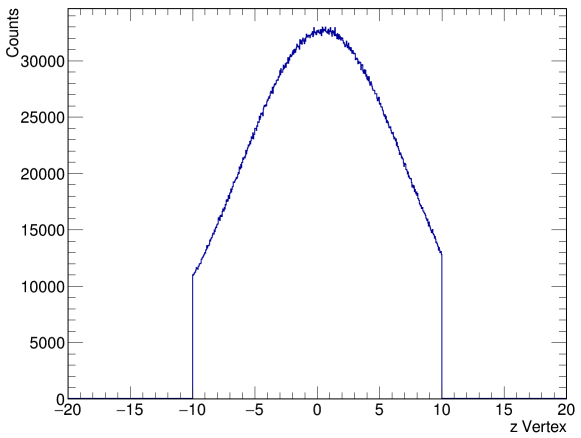

Figure 4.2: Distribution of z vertex of all used runs after z vertex cut.

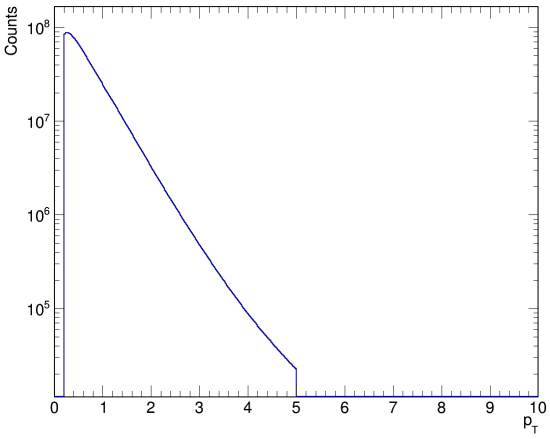

Figure 4.3: Distribution of transverse momentum p_T of all used runs after track selection.

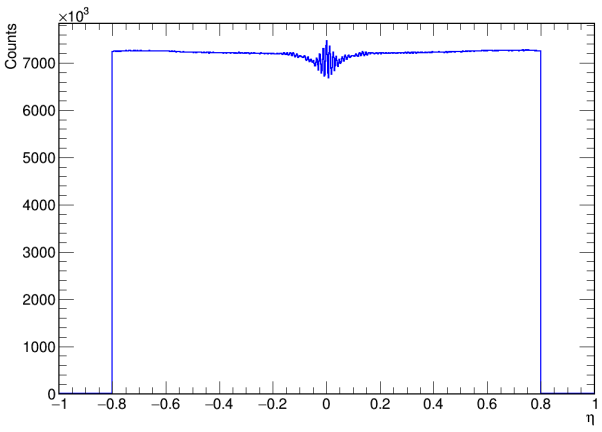

Figure 4.4: Distribution of pseudorapidity η of all used runs after track selection.

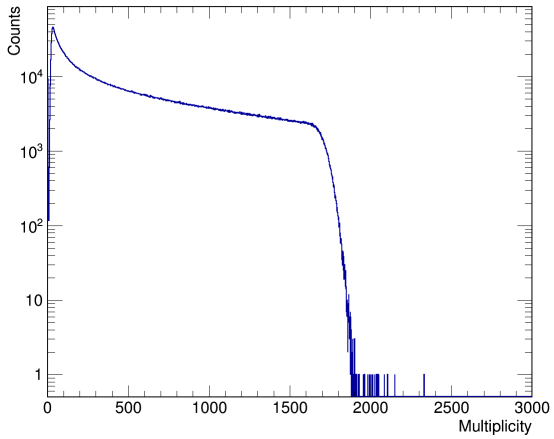

Figure 4.5: Multiplictiy distribution of all used runs after track selection. All centralities are presented.

4.2 Centrality-dependent SPC

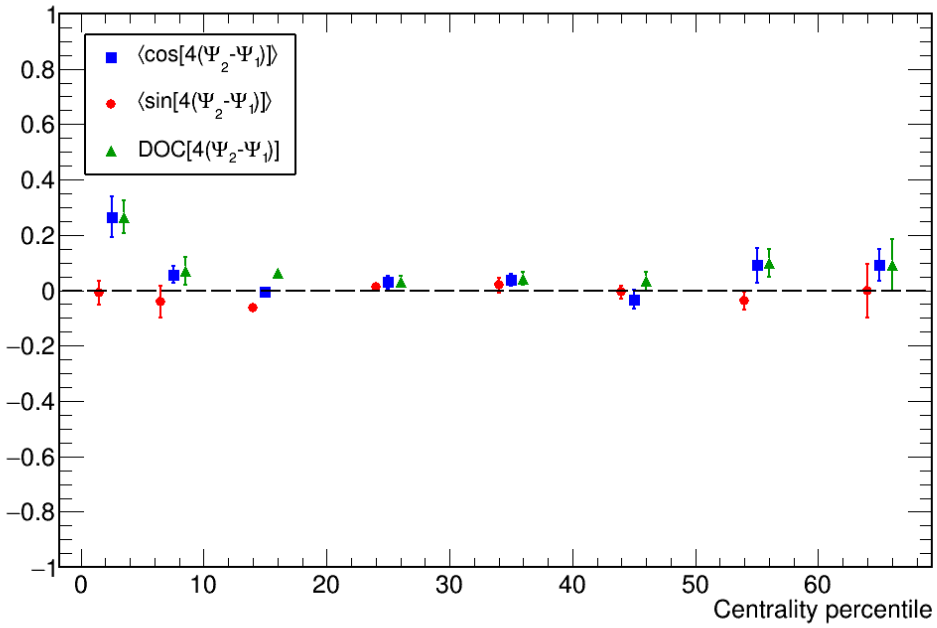

Figure 4.6: SPC for Ψ_2 and Ψ_1 for centrality 0 % to 70 %.

The results of the first look at experimental SPC are presented in this section. They have been obtained with the AE-approach, thus they represent SPC without any contributions of correlations between the flow amplitudes v_n. Though, a bias through correlations between flow amplitudes in the (difference) of symmetry-planes cannot be excluded. Only statistical errors, which were obtained by the "bootstrap-method" (see Appendix G.2), are presented. The EbE-approach and the Expansion-approach will not be presented due to problems with statistical instability.

Figure 4.6 shows the obtained SPC between Ψ_2 and Ψ_1. These results show that Ψ_2 and Ψ_1 are different. The $DOC\left[4\left(\Psi_2 - \Psi_1\right)\right]$ is consistent with 0 for centrality classes bigger 10 %. This hints to the possible observation, that Ψ_2 and Ψ_1 are not correlated for mid-central and peripheral collisions. For very central collisions, there might be an indication for a slight correlation, as here the DOC is not consistent with 0.

The SPC between Ψ_3 and Ψ_1 is presented in Fig. 4.7. The errors of the obtained results are very large within the presented centrality classes. Thus, more data have to be analysed to constraint more precise information about this correlation as this is not feasible with the current statistics.

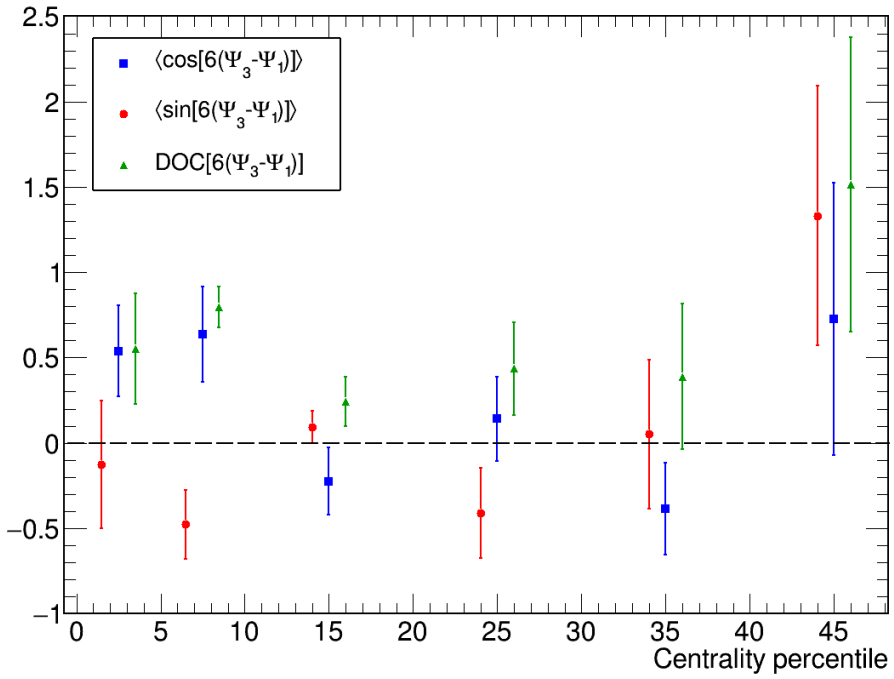

Figure 4.7: SPC for Ψ_3 and Ψ_1 for centrality 0 % to 50 %.

Figure 4.8 presents the SPC between Ψ_3 and Ψ_2. It can be observed that Ψ_3 and Ψ_2 differ and for centralities up to 30 % seem to be uncorrelated. For higher centralities this statement is less certain, more data have to be analysed to gain further constraints.

The SPC between Ψ_4 and Ψ_2 is shown in Fig. 4.9. The results show that Ψ_4 and Ψ_2 are not the same, further the results show that these symmetry-planes seem to be correlated (in mid-central collisions). The degree of correlation has a maximum for mid-central collisions (centrality $\approx$ 40 %), thus the symmetry-planes tend to be "more strongly" correlated in this regime. For very central and increasing peripheral collisions, Ψ_4 and Ψ_2 seem to be less correlated, in the extreme cases even uncorrelated.

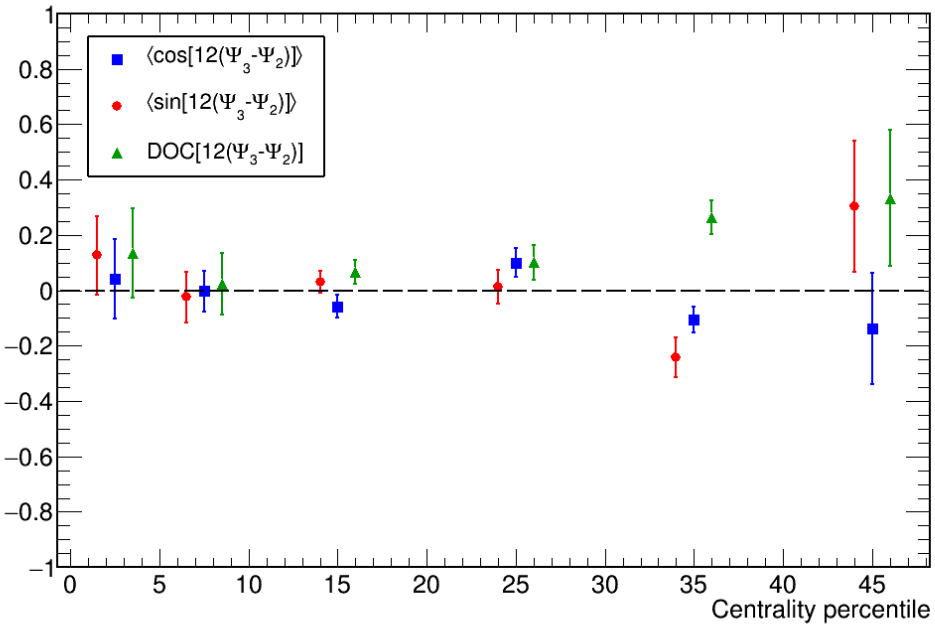

Figure 4.8: SPC for Ψ_3 and Ψ_2 for centrality 0 % to 50 %.

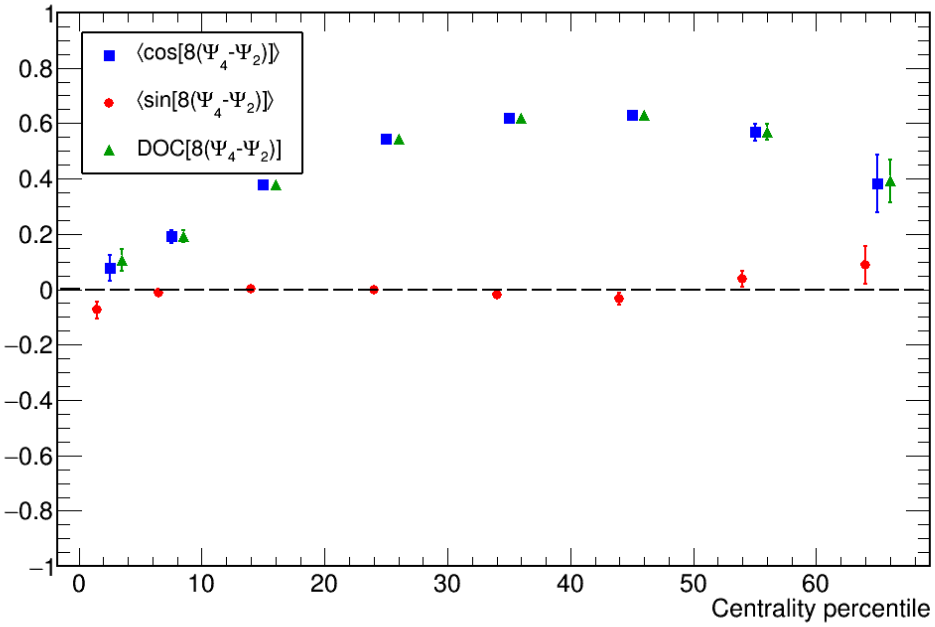

Figure 4.9: SPC for Ψ_4 and Ψ_2 for centrality 0 % to 70 %.

Chapter 5

Summary

In this thesis, new approaches for the measurement of symmetry-plane correlations (SPC), which correct for the bias originating from correlated flow amplitudes v_n, have been presented. Such bias is not negligible and it affects all currently available measurements of SPC. Study of quantities in the initial geometry of heavy ion collisions, obtained by the Monte Carlo-Glauber model, indicated a possible correlation between flow amplitudes and symmetry-planes. Therefore, various additional approaches have been introduced which hold the potential for a complete bias-free SPC by additionally removing bias through correlations between flow amplitudes and the (difference of) symmetry-planes. In future studies, properties of these completely bias-free approaches will be investigated to further improve measurements in the field of SPC.
Lastly, a first look at experimental analyses of different SPC built in terms of the AE-approach have been presented and shortly discussed. These results present the first measurement of SPC without any bias from correlations between flow amplitudes v_n. Further analyses and systematic checks will be done in this direction in the future.

Appendix A

Flow

A.1 Flow harmonic

One has to prove that

$$\langle \cos[n(\varphi - \psi_n)] \rangle = v_n \tag{A.1}$$

The mean value of a random observable x can be written as

$$\langle x \rangle = \int_0^{2\pi} x \cdot f(x)\, dx\,. \tag{A.2}$$

We define $z(n) \coloneqq \cos[n(\varphi - \psi_n)]$ and use a normalized version of Eq. (1.5)

$$f(z(n)) \coloneqq \frac{1}{2\pi}\left[1 + 2\sum_{n=1}^{\infty} v_n z(n)\right], \tag{A.3}$$

which leads to

$$\langle \cos[n(\varphi - \psi_n)] \rangle = \int_0^{2\pi} z(n) \cdot \frac{1}{2\pi}\left[1 + 2\sum_{n=1}^{\infty} v_n \cdot z(n)\right] d\varphi \tag{A.4}$$

$$\tag{A.5}$$

$$= \frac{1}{2\pi}\left[\underbrace{\int_0^{2\pi} z(n) d\varphi}_{=0} + 2\int_0^{2\pi} z(n) \sum_{n=1}^{\infty} v_n \cdot z(n)\; d\varphi\right]. \tag{A.6}$$

For the second integral one can write

$$\int_0^{2\pi} z(n) \sum_{n=1}^{\infty} v_n \cdot z(n)\; d\varphi \tag{A.7}$$

$$= \int_0^{2\pi} \sum_{n=1}^{\infty} v_n \cdot z(n) \cdot z(m)\; d\varphi \tag{A.8}$$

$$= \sum_{n=1}^{\infty} v_n \int_0^{2\pi} z(n) \cdot z(m)\; d\varphi\,. \tag{A.9}$$

The sum and the integral can be switched, as both of them have to converge (and we assume they converge). Flow amplitudes v_n can be taken out of the integral as they are

independent of φ. With the help of the orthogonality relations of trigonometric functions, one gets

$$\int_0^{2\pi} z(n) \cdot z(m)\ d\varphi \tag{A.10}$$

$$= \int_0^{2\pi} \cos[n(\varphi - \psi_n)] \cdot \cos[m(\varphi - \psi_m)]\ d\varphi \tag{A.11}$$

$$= \cos(n \cdot \psi_n - m \cdot \psi_m) \cdot \pi \cdot \delta_{mn}\,, \tag{A.12}$$

where δ_{mn} is the Kronecker delta symbol. Therefore,

$$\sum_{n=1}^{\infty} v_n \int_0^{2\pi} z(n) \cdot z(m)\ d\varphi \tag{A.13}$$

$$= \sum_{n=1}^{\infty} v_n\, cos(n \cdot \psi_n - m \cdot \psi_m) \cdot \pi \cdot \delta_{mn}\,. \tag{A.14}$$

By explicitly using the properties of the Kronecker delta in the case of $m = n$, it simplifies to

$$\cos(n \cdot \psi_n - m \cdot \psi_m) = \cos(n \cdot \psi_n - n \cdot \psi_n) = \cos(0) = 1\,. \tag{A.15}$$

In all other cases $\delta_{mn} = 0$. Therefore, the sum simplifies to:

$$\sum_{n=1}^{\infty} v_n \cos(n \cdot \psi_n - m \cdot \psi_m) \cdot \pi \cdot \delta_{mn} \tag{A.16}$$

$$= \pi v_n \tag{A.17}$$

This leads to the wanted result

$$\langle \cos[n(\varphi - \psi_n)] \rangle = \frac{1}{2\pi} \cdot 2\pi \cdot v_n = v_n\,. \tag{A.18}$$

A.2 Q-vector in two-particle correlation

By introducing the so-called Q-vector

$$Q_n = \sum_{j=1}^{M} e^{in\varphi_j}\,, \tag{A.19}$$

one can show that

$$\langle 2 \rangle \equiv \left\langle e^{in(\varphi_1 - \varphi_2)} \right\rangle \tag{A.20}$$

$$= \frac{1}{\binom{M}{2} 2!} \sum_{\substack{j,k=1 \\ (j \neq k)}}^{M} e^{in(\varphi_j - \varphi_k)} \tag{A.21}$$

$$= \frac{1}{\binom{M}{2} 2!} \times [|Q_n|^2 - M]\,. \tag{A.22}$$

Here $\left\langle e^{in(\varphi_1 - \varphi_2)} \right\rangle$ is the sum of all possible pairs between the azimuthal angles φ_1 and φ_2 divided by the total number of all possible pairs (i.e. the event weight).

As mentioned in Sec. 1.5, one has to be aware of autocorrelations. Therefore, the sum of all possible pairs between the two azimuthal angles is given as

$$\sum_{\substack{j,k=1 \\ (j\neq k)}}^{M} e^{in(\varphi_j-\varphi_k)}\,. \tag{A.23}$$

The number of all possible pairs N for a event consisting of M particles can be derived as the following: Taking the first particle, one can correlate it with $M-1$ particles as one must not correlate it with itself. As there are M particles, this process can be repeated M times, therefore the number of all possibles pairs is $N = M\cdot(M-1)$. This expression can be rewritten as

$$N = M\cdot(M-1) = \frac{M!}{(M-2)!} = 2!\cdot\frac{M!}{2!(M-2)!} = \binom{M}{2}2!, \tag{A.24}$$

representing the event weight of the 2-particle correlation. This results to

$$\left\langle e^{in(\varphi_1-\varphi_2)}\right\rangle = \frac{1}{\binom{M}{2}2!}\sum_{\substack{j,k=1 \\ (j\neq k)}}^{M} e^{in(\varphi_j-\varphi_k)} \tag{A.25}$$

To prove

$$\left\langle e^{in(\varphi_1-\varphi_2)}\right\rangle \equiv \frac{1}{\binom{M}{2}2!}\times\left[|Q_n|^2 - M\right] \tag{A.26}$$

one has to prove that

$$|Q_n|^2 = \sum_{j,k=1}^{M} e^{in(\varphi_j-\varphi_k)}\,. \tag{A.27}$$

As shown in [2]

$$|Q_n|^2 = Q_nQ_n^* = \sum_{j=1}^{M} e^{in\varphi_j}\cdot\sum_{k=1}^{M} e^{-in\varphi_k} = \sum_{j,k=1}^{M} e^{in(\varphi_j-\varphi_k)}\,. \tag{A.28}$$

Therefore,

$$|Q_n|^2 = \sum_{j,k=1}^{M} e^{in(\varphi_j-\varphi_k)} = \sum_{\substack{j,k=1 \\ (j\neq k)}}^{M} e^{in(\varphi_j-\varphi_k)} + M\,. \tag{A.29}$$

As the autocorrelation is removed M times, one has to add M itself again. This results out of the fact, that for any autocorrelation ($j=k$) the term $\exp(in(\varphi_j-\varphi_k)) = \exp(in\cdot 0) = 1$ is taken out. In the end this provides the wanted result

$$\langle 2\rangle \equiv \left\langle e^{in(\varphi_1-\varphi_2)}\right\rangle \tag{A.30}$$

$$= \frac{1}{\binom{M}{2}2!}\sum_{\substack{j,k=1 \\ (j\neq k)}}^{M} e^{in(\varphi_j-\varphi_k)} \tag{A.31}$$

$$= \frac{1}{\binom{M}{2}2!}\times\left[|Q_n|^2 - M\right]. \tag{A.32}$$

Appendix B

Monte Carlo-Glauber

B.1 Parameters for Woods-Saxon-Distribution

Nucleus	R in fm	a in fm	w in fm
^{2}H	0.01	0.5882	0
^{16}O	2.608	0.513	-0.51
^{28}Si	3.34	0.580	-0.233
^{32}S	2.54	2.191	0.16
^{40}Ca	3.766	0.586	-0.161
^{58}Ni	4.309	0.517	-0.1308
^{62}Cu	4.2	0.596	0
^{186}W	6.58	0.480	0
^{197}Au	6.38	0.535	0
^{207}Pb	6.62	0.546	0
^{238}U	6.81	0.6	0

Table B.1: Parameters for Woods-Saxon-Distribution, taken from [22].

B.2 Nucleon-Nucleon Overlap Function

The nucleon-nucleon interaction takes a function $p(b)$ which gives the probability of interaction between those nucleons. Here b represents the distance of the two nucleons in the transverse plane. For this Monte Carlo-Glauber model, two options are available:

1. *Black Disk:* The interaction function $p(b)$ is given as

$$p_{BD}(b) = \Theta\left(R - b\right) \tag{B.1}$$

   where Θ represents the Heaviside function. This leads to an interaction of two different nucleons if they undershoot a certain distance R.

2. *Gaussian Overlap:* The Gaussian overlap function is given as

$$p_G(b) = 1 - \left[1 - \alpha \exp\left(-\gamma b^2\right)\right]^2 \tag{B.2}$$

   with two parameters α and γ (taken from [23]).

As stated in [23], Eq. (B.2) has two fulfil

$$\int \mathrm{d}^2 b p(b) = \sigma_{inel}^{NN} \tag{B.3}$$

and

$$2\int \mathrm{d}^2 b \Gamma(b) = \sigma_{tot}^{NN}, \text{ with } \Gamma(b) = 1 - \sqrt{1 - p(b)} \tag{B.4}$$

where σ_{inel}^{NN} is the total inelastic nucleon-nucleon cross-section and σ_{tot}^{NN} the total nucleon-nucleon cross-section. Values for these cross-sections at certain energies can be found Tab. B.2.
Furthermore, Eq. (B.1) has to fulfil Eq. (B.3). Using Eq. (B.3) and (B.4) one obtains dependencies of the parameters R in Eq. (B.1) and α and γ in Eq. (B.2).

$\sqrt{s}$ (GeV)	σ_{el}^{NN}	σ_{tot}^{NN} (mb)	$\sigma_{inel}^{NN} = (\sigma_{tot}^{NN} - \sigma_{el}^{NN})$ (mb)
200	10	52	42
2760	19	83	64

Table B.2: pp cross-sections, taken from [40] and [41].

B.3 Parameter Calculation Black Disk NN-Overlap

Using Eq. (B.1) and Eq. (B.3), one obtains

$$\begin{aligned} &\int \mathrm{d}^2 b \;\; p_{BD}(b) \\ &= 2\pi \int_0^\infty \mathrm{d}b \;\; \Theta\left(R - b\right) \\ &= 2\pi \int_0^R \mathrm{d}b = \sigma_{inel}^{NN} \,. \end{aligned} \tag{B.5}$$

Therefore,

$$R = \sqrt{\frac{\sigma_{inel}^{NN}}{\pi}} \,. \tag{B.6}$$

B.4 Parameter Calculation Gaussian NN-Overlap

Using the Gaussian NN-overlap function $p_G(b)$ (Eq. (B.2)) one obtains

$$\begin{aligned} \Gamma_G(b) &= 1 - \sqrt{1 - p_G(b)} \\ &= 1 - \sqrt{\underbrace{\left[1 - \alpha \exp\left(-\gamma b^2\right)\right]^2}_{>0 \;\; \forall \;\; b, \;\; \gamma \geq 0 \, \text{(Assumption)}}} \\ &= \alpha \exp\left(-\gamma b^2\right) \,. \end{aligned} \tag{B.7}$$

for $\Gamma(b)$ in Eq. (B.4). Therefore, using Eq. (B.4)

$$\begin{aligned} & 2\int \mathrm{d}^2b \;\; \Gamma_G(b) \\ & = 2\pi \int_0^\infty \mathrm{d}b \;\; 2b \;\; \alpha \exp\left(-\gamma b^2\right) \\ & = 2\pi \frac{\alpha}{\gamma} = \sigma_{tot}^{NN} \end{aligned} \tag{B.8}$$

leads to the relation

$$\frac{\gamma}{2\pi} = \frac{\alpha}{\sigma_{tot}^{NN}} \,. \tag{B.9}$$

between the parameters α and γ of the Gaussian NN-overlap function. From Eq. (B.3) it follows that

$$\begin{aligned} & \int \mathrm{d}^2b \;\; p_g(b) = 2\pi \int_0^\infty \mathrm{d}b \; b \; p_G(b) \\ & = 2\pi \int_0^\infty \mathrm{d}b \;\; \left[2\alpha b \exp\left(-\gamma b^2\right) - \alpha^2 b \exp\left(-2\gamma b^2\right)\right] \\ & = 2\pi \left[\frac{\alpha}{\gamma} - \frac{\alpha^2}{4\gamma}\right] \\ & \underset{Eq.(B.9)}{=} \\ & = \sigma_{tot}^{NN} - \alpha \frac{\sigma_{tot}^{NN}}{4} = \sigma_{inel}^{NN} \,. \end{aligned} \tag{B.10}$$

Therefore,

$$\alpha = 4 \frac{\sigma_{tot}^{NN} - \sigma_{inel}^{NN}}{\sigma_{tot}^{NN}} \,. \tag{B.11}$$

The parameter γ is implicitly given by

$$\gamma = 2\pi \frac{\alpha}{\sigma_{tot}^{NN}} = 8\pi \frac{\sigma_{tot}^{NN} - \sigma_{inel}^{NN}}{\left(\sigma_{tot}^{NN}\right)^2} \,. \tag{B.12}$$

Appendix C

General SPC

C.1 Proof of Eq. (3.15)

It has to be shown that

$$\nexists\, m, n \in \mathbb{N}: \ \frac{LCM(m,n)}{m} = 2j \wedge \frac{LCM(m,n)}{n} = 2k \text{ with } j,k \in \mathbb{N}. \tag{C.1}$$

Proof:
Taking the fundamental theorem of arithmetic, every positive natural number a can be built up as a unique product of prime numbers:

$$a = \prod_p p^{a_p} \tag{C.2}$$

where $\prod_p$ denotes the product of all prime numbers starting from 2 and a_p are the unique exponents of the prime number p to build a. Taking a second integer

$$b = \prod_p p^{b_p}\,, \tag{C.3}$$

the least common multiple between a and b ($LCM(a,b)$) can be written as

$$LCM(a,b) = \prod_p p^{max(a_p,b_p)}\,. \tag{C.4}$$

For an integer a we now use the notation

$$a = 2^{a_2} \cdot \tilde{a} \tag{C.5}$$

with

$$\tilde{a} = \prod_{\tilde{p}} \tilde{p}^{\,a_{\tilde{p}}}\,. \tag{C.6}$$

$\prod_{\tilde{p}}$ denotes the product of all prime numbers starting from 3 and $a_{\tilde{p}}$ are the unique exponents of the prime number $\tilde{p}$ to build $\tilde{a}$. $\tilde{a}$ is odd as it is a product of odd numbers. Using the same notation with $\tilde{p}$ being the prime numbers starting from 3, the $LCM(m,n)$ can be written as

$$LCM(m,n) = 2^{max(m_2,n_2)} \cdot \tilde{\beta} \tag{C.7}$$

where

$$\tilde{\beta} = \prod_{\tilde{p}} \tilde{p}^{\,max\left(m_{\tilde{p}},n_{\tilde{p}}\right)}\,. \tag{C.8}$$

It has to be stressed that $\tilde{\beta}$ is odd as it is a product of odd numbers. Possible combinations between

$$m = 2^{m_2} \cdot \tilde{m} \text{ and } n = 2^{n_2} \cdot \tilde{n}\,.$$

	m odd ($m_2 = 0$)	m even ($m_2 > 0$)
n odd ($n_2 = 0$)	$LCM(m,n) = \tilde{\beta}$ (odd) $\frac{LCM(m,n)}{m} = \frac{\tilde{\beta}}{\tilde{m}} \implies$ odd $\frac{LCM(m,n)}{n} = \frac{\tilde{\beta}}{\tilde{n}} \implies$ odd	$LCM(m,n) = 2^{m_2}\ \tilde{\beta}$ (even) $\frac{LCM(m,n)}{m} = \frac{\tilde{\beta}}{\tilde{m}} \implies$ odd $\frac{LCM(m,n)}{n} = 2^{m_2}\ \frac{\tilde{\beta}}{\tilde{n}} \implies$ even
n even ($n_2 > 0$)	$LCM(m,n) = 2^{n_2}\ \tilde{\beta}$ (even) $\frac{LCM(m,n)}{m} = 2^{n_2}\ \frac{\tilde{\beta}}{\tilde{m}} \implies$ even $\frac{LCM(m,n)}{n} = \frac{\tilde{\beta}}{\tilde{n}} \implies$ odd	w.l.o.g. $m_2 \geq n_2$ $LCM(m,n) = 2^{m_2} \cdot \tilde{\beta}$ (even) $\frac{LCM(m,n)}{m} = \frac{\tilde{\beta}}{\tilde{m}} \implies$ odd $\frac{LCM(m,n)}{n} = 2^{m_2-n_2}\ \frac{\tilde{\beta}}{\tilde{n}}$ $\implies \begin{cases} \text{odd} & \text{for } m_2 = n_2 \\ \text{even} & \text{for } m_2 > n_2 \end{cases}$

Table C.1: All possible combinations between $m = 2^{m_2} \cdot \tilde{m}$ and $n = 2^{n_2} \cdot \tilde{n}$ in respect to $LCM(m,n)$

Note: The Ratio of two dividable odd numbers is odd again. As seen in Tab. C.1:

$$\nexists\, m,n \in \mathbb{N}: \ \frac{LCM(m,n)}{m} = 2j \wedge \frac{LCM(m,n)}{n} = 2k \text{ with } j,k \in \mathbb{N} \quad \square \tag{C.9}$$

C.2 LCM-Method Smaller Order

It has to be shown that for any integer m and n the order of the correlators using the LCM-Method is always smaller equal than the ones for the Direct Method presented above. The orders of the correlators are given as

1. Direct Method $\begin{cases} n+m & \text{for } m \wedge n \text{ even} \\ 2\,(n+m) & \text{for } m \vee n \text{ odd} \end{cases}$
2. LCM-Method: $2 \cdot LCM(m,n)\left(\frac{1}{m} + \frac{1}{n}\right)$

Proof:
In general, $LCM(m,n) \leq m \cdot n$. Therefore, in cases of $m \vee n$ odd, the LCM-Method reduces the order of the particle correlator compared to the Direct Method as

$$2 \cdot LCM(m,n)\left(\frac{1}{m}+\frac{1}{n}\right) \leq 2\,(n \cdot m)\left(\frac{1}{m}+\frac{1}{n}\right) \equiv 2(n+m)\,. \tag{C.10}$$

In case of $m \wedge n$ even, the order of the particle correlator of the Direct Method is also bigger equal than the LCM-Method:
For two positive integers $m, n > 0$

$$GCD(m,n) \cdot LCM(m,n) = m \cdot n \tag{C.11}$$

where $GCD(m,n)$ is the greatest common divisor of m and n.

As m and n are both even, we can show that $GCD(m,n)$ is even:

$$GCD(m,n) = 2k \text{ with } k \in \mathbb{N}\,. \tag{C.12}$$

An integer a can be written as

$$a = 2^{a_2} \cdot \tilde{a} \tag{C.13}$$

with

$$\tilde{a} = \prod_{\tilde{p}} \tilde{p}^{\,a_{\tilde{p}}} \tag{C.14}$$

due to the fundamental theorem of arithmetic. $\prod_{\tilde{p}}$ denotes the product of all prime numbers starting from 3 and $a_{\tilde{p}}$ are the unique exponents of the prime number $\tilde{p}$ to build $\tilde{a}$. $\tilde{a}$ is odd as it is a product of odd numbers. The greatest common divisor of a and b ($GCD(a,b)$) is given as

$$GCD(a,b) = 2^{min(a_2,b_2)} \cdot \tilde{\gamma} \tag{C.15}$$

where

$$\tilde{\gamma} = \prod_{\tilde{p}} \tilde{p}^{\,min\left(a_{\tilde{p}},b_{\tilde{p}}\right)}\,. \tag{C.16}$$

It has to be stressed that $\tilde{\gamma}$ is odd as it is a product of odd numbers and $\tilde{p}$ denotes all prime numbers starting from 3. As a and b are even, we know that $a_2 > 0$ and $b_2 > 0$. Therefore, $min(a_2, b_2) > 0$:

$$2^{min(a_2,b_2)} = 2k \text{ with } k \in \mathbb{N} \implies GCD(a,b) \text{ even}\,. \tag{C.17}$$

Taking this statement into account

$$\begin{aligned} GCD(m,n) \cdot LCM(m,n) &= m \cdot n \\ \Leftrightarrow 2k \cdot LCM(m,n) &= m \cdot n \\ \Leftrightarrow 2k \cdot LCM(m,n) \cdot (m+n) &= \underbrace{m \cdot n}_{\neq 0}(m+n) \\ \Leftrightarrow 2k \cdot LCM(m,n) \cdot (\frac{1}{m}+\frac{1}{n}) &= (m+n)\,. \end{aligned} \tag{C.18}$$

As k is a positive integer

$$2 \cdot LCM(m,n) \cdot (\frac{1}{m}+\frac{1}{n}) \leq 2k \cdot LCM(m,n) \cdot (\frac{1}{m}+\frac{1}{n}) = (m+n) \tag{C.19}$$

and therefore also in this case, the LCM-Method is in general a smaller set of correlators.

□

C.3 Proof Eq. (3.23)

It has to be shown that

$$\nexists\, m,n,q \in \mathbb{N}: \frac{LCM(m,n,q)}{m} = 2i \wedge \frac{LCM(m,n,q)}{n} = 2j \wedge \frac{LCM(m,n,q)}{q} = 2k \quad \text{with } i,j,k \in \mathbb{N}\,. \tag{C.20}$$

Proof:
As before, using the fundamental theorem of arithmetic, an integer a can be built up as a multiplication of prime numbers:

$$a = 2^{a_2} \cdot \tilde{a}\,, \tag{C.21}$$

with

$$\tilde{a} = \prod_{\tilde{p}} \tilde{p}^{\,a_{\tilde{p}}}\,. \tag{C.22}$$

$\prod_{\tilde{p}}$ denotes the product of all prime numbers starting from 3 and $a_{\tilde{p}}$ are the unique exponents of the prime number $\tilde{p}$ to build $\tilde{a}$. $\tilde{a}$ is odd as it is a product of odd numbers.
Using the same notation with $\tilde{p}$ being the prime numbers starting from 3, the $LCM(m,n,q)$ can be written as

$$LCM(m,n,q) = 2^{max(m_2,n_2,q_2)} \cdot \tilde{\beta}\,, \tag{C.23}$$

where

$$\tilde{\beta} = \prod_{\tilde{p}} \tilde{p}^{\,max\left(m_{\tilde{p}},n_{\tilde{p}},q_{\tilde{p}}\right)}\,. \tag{C.24}$$

It has to be stressed that $\tilde{\beta}$ is odd as it is a product of odd numbers.
Possible combinations between

$$m = 2^{m_2} \cdot \tilde{m},\ n = 2^{n_2} \cdot \tilde{n} \text{ and } q = 2^{q_2} \cdot \tilde{q}$$

where we use w.l.o.g.

$$m_2 \geq n_2 \geq p_2\,. \tag{C.25}$$

	m odd ($m_2 = 0$)	m even ($m_2 > 0$)
n odd ($n_2 = 0$)	not possible as $m_2 \geq n_2 \geq q_2$	not possible as $m_2 \geq n_2 \geq q_2$
n even ($n_2 > 0$)	not possible as $m_2 \geq n_2 \geq q_2$	$LCM(m,n,q) = 2^{m_2} \cdot \tilde{\beta}$ (even) $\frac{LCM(m,n,q)}{m} = \frac{\tilde{\beta}}{\tilde{m}} \implies$ odd $\frac{LCM(m,n,q)}{n} = 2^{m_2-n_2}\,\frac{\tilde{\beta}}{\tilde{n}}$ $\implies \begin{cases} \text{odd} & \text{for } m_2 = n_2 \\ \text{even} & \text{for } m_2 > n_2 \end{cases}$ $\implies \begin{cases} \text{odd} & \text{for } m_2 = q_2 \\ \text{even} & \text{for } m_2 > q_2 \end{cases}$

Table C.2: Case p even ($q_2 > 0$).

	m odd ($m_2 = 0$)	m even ($m_2 > 0$)
n odd ($n_2 = 0$)	$LCM(m,n,q) = \tilde{\beta}$ (odd) $\frac{LCM(m,n,q)}{m} = \frac{\tilde{\beta}}{\tilde{m}} \implies$ odd $\frac{LCM(m,n,q)}{n} = \frac{\tilde{\beta}}{\tilde{n}} \implies$ odd $\frac{LCM(m,n,q)}{q} = \frac{\tilde{\beta}}{\tilde{q}} \implies$ odd	$LCM(m,n,q) = 2^{m_2}\ \tilde{\beta}$ (even) $\frac{LCM(m,n,q)}{m} = \frac{\tilde{\beta}}{\tilde{m}} \implies$ odd $\frac{LCM(m,n,q)}{n} = 2^{m_2}\ \frac{\tilde{\beta}}{\tilde{n}} \implies$ even $\frac{LCM(m,n,q)}{q} = 2^{m_2}\ \frac{\tilde{\beta}}{\tilde{q}} \implies$ even
n even ($n_2 > 0$)	not possible as $m_2 \geq n_2 \geq q_2$	$LCM(m,n,q) = 2^{m_2} \cdot \tilde{\beta}$ (even) $\frac{LCM(m,n,q)}{m} = \frac{\tilde{\beta}}{\tilde{m}} \implies$ odd $\frac{LCM(m,n,q)}{n} = 2^{m_2-n_2}\ \frac{\tilde{\beta}}{\tilde{n}}$ $\implies \begin{cases} \text{odd} & \text{for } m_2 = n_2 \\ \text{even} & \text{for } m_2 > n_2 \end{cases}$ $\frac{LCM(m,n,q)}{q} = 2^{m_2}\ \frac{\tilde{\beta}}{\tilde{q}} \implies$ even

Table C.3: Case q odd ($q_2 = 0$).

□

Appendix D

Wolverine-Plots

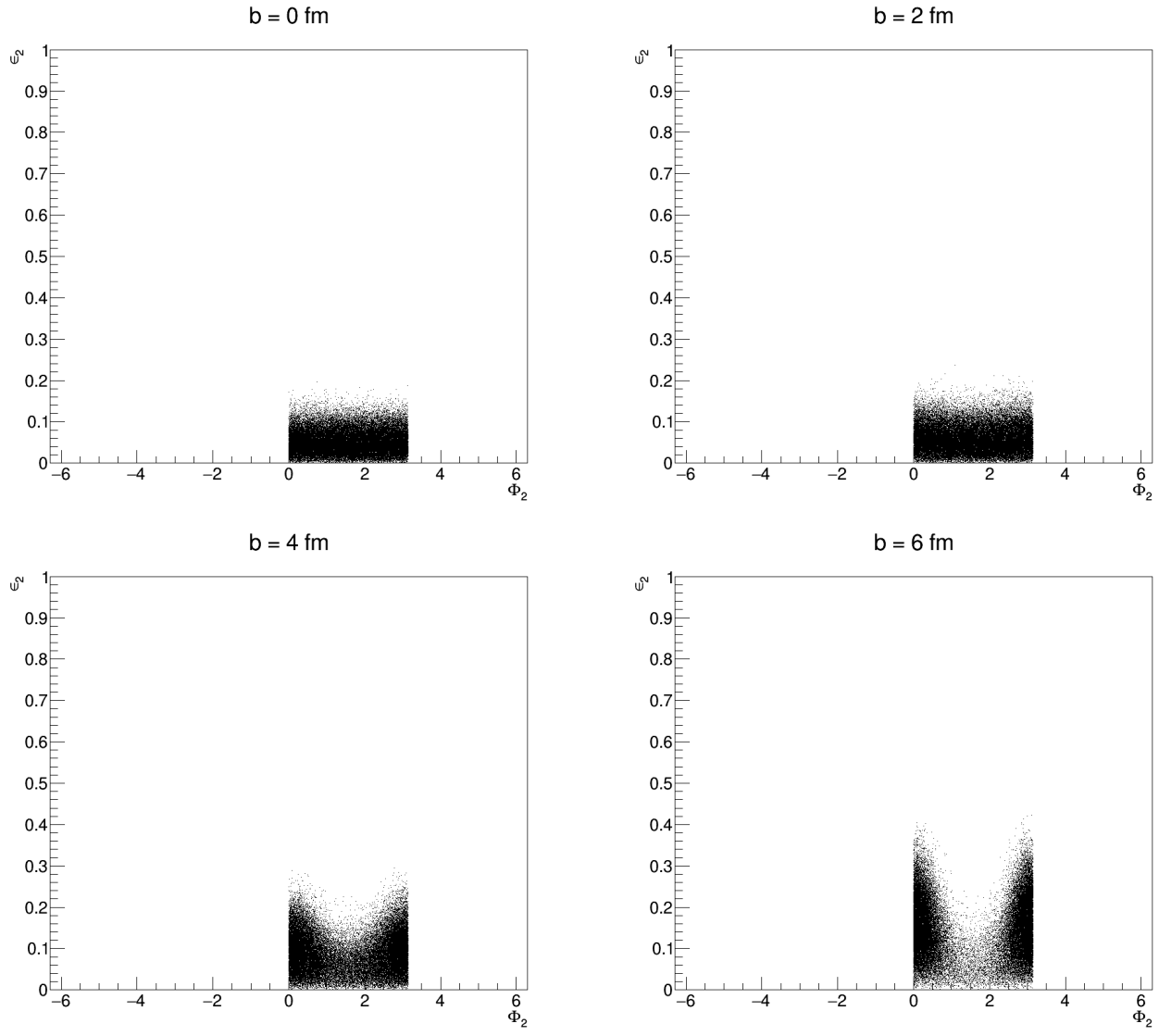

Figure D.1: Correlation plots between ϵ_2 and Φ_2 for impact parameters $b \in [0\,\mathrm{fm}, 16\,\mathrm{fm}]$.

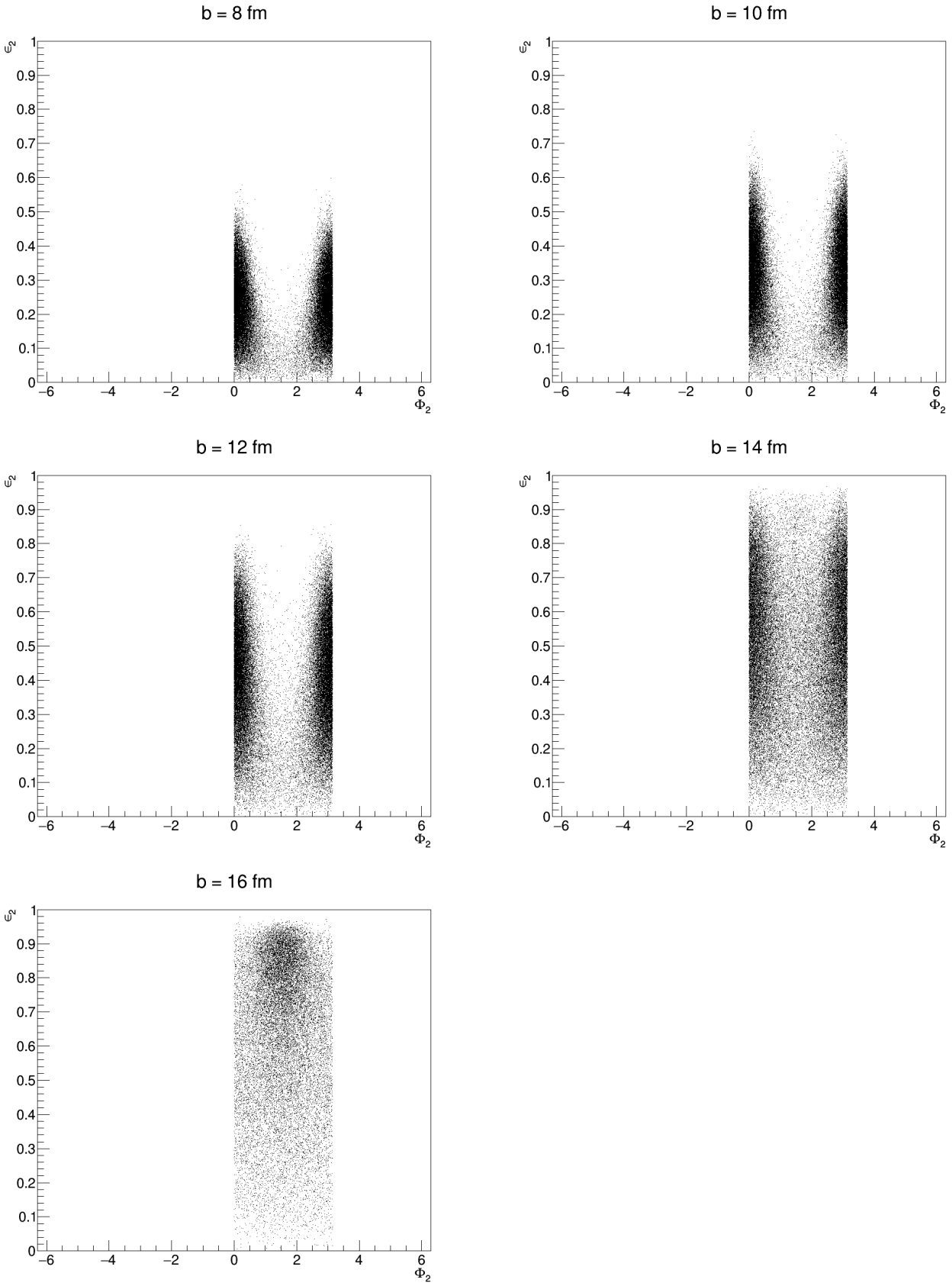

Figure D.1: Correlation plots between ϵ_2 and Φ_2 for impact parameters $b \in [0\,\text{fm}, 16\,\text{fm}]$.

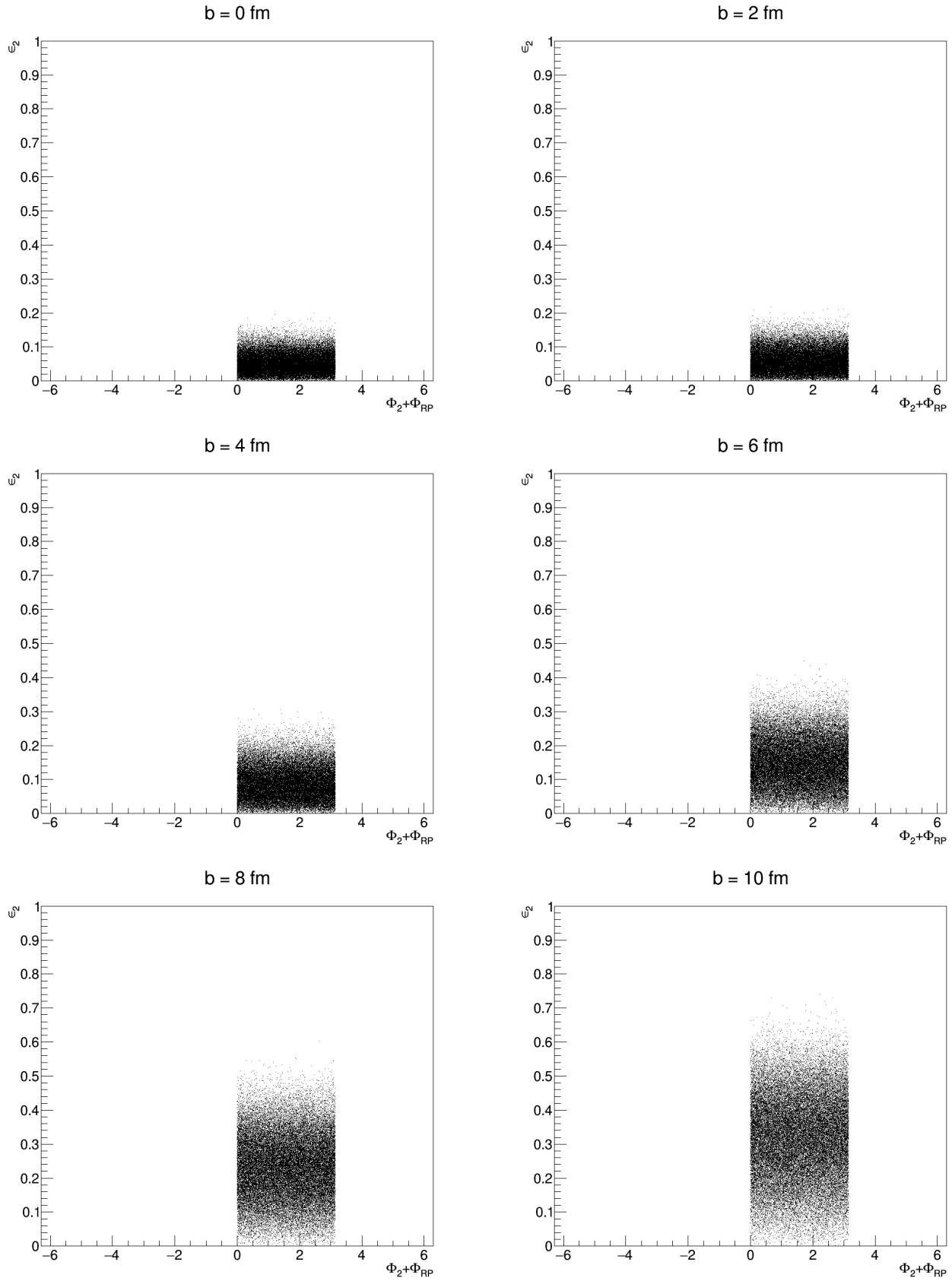

Figure D.2: Correlation plots between ϵ_2 and $\Phi_2 + \Phi_{RP}$ for impact parameters $b \in [0\,\text{fm}, 16\,\text{fm}]$.

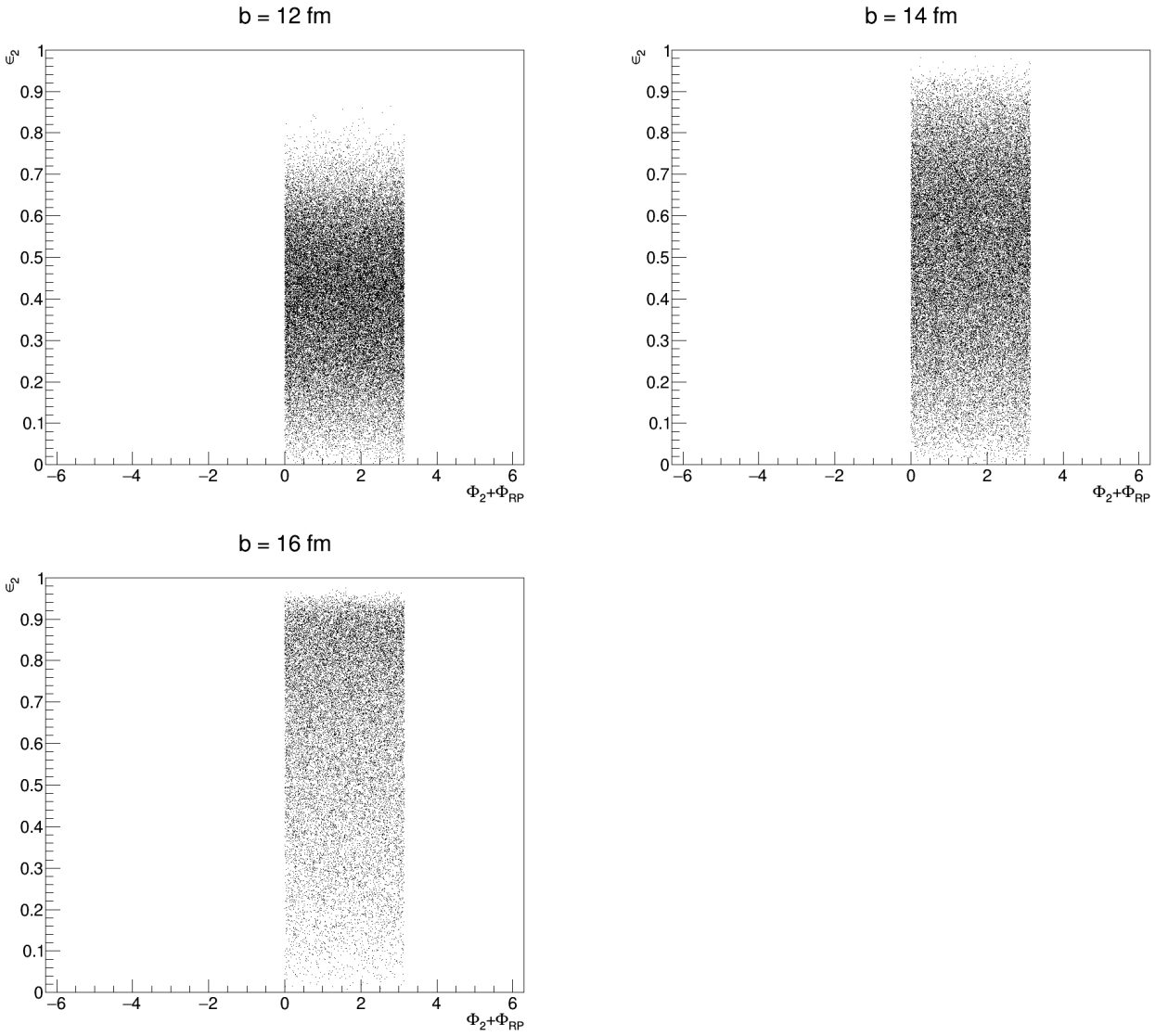

Figure D.2: Correlation plots between ϵ_2 and $\Phi_2 + \Phi_{RP}$ for impact parameters $b \in [0\,\text{fm}, 16\,\text{fm}]$.

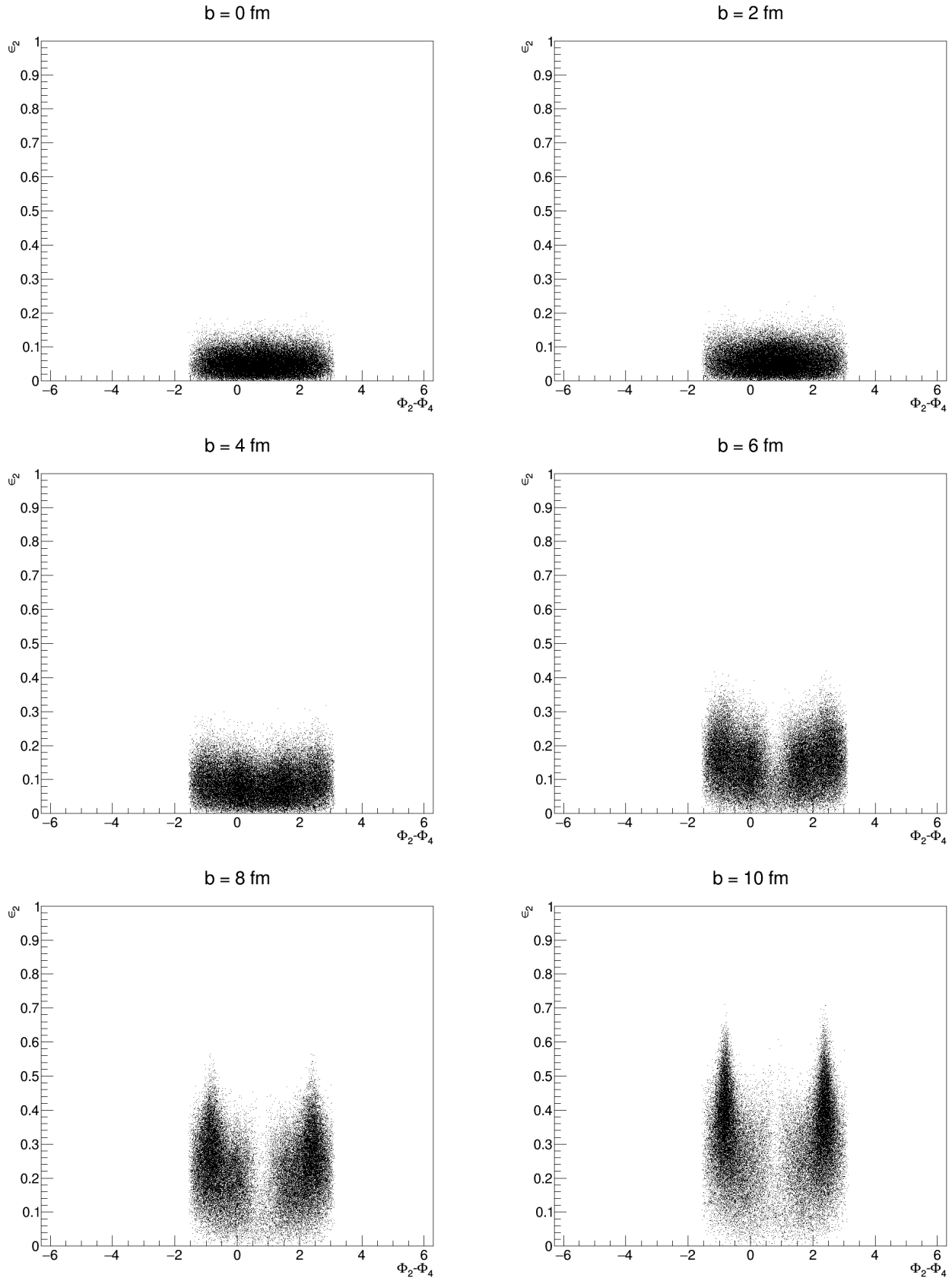

Figure D.3: Correlation plots between ϵ_2 and $\Phi_2 - \Phi_4$ for impact parameters $b \in [0\,\text{fm}, 16\,\text{fm}]$.

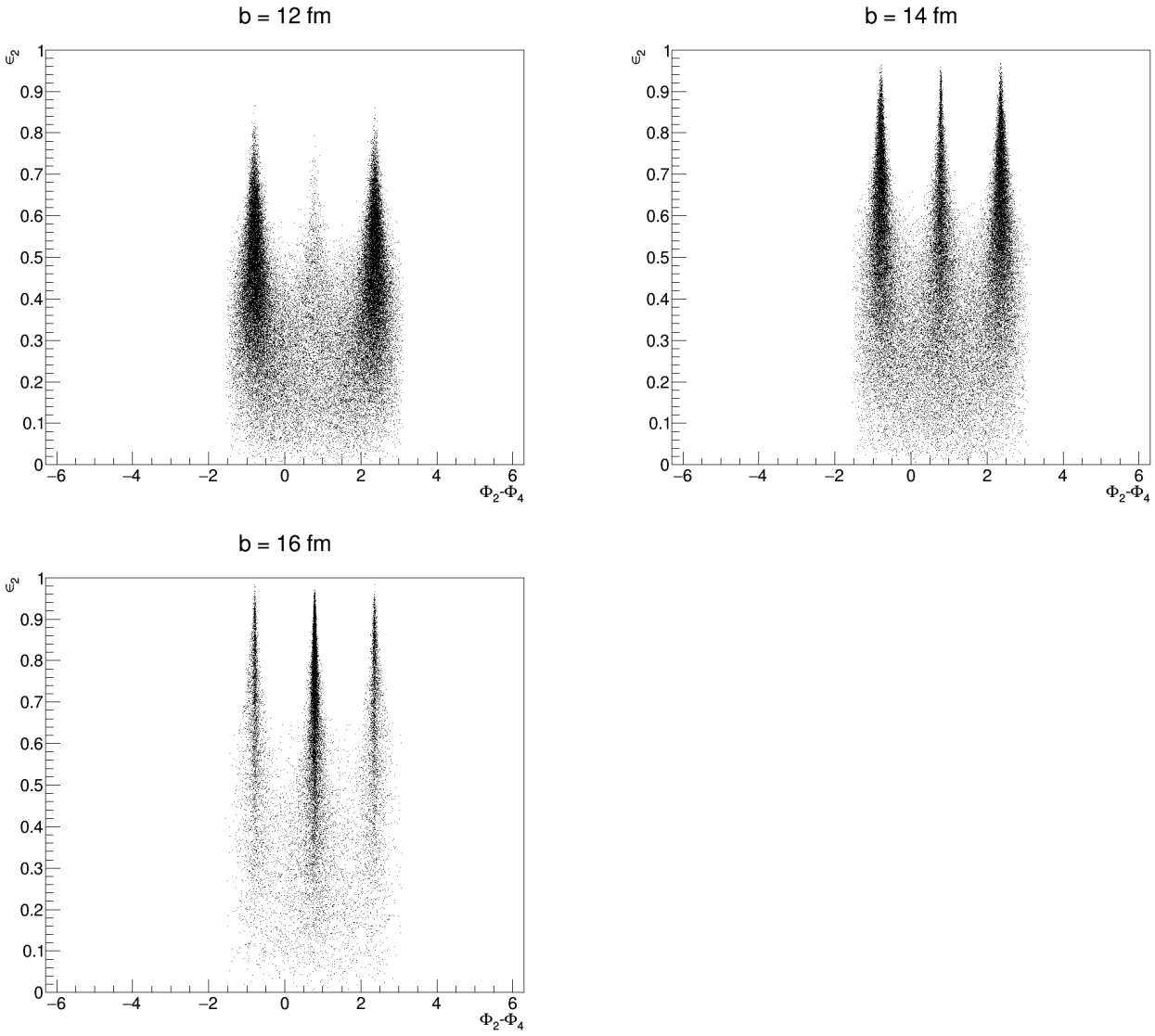

Figure D.3: Correlation plots between ϵ_2 and $\Phi_2 - \Phi_4$ for impact parameters $b \in [0\,\text{fm}, 16\,\text{fm}]$.

Appendix E

Expansion Approach

E.1 Second Order Expansion

[1]The second order Taylor Expansion $T_2(f(X,Y))$ of the function $f(X,Y) = \frac{X}{Y}$ around the expansion point $\Theta = (\mu_X, \mu_Y)$ (with $\mu_Y \neq 0$) is

$$\begin{aligned} T_2(f(X,Y)) =& \frac{\mu_X}{\mu_Y}\left[1 - \frac{1}{\mu_Y}(Y-\mu_Y) + \frac{1}{\mu_Y^2}(Y-\mu_Y)^2\right] \\ &+ \frac{(x-\mu_X)}{\mu_Y}\left[1 - \frac{1}{\mu_Y}(Y-\mu_Y)\right]. \end{aligned} \tag{E.1}$$

By using the approximation

$$\mathrm{E}(f(x,y)) = \mathrm{E}\left(\frac{X}{Y}\right) \approx \mathrm{E}(T_2(f(X,Y))) \tag{E.2}$$

one obtains the second order approximation of the mean of the ratio distribution $\mathrm{E}\left(\frac{X}{Y}\right)$ as

$$\mathrm{E}\left(\frac{X}{Y}\right) \approx \frac{\mathrm{E}(X)}{\mathrm{E}(Y)}\left[1 + \frac{\mathrm{E}(Y^2)}{\mathrm{E}(Y)^2}\right] - \frac{\mathrm{E}(XY)}{\mathrm{E}(Y)^2}. \tag{E.3}$$

E.2 Third Order Expansion

Analogous to the second order expansion, in this section the third order expansion will be presented. The third order Taylor expansion $T_3(f(X,Y))$ of a function $f(X,Y) = \frac{X}{Y}$ around the expansion point $\Theta = (\mu_X, \mu_Y)$ (with $\mu_Y \neq 0$) is

$$\begin{aligned} T_3(f(X,Y)) =& \frac{\mu_X}{\mu_Y}\left[1 - \frac{1}{\mu_Y}(Y-\mu_Y) + \frac{1}{\mu_Y^2}(Y-\mu_Y)^2 - \frac{1}{\mu_Y^3}(Y-\mu_Y)^3\right] \\ &+ \frac{(x-\mu_X)}{\mu_Y}\left[1 - \frac{1}{\mu_Y}(Y-\mu_Y) + \frac{1}{\mu_Y^2}(Y-\mu_Y)^2\right] \end{aligned} \tag{E.4}$$

Taking the approximation that

$$\mathrm{E}(f(x,y)) = \mathrm{E}\left(\frac{X}{Y}\right) \approx \mathrm{E}(T_3(f(X,Y))) \tag{E.5}$$

the mean of the ratio distribution of $\mathrm{E}\left(\frac{X}{Y}\right)$ can be approximated as

$$\mathrm{E}\left(\frac{X}{Y}\right) \approx \frac{\mathrm{E}(X)}{\mathrm{E}(Y)}\left[1 + 3\frac{\mathrm{E}(Y^2)}{\mathrm{E}(Y)^2} - \frac{\mathrm{E}(Y^3)}{\mathrm{E}(Y)^3}\right] - 3\frac{\mathrm{E}(XY)}{\mathrm{E}(Y)^2} + \frac{\mathrm{E}(XY^2)}{\mathrm{E}(Y)^3}. \tag{E.6}$$

[1]This section is based on [39].

Appendix F

First Look at Experimental SPC

F.1 List of Runs

The runs used in the presented first look at experimental data analyses are taken from LHC10h. The list of used runs is:
139510, 139507, 139505, 139503, 139465, 139438, 139437, 139360, 139329, 139328, 139314, 139310, 139309, 139173, 139107, 139105, 139038, 139037, 139036, 139029, 139028, 138872, 138871, 138870, 138837, 138732, 138730, 138666, 138662, 138653, 138652, 138638, 138624, 138621, 138583, 138582, 138578, 138534, 138469, 138442, 138439, 138438, 138396, 138364, 138275, 138225, 138201, 138197, 138192, 138190, 137848, 137844, 137752, 137751, 137724, 137722, 137718, 137704, 137693, 137692, 137691, 137686, 137685, 137639, 137638, 137608, 137595, 137549, 137546, 137544, 137541, 137539, 137531, 137530, 137443, 137441, 137440, 137439, 137434, 137432, 137431, 137430, 137243, 137236, 137235, 137232, 137231, 137230, 137162, 137161

F.2 High Multiplicity Outliers

[1]High multiplicity outliers (HMO's) describe peripheral events (centrality > 60 %), in which the reconstruction went wrong in such a way, that this event carries an unrealistically large multiplicity. This happens only on a per-mill level. However, as multiplicity weights are used as event weights in multi-particle correlation techniques, such HMO's will strongly bias the measurement in high centrality classes (peripheral collisions).
The removal of the HMO's was performed by introducing a rejection criteria based on the number of tracks in the filter 768 (hybrid tracks) and filter 256 (global hybrid tracks). Filter 768 is used as the primary filter in the analysis due to its uniform azimuthal coverage. Though, as Fig. F.1 shows, this filter contains HMO's. As the rejection criteria

$$\begin{cases} (\text{Tracks-Filter-768}) > 1.63 \cdot (\text{ Tracks-Filter-256 }) + 70 \implies \text{reject event} \\ (\text{Tracks-Filter-768}) < 1.14 \cdot (\text{ Tracks-Filter-256 }) - 35 \implies \text{reject event} \end{cases}$$

is applied, HMO's in filter 768 are removed (Fig. F.2).

[1]See acknowledgements.

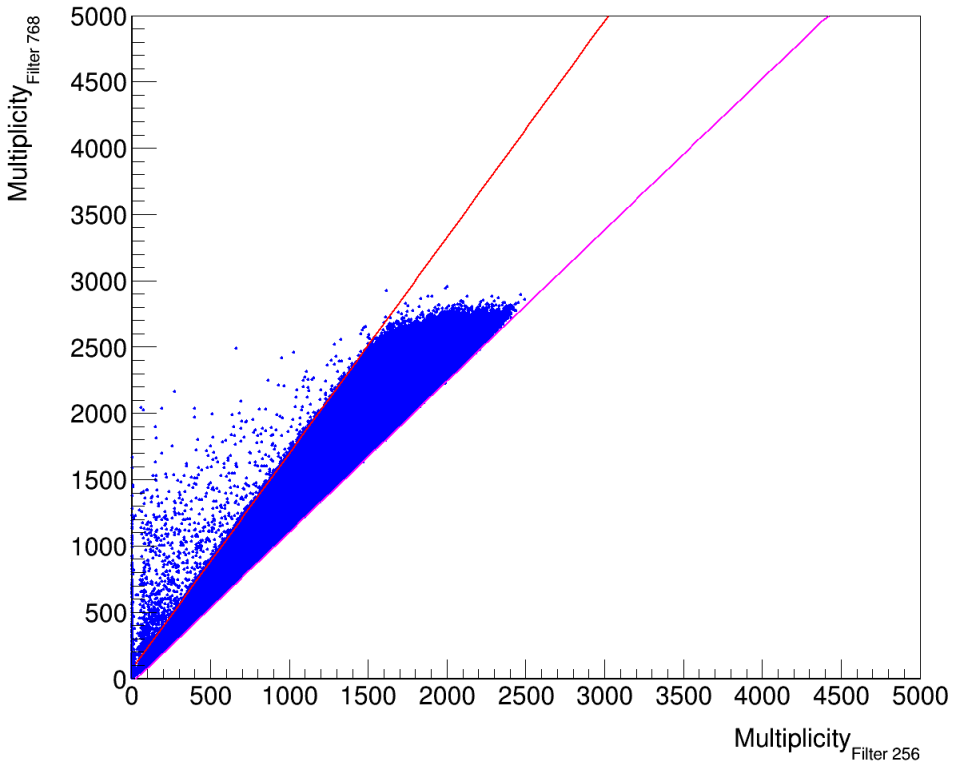

Figure F.1: Correlation plot between filter 256 and filter 768 without application of the HMO-cut (indicated by the lines).

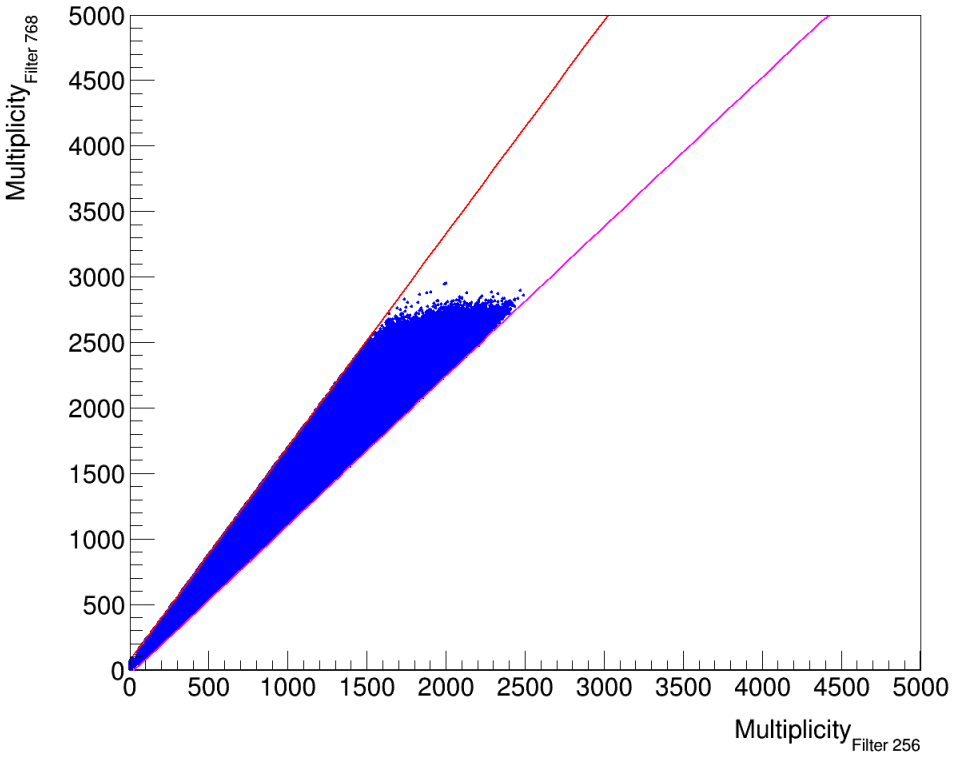

Figure F.2: Correlation plot between filter 256 and filter 768 with application of the HMO-cut (indicated by the lines).

Appendix G

Error Propagation

G.1 All-Event-Average Approach

In general, an observable Z which is built as

$$Z = \frac{\langle X \rangle}{\langle Y \rangle} \tag{G.1}$$

has a first order error propagation of

$$\sigma_Z = |Z| \sqrt{\left(\frac{\sigma_{\langle X \rangle}}{\langle X \rangle}\right)^2 + \left(\frac{\sigma_{\langle Y \rangle}}{\langle Y \rangle}\right)^2 - 2\frac{\mathrm{Cov}(X,Y)}{\langle X \rangle \langle Y \rangle}}\,. \tag{G.2}$$

In Eq. (G.2), $\langle X \rangle$ is the mean of X and $\sigma^2_{\langle X \rangle}$ its variance (same notation for Y). Additionally, $\mathrm{Cov}(X,Y)$ denotes the covariance between X and Y.
Under neglect of the covariance term, the error propagation of Eq. (G.2) leads to

$$\sigma_Z = |Z| \sqrt{\left(\frac{\sigma_{\langle X \rangle}}{\langle X \rangle}\right)^2 + \left(\frac{\sigma_{\langle Y \rangle}}{\langle Y \rangle}\right)^2}\,. \tag{G.3}$$

In case of an AE-Approach with factorised denominator

$$P = \frac{\langle A \rangle}{\langle B \rangle \langle C \rangle} \tag{G.4}$$

the error propagation under neglect of covariance terms can be written as

$$\sigma_P = |P| \sqrt{\left(\frac{\sigma_{\langle A \rangle}}{\langle A \rangle}\right)^2 + \left(\frac{\sigma_{\langle B \rangle}}{\langle B \rangle}\right)^2 + \left(\frac{\sigma_{\langle C \rangle}}{\langle C \rangle}\right)^2}\,. \tag{G.5}$$

G.2 Bootstrap

The bootstrap method allows the estimation of statistical errors of compound observables which would otherwise need to be estimated by a possibly more complicated error propagation.
Consider a general compound observable x, which represents the observable of interest. First, the initial sample will be divided into N subsamples with about the same statistics (in this analyses by default $N = 10$). For each subsample i ($i \in \{1, ..., N\}$), its compound

observable x_i can be computed. With the mean $\langle x \rangle$ of our observable of interest, its standard deviation σ_x can be computed as

$$\sigma_x = \sqrt{\frac{1}{N(N-1)} \sum_{i=1}^{N} \left(\langle x \rangle - x_i \right)^2}. \tag{G.6}$$

Appendix H

MC-Glauber Code

```
#include "TComplex.h"
#include "TProfile.h"
#include "TStopwatch.h"
#include "Riostream.h"
#include "TMath.h"
#include "TGraphErrors.h"
#include "TF1.h"
#include <iostream>
#include <fstream>
#include <cmath>
#include <cstdio>
#include "TMultiGraph.h"
#include "TGraph.h"
#include "TAxis.h"
#include "TCanvas.h"
#include "TList.h"
#include "TFile.h"
#include "TDirectory.h"
#include "TObject.h"
#include "TDirectoryFile.h"
#include "TRandom3.h"
#include "TClass.h"
#include "TROOT.h"
#include "TString.h"
#include "TH1.h"
#include <string>
#include "TH2.h"
#include "TAxis.h"
#include "TPaveStats.h"

using namespace std;

//Global
TFile *file = new TFile("output.root","recreate");
const Int_t Steps = 22;
TProfile *Ecc[Steps] = {NULL}; //will store epsilon_1 (Bin 1) to epsilon_8 (Bin 8)
TProfile *Ecc_Sqr[Steps] = {NULL}; //will store (epsilon_1)^2 (Bin 1) to (epsilon_8)^2 (Bin 8)
TProfile *Ecc_Quadr[Steps] = {NULL}; //will store (epsilon_1)^4 (Bin 1) to (epsilon_8)^4 (Bin 8)
TProfile *SP[Steps] = {NULL}; //will store symmetryplane psi_1 (Bin 1) to psi_8 (Bin 8)
TProfile *CollStats[Steps] = {NULL}; //will store Impactparameter in fm (Bin 1), <N_Part> (Bin 2) and <N_Coll> (Bin 3)
TDirectoryFile *Basics = new TDirectoryFile("Basics","Basics");
TList *List[Steps] = {NULL};
Bool_t bMinDist = kTRUE; //if kTrue: Hard-core nucleons with radius 0.4 fm -> min. distance of 0.8 fm between nucleon centres of same nucleus
Bool_t bModWoodsSaxon = kTRUE; //if kTRUE: Usage of normal Woods-Saxon-Distribution for building the nuclei (usage of sphere parameter)
Bool_t bGaussianSmearing = kTRUE; //if kTRUE: Usage of Gaussian Smearing
Bool_t bGaussianOverlap = kTRUE; //if kTRUE: Usage of Gaussian NN overlap function
//=============================================================================================================================================
//Function declaration
void Glauber();

void Cosmetics(const Int_t Num);

void Storing(const Int_t Number);

void GetNucleusData(string Nucleus_Typ, Float_t Data[4], Float_t *Impact, const Int_t Counter);

void GetEnergyData(string Energy, Float_t Data[2]);

void BuildNucleus(const Int_t Mass_Number, const Float_t Impact_Parameter, const Float_t Radius, const Float_t Skin,const Float_t Sphere_Parameter,
                  Float_t *Nuc, Int_t *Nuc_Inter);
```

```
void CollideNuclei(const Int_t Mass_Number, Float_t *Nuc_1, Float_t *Nuc_2, Int_t *Nuc_1_Inter, Int_t *Nuc_2_Inter,
                   Int_t *Coll_Para, Float_t Energy[2]);

void EccentricityAndSymmetryplanes(const Int_t NuPart, Float_t *Coordinates_Participants, Float_t *Ecco, Float_t *Symmo);

void ReFill(const Int_t NuPart, const Int_t Mass_Number, Float_t *Coordinates_Participants, Float_t *Nuc_1, Float_t *Nuc_2,
            Int_t *Nuc_1_Inter, Int_t *Nuc_2_Inter);

void PlotNucleus(const Int_t Mass_Number, Float_t* Nuc_1, Float_t* Nuc_2, Int_t* Nuc_1_Inter, Int_t* Nuc_2_Inter, Int_t* Coll_Para);

//=============================================================================================================================

void Glauber() {

        if(gRandom) delete gRandom;
        gRandom = new TRandom3(0);

        //List of actions:
        //1. Cosmetics
        //2. Get Nucleus and Energy Data
        //3. Setup the Nuclei
        //4. Collide the Nuclei
        //5. Refill Participant Coordinates
        //6. Calculate Exccentricities
        //7. Plot
        //8. Monitor Progress
        //9. Store Data

    //~~~~~~~~~~~~~~~~~~~~~~~~~~~~~~~~~~~~~~~~~~~~~~~~~~~~~~~~~~~
        //1. Cosmetics
        Cosmetics(Steps); //Book everything

        //~~~~~~~~~~~~~~~~~~~~~~~~~~~~~~~~~~~~~~~~~~~~~~~~~~~~~~~~
        //2. Get Nucleus and Energy Data

        Float_t Data[4] = {0.}; //Data[0] Mass_Number, Data[1] Radius, Data[2] Skin depth, Data[3] Sphere parameter
        Float_t b_Arr[Steps] = {0.};
        Float_t Energy_Data[2] = {0.};

        GetNucleusData("Pb207",Data,b_Arr,Steps);
        GetEnergyData("2.76TeV",Energy_Data);

        const Int_t A = (Int_t)(Data[0]); //number of nucleons in the nucleus

        //for Woods-Saxon-Distribution:
        const Float_t R = Data[1]; //radius of the nucleus in fm
        const Float_t a = Data[2]; //skin depth in fm
        const Float_t w = Data[3]; //sphere parameter

        //~~~~~~~~~~~~~~~~~~~~~~~~~~~~~~~~~~~~~~~~~~~~~~~~~~~~~~~~

        //Measure total execution time:
        TStopwatch timerRecursion;
        timerRecursion.Start();

        //output for tracing what setup was used:
        if(bMinDist==kFALSE){cout<<"No minimal distance between nucleons within the same atom"<<endl;}
        else{cout<<"Minimal distance between centre of nucleons within the same atom: 0.8 fm. (nucleons with hard core)"<<endl;}
        if(bModWoodsSaxon==kFALSE){cout<<"Usage of stripped Woods-Saxon distribution for building the nuclei (no sphere parameter)"<<endl;}
        else{cout<<"Usage of normal Woods-Saxon distribution for building the nuclei (usage of sphere parameter)"<<endl;}
        if(bGaussianSmearing==kFALSE){cout<<"No Gaussian Smearing"<<endl;}
        else{cout<<"Usage of Gaussian Smearing"<<endl;}
        if(bGaussianOverlap==kFALSE){cout<<"Black disk NN overlap"<<endl;}
        else{cout<<"Usage of Gaussian NN overlap"<<endl;}

        const Int_t NE=1000; //number of events per impact parameter

        //~~~~~~~~~~~~~~~~~~~~~~~~~~~~~~~~~~~~~~~~~~~~~~~~~~~~~~~~

        for(Int_t q=0; q<Steps; q++){

        Float_t b = b_Arr[q];
        CollStats[q]->Fill(0.5,b);


        for(Int_t j=0; j<NE; j++){

        //Data storing for each Nucleus
        Float_t *Nucleus_1 = new Float_t[2*A]; // x_1, ... , x_A, y_1, ... y_A
```

```
Int_t *Nucleus_1_Inter = new Int_t[A]; // no interaction if interaction_n = 0 , interaction if interaction_n = 1

Float_t *Nucleus_2 = new Float_t[2*A];
Int_t *Nucleus_2_Inter = new Int_t[A];

//Data storing collision for each event
//Int_t *Coll = new Int_t[4];
Int_t Coll[4] = {0}; // {N_Part, N_Coll, N_Part_1, N_Part_2}
                                                //N_Part number of participants
                                                //N_Coll number of collisions
                                                //N_Part_1 number of participants in nucleus 1
                                                //N_Part_2 number of participants in nucleus 2
Coll[0] = 0;
Coll[2] = 0;
Coll[1] = 0;
Coll[3] = 0;

Float_t Eccent[9] = {0.}; //EbE data storing of epsilon_0 (dummy), epsilon_1 ... epsilon_9
Float_t Symm[9] = {0.};
 //’’’’’’’’’’’’’’’’’’’’’’’’’’’’’’’’’’’’’’’’’’’’’’’’’’’’’’’’’’’’’’’’’’’’’’’’’’’’
 //3. Setup the nuclei
 BuildNucleus(A,b,R,a,w,Nucleus_1,Nucleus_1_Inter);
 BuildNucleus(A,-b,R,a,w,Nucleus_2,Nucleus_2_Inter);

 //’’’’’’’’’’’’’’’’’’’’’’’’’’’’’’’’’’’’’’’’’’’’’’’’’’’’’’’’’’’’’’’’’’’’’’’’’’’’
 //4. Collide the nuclei
 CollideNuclei(A,Nucleus_1,Nucleus_2,Nucleus_1_Inter,Nucleus_2_Inter,Coll,Energy_Data);

 if(Coll[0]>0) //take only events into account that actually collide!
 {
        //Fill in stats about N_Part and N_Coll for this collision
        CollStats[q]->Fill(1.5,(Float_t)(Coll[0]));
        CollStats[q]->Fill(2.5,(Float_t)(Coll[1]));

        //’’’’’’’’’’’’’’’’’’’’’’’’’’’’’’’’’’’’’’’’’’’’’’’’’’’’’’’’’’’’’’’’’’’’’’’’’’’’
        // 5. Refill Participant Coordinates
        const Int_t NPart = Coll[0]; //get new constant for number of participants for this event
        Float_t *Participants = new Float_t[2*NPart]; //will store x and y coordinates of the participants
        ReFill(NPart, A, Participants, Nucleus_1, Nucleus_2, Nucleus_1_Inter, Nucleus_2_Inter); //Refill into new array

        //’’’’’’’’’’’’’’’’’’’’’’’’’’’’’’’’’’’’’’’’’’’’’’’’’’’’’’’’’’’’’’’’’’’’’’’’’’’’
        //6. Calculate Exccentricities
        EccentricityAndSymmetryplanes(NPart,Participants,Eccent,Symm);

        for(Int_t r=1; r<9; r++)
        {
                Ecc[q]->Fill((Float_t)(r)-0.5,Eccent[r],1.); //Unit weight
                SP[q]->Fill((Float_t)(r)-0.5,Symm[r],1.);
                Ecc_Sqr[q]->Fill((Float_t)(r)-0.5,Eccent[r]*Eccent[r],1.); //Unit weight
                Ecc_Quadr[q]->Fill((Float_t)(r)-0.5,Eccent[r]*Eccent[r]*Eccent[r]*Eccent[r],1.);
        }//for(Int_t r=0; r<9; r++)

         delete [] Participants;

 } //if(Coll[0]>0)

 //’’’’’’’’’’’’’’’’’’’’’’’’’’’’’’’’’’’’’’’’’’’’’’’’’’’’’’’’’’’’’’’’’’’’’’’’’’’’
 //7. Plot
 //PlotNucleus(A,Nucleus_1,Nucleus_2,Nucleus_1_Inter,Nucleus_2_Inter,Coll);

 //’’’’’’’’’’’’’’’’’’’’’’’’’’’’’’’’’’’’’’’’’’’’’’’’’’’’’’’’’’’’’’’’’’’’’’’’’’’’
 //8. Monitor Progress
 if(j%20==0){
 cout<<Form("␣␣␣␣␣=>␣Calculations␣for␣%d.-Impact-Parameter...␣␣␣␣␣␣␣",q)<<Form("%.1f%%\r",100.*(j)/NE)<<"␣␣␣"<<flush;
 }

 delete [] Nucleus_1; //no memory leak
 delete [] Nucleus_2;
 delete [] Nucleus_1_Inter;
 delete [] Nucleus_2_Inter;

}//end for(Int_t j=0; j<NE; j++)


}//end for(Int_t q=0; q<Steps; q++)

//~~~~~~~~~~~~~~~~~~~~~~~~~~~~~~~~~~~~~~~~~~~~~~~~~~~~~~~~~~~~~~~~~~~~~~~~~~~~~~~~~~~~~~~~~~
//9. Store Data
Storing(Steps);
Basics->Write(Basics->GetName(),TObject::kSingleKey); // dumping TDirectoryFile in the  ROOT file:
```

```
        file->Close();
        delete file;

        //~~~~~~~~~~~~~~~~~~~~~~~~~~~~~~~~~~~~~~~~~~~~~~~~~~~~~~~~~~~~~~~~~~~~~~~~~~~~~~~~~~~~~~~~~~

        timerRecursion.Stop();
        cout<<""<<endl;
    cout<<"cpu time is "<<timerRecursion.CpuTime()<<" s"<<endl; //giving out the cpu time, measured by the stopwatch

        return;

}//void Glauber()

//==================================================================================================================================================

void Cosmetics (const Int_t Num){

  for(Int_t c=0;c<Num;c++)
  {

   Ecc[c] = new TProfile("Ecc","Ecc",8,0.,8.); //will store epsilon_1 (Bin 1) to epsilon_8 (Bin 8)
   CollStats[c] = new TProfile("CollStats","CollStats",3,0.,3.); //will store impact parameter in fm (Bin 1), <N_Part> (Bin 2) and <N_Coll> (Bin 3)
   SP[c] = new TProfile("SP","SP",8,0.,8.); //will store symmetryplane Psi_1 (Bin 1) to Psi_8 (Bin 8)
   Ecc_Sqr[c] = new TProfile("Ecc_Sqr","Ecc_Sqr",8,0.,8.); //will store (epsilon_1)^2 (Bin 1) to (epsilon_8)^2 (Bin 8)
   Ecc_Quadr[c] = new TProfile("Ecc_Quadr","Ecc_Quadr",8,0.,8.); //will store (epsilon_1)^4 (Bin 1) to (epsilon_8)^4 (Bin 8)

   Ecc[c]->SetDirectory(0);
   Ecc[c] -> Sumw2();
   Ecc_Sqr[c]->SetDirectory(0);
   Ecc_Sqr[c] -> Sumw2();
   Ecc_Quadr[c]->SetDirectory(0);
   Ecc_Quadr[c] -> Sumw2();
   SP[c]->SetDirectory(0);
   SP[c] -> Sumw2();
   CollStats[c]->SetDirectory(0);

  } // end of for(Int_t c=0;c<Num;c++)

}//void Cosmetics (const Int_t Num)

//~~~~~~~~~~~~~~~~~~~~~~~~~~~~~~~~~~~~~~~~~~~~~~~~~~~~~~~~~~~~~~~~~~~~~~~~~~~~~~~~~~~~~~~~~~~~~~~~~~~~~~~~~~~~~~~~~~~~~~~~~~~~~~~~~

void Storing(const Int_t Number){

  for(Int_t c=0;c<Number;c++)
  {
  List[c] = new TList();
  List[c]->SetName(Form("%d",c));

  List[c]->Add(Ecc[c]);
  List[c]->Add(Ecc_Sqr[c]);
  List[c]->Add(Ecc_Quadr[c]);
  List[c]->Add(CollStats[c]);
  List[c]->Add(SP[c]);

  Basics->Add(List[c]);
  }// end of for(Int_t c=0;c<Number;c++)

}//void Storing(const Int_t Number)

//~~~~~~~~~~~~~~~~~~~~~~~~~~~~~~~~~~~~~~~~~~~~~~~~~~~~~~~~~~~~~~~~~~~~~~~~~~~~~~~~~~~~~~~~~~~~~~~~~~~~~~~~~~~~~~~~~~~~~~~~~~~~~~~~~

void GetNucleusData(string Nucleus_Typ, Float_t Data[4], Float_t *Impact, const Int_t Counter)
{
        if(Nucleus_Typ == "Pb207")
        {
                Data[0] = 207;
                Data[1] = 6.62;
                Data[2] = 0.546;
                Data[3] = 0.;

                Float_t b[22] = {0.,1.,2.,3.,4.,5.,6.,7.,8.,9.,10.,11.,12.,13.,14.,15.,16.,17.,18.,19.,20.,21.};

                for(Int_t c=0;c<Counter;c++)
                {
                        Impact[c] = b[c];
                }

                cout<<"Nucleus Typ: Pb207"<<endl;
        }
```

```
        else if(Nucleus_Typ == "Au197")
        {
                Data[0] = 197;
                Data[1] = 6.38;
                Data[2] = 0.535;
                Data[3] = 0.;

                Float_t b[22] = {0., 0.3, 0.6, 1.,2.,3.,4.,5.,6.,7.,8.,9.,10.,11.,12.,13.,14.,15.,15.5,16.,16.5,17.};

                for(Int_t c=0;c<Counter;c++)
                {
                        Impact[c] = b[c];
                }

                cout<<"Nucleus Typ: Au197"<<endl;

        }

        else if (Nucleus_Typ == "Cu62") {

                Data[0] = 62;
                Data[1] = 4.2;
                Data[2] = 0.596;
                Data[3] = 0.;

                Float_t b[22] = {0., 0.3, 0.6, 1.,2., 2.5 ,3.,3.5,4.,5.,5.5,6.,7.,7.5,8.,9.,10.,11.,11.5,12.,12.5,13.};

                for(Int_t c=0;c<Counter;c++)
                {
                        Impact[c] = b[c];
                }

                cout<<"Nucleus Typ: Cu62"<<endl;

        }

        else { cout<<"Nucleus typ not in data bank"<<endl; exit(0);
        }

}//end void GetNucleusData(string Nucleus_Typ, Float_t Data[4], Float_t* Impact, const Int_t Counter)

//-----------------------------------------------------------------------------------------------------------------------

void GetEnergyData(string Energy, Float_t Data[2])
{
        if(Energy == "2.76TeV")
        {
                Data[0] = 8.3; //sigma_tot in fm^2
                Data[1] = 6.4; //sigma_inel in fm^2

                cout<<"Energy: 2.76 TeV"<<endl;
        }

        else if(Energy == "200GeV")
        {
                Data[0] = 5.2; //sigma_tot in fm^2
                Data[1] = 4.2; //sigma_inel  in fm^2

                cout<<"Energy: 200 GeV"<<endl;
        }

        else { cout<<"Energy not in data bank"<<endl; exit(0); }

}// end void GetEnergyData(string Energy, Float_t Data[2])

//-----------------------------------------------------------------------------------------------------------------------

void BuildNucleus(const Int_t Mass_Number, const Float_t Impact_Parameter, const Float_t Radius, const Float_t Skin,
                  const Float_t Sphere_Parameter, Float_t *Nuc, Int_t *Nuc_Inter)
{

        TF1* Woods_Saxon;

        if(bModWoodsSaxon==kTRUE) //normal Woods-Saxon
        {

        Woods_Saxon = new TF1("Woods_Saxon","4*TMath::Pi()*TMath::Power(x,2.)*((1.+[1]*TMath::Power(x/[2],2.))/(1.+TMath::Exp((x-[2])/[3])))", 0., 50.);
        Woods_Saxon->SetParameter(1, Sphere_Parameter);
        Woods_Saxon->SetParameter(2, Radius);
```

```
Woods_Saxon->SetParameter(3, Skin);

} // if(bModWoodsSaxon==kTRUE)

if(bModWoodsSaxon==kFALSE) //stripped Woods-Saxon
{

Woods_Saxon = new TF1("Woods_Saxon","4*TMath::Pi()*TMath::Power(x,2.)*(1./(1+TMath::Exp((x-[2])/[3])))", 0., 50.);
Woods_Saxon->SetParameter(2, Radius);
Woods_Saxon->SetParameter(3, Skin);

} // if(bModWoodsSaxon==kTRUE)

//spherical coordinates
Float_t r=0.;
Float_t phi=0.;
Float_t theta=0.;

//polar angle distribution
TF1* polar = new TF1("polar","TMath::Sin(x)",0.,TMath::Pi());

//-------------------------------------------------------------------------------------------------------------------

if(bMinDist == kFALSE) //no min. distance between nucleons
{
        for(Int_t i=0; i<Mass_Number; i++)
        {
                //Get spherical coordinates
                r=Woods_Saxon->GetRandom(); //radius
                phi=gRandom->Uniform(0.,TMath::TwoPi()); //phi
                theta = polar->GetRandom(); //theta

                //convert to standard cartesian coordinates and fill Nuc with x and y coordinates
                Nuc[i] = TMath::Sin(theta) * TMath::Cos(phi) * r + Impact_Parameter/2.;
    //fill x + shift it from centering at 0 to centering at b/2 (for Nuclues 1)/ - b/2 for Nucleus 2
                Nuc[i+Mass_Number] = TMath::Sin(theta) * TMath::Sin(phi) * r; //fill y
                Nuc_Inter[i] = 0; //no interaction (yet)

        } //end for(Int_t i=0; i<Mass_Number; i++)

} //end if(bMinDist == kFALSE)

//.....................................................................

if(bMinDist == kTRUE)
{
        Float_t *z = new Float_t[Mass_Number]; //z-component. Will not be stored in final projection output
        Int_t Counter=0;

        while(Counter<Mass_Number)
  {

    //Get spherical coordinates
        r = Woods_Saxon->GetRandom(); //radius
        phi = gRandom->Uniform(0.,TMath::TwoPi()); //phi
        theta = polar->GetRandom();  //theta

        //convert to standard cartesian coordinates and fill Nuc with x and y coordinates
        Nuc[Counter] = TMath::Sin(theta) * TMath::Cos(phi) * r + Impact_Parameter/2.;
//fill x + shift it from centering at 0 to centering at b/2 (for Nuclues 1)/ - b/2 for Nucleus 2
        Nuc[Counter+Mass_Number] = TMath::Sin(theta) * TMath::Sin(phi) * r; //fill y
        Nuc_Inter[Counter] = 0; //no interaction (yet)

        z[Counter]= r* TMath::Cos(theta);

        if(Counter>0)
        {
                for(Int_t i=0; i<Counter; i++)
                 {

                        Float_t x_square = pow(Nuc[i]-Nuc[Counter],2.);
                    Float_t y_square = pow(Nuc[i+Mass_Number]-Nuc[Counter+Mass_Number],2.);
                    Float_t z_square = pow(z[i]-z[Counter],2.);

                         if(x_square + y_square + z_square < 0.64) //if under minimal distance
                         {
                                //reset latest nucleon back to 0
                                Nuc[Counter] = 0.;
                                Nuc[Counter+Mass_Number] = 0.;
                                z[Counter]=0.;
```

```
                                        --Counter; //step one back
                                        break;
                                 } //end if(x_square + y_square + z_square < 0.64)

                         } //end for(Int_t i=0; i<Counter; i++)

                }// end if(Counter>0)

                Counter++;

          } //end while(Counter<Mass_Number)

        delete [] z;

    }//end if(bMinDist == kTrue)

    //....................................................................

    //Set center of mass correctly
    Float_t Mean_x = 0.;
    Float_t Mean_y = 0.;

    for(Int_t i=0; i<Mass_Number; i++)
    {
        Mean_x += Nuc[i];
        Mean_y += Nuc[i+Mass_Number];

        } //for(Int_t i=0; i<Mass_Number; i++)

        Mean_x /= Mass_Number;
        Mean_y /= Mass_Number;

    for(Int_t i=0; i<Mass_Number; i++)
    {
        Nuc[i] = Nuc[i] + Impact_Parameter/2. - Mean_x;
        Nuc[i+Mass_Number] = Nuc[i+Mass_Number] - Mean_y;

        } //for(Int_t i=0; i<Mass_Number; i++)

    //....................................................................

    //clearing up space
        delete Woods_Saxon;
        delete polar;

} //void BuildNucleus(const Int_t Mass_Number, const Float_t Impact_Parameter,
  //                   const Float_t Radius, const Float_t Skin, const Float_t Sphere_Parameter, Float_t* Nuc)

//~~~~~~~~~~~~~~~~~~~~~~~~~~~~~~~~~~~~~~~~~~~~~~~~~~~~~~~~~~~~~~~~~~~~~~~~~~~~~~~~~~~~~~~~~~~~~~~~~~~~~~~~~~~~~~~~~~~~~~~~~~~~~~~~

void CollideNuclei(const Int_t Mass_Number, Float_t *Nuc_1, Float_t *Nuc_2, Int_t *Nuc_1_Inter, Int_t *Nuc_2_Inter, Int_t *Coll_Para, Float_t Energy[2])
{
        if(bGaussianOverlap==kFALSE)
        {
         const Float_t d_square = Energy[1]/TMath::Pi();

     for(Int_t i=0; i<Mass_Number; i++)
         {
                for(Int_t j=0; j<Mass_Number; j++)
                {
                        Float_t x_square = pow(Nuc_1[i]-Nuc_2[j],2.);
                        Float_t y_square = pow(Nuc_1[i+Mass_Number]-Nuc_2[j+Mass_Number],2.);

                        if(x_square+y_square<=d_square)
                        {
                                Coll_Para[1]++; //one collision more

                                //if no interaction accounted yet, raise N_Part and N_Part_n and set collision indicator to 1
                                if(Nuc_1_Inter[i]==0) { Coll_Para[0]++; Coll_Para[2]++; Nuc_1_Inter[i]=1;}
                                if(Nuc_2_Inter[j]==0) { Coll_Para[0]++; Coll_Para[3]++; Nuc_2_Inter[j]=1;}

                        }//if(abs(Nuc_1[i] - Nuc_2[j] )<d.)

                } //for(Int_t j=0; j<Mass_Number; j++)

         }  //for(Int_t i=0; i<Mass_Number; i++)

        } //if(bGaussianOverlap==kFALSE)

        if(bGaussianOverlap==kTRUE)
```

```
        {

         const Float_t para_1 = 4. *( (Energy[0]-Energy[1])/Energy[0] );
         const Float_t para_2 = (TMath::TwoPi()* para_1)/Energy[0]; //fm^-2

     for(Int_t i=0; i<Mass_Number; i++)
         {
                for(Int_t j=0; j<Mass_Number; j++)
                {
                        Float_t x_square = pow(Nuc_1[i]-Nuc_2[j],2.);
                        Float_t y_square = pow(Nuc_1[i+Mass_Number]-Nuc_2[j+Mass_Number],2.);
                        Float_t dist_square = x_square + y_square;

                        Float_t prob = 1 - pow((1-para_1*TMath::Exp(-para_2*dist_square)),2.); //interaction probability
                        Float_t random = gRandom->Uniform(0.,1.); //random value

                        if(random<=prob)
                        {
                                Coll_Para[1]++; //one collision more

                                //if no interaction accounted yet, raise N_Part and N_Part_n and set collision indicator to 1
                                if(Nuc_1_Inter[i]==0) { Coll_Para[0]++; Coll_Para[2]++; Nuc_1_Inter[i]=1;}
                                if(Nuc_2_Inter[j]==0) { Coll_Para[0]++; Coll_Para[3]++; Nuc_2_Inter[j]=1;}

                        }//if(random<=prob)

                } //for(Int_t j=0; j<Mass_Number; j++)

         }  //for(Int_t i=0; i<Mass_Number; i++)

        } //if(bGaussianOverlap==kTRUE)

} // end void CollideNuclei(const Int_t Mass_Number, Float_t* Nuc_1, Float_t* Nuc_2)


//-----------------------------------------------------------------------------------------------------------------------

void EccentricityAndSymmetryplanes(const Int_t NuPart, Float_t *Coordinates_Participants, Float_t *Ecco, Float_t *Symmo){

        Float_t Coso[9]={0.};
        Float_t Sino[9]={0.};
        Float_t Ro[9]={0.};

        if(bGaussianSmearing == kFALSE)
        {
                Float_t Mean_x = 0.;
                Float_t Mean_y = 0.;

                Float_t Mean_x_sqr = 0.;
                Float_t Mean_y_sqr = 0.;

                for(Int_t i=0; i<NuPart; i++)
                {
                                Mean_x += Coordinates_Participants[i];
                                Mean_y += Coordinates_Participants[i+NuPart];

                }//for(Int_t i=0; i<NuPart; i++)

                Mean_x /= NuPart;
                Mean_y /= NuPart;

                  for(Int_t g=1; g<9; ++g)
            {

                        for(Int_t i=0; i<NuPart; i++)
                        {
                                Float_t x = Coordinates_Participants[i] - Mean_x;
                                Float_t y = Coordinates_Participants[i+NuPart] - Mean_y;
                                Float_t r = TMath::Sqrt((x*x)+(y*y));
                                Float_t phi = TMath::ATan2(y,x);

                                Float_t w = (Float_t)(g);

                        if (g==1){w = 3.;} // use r^3 weighting for Ecc1/Psi1

                        Coso[g] += TMath::Power(r,w)*TMath::Cos((Float_t)(g)*phi);
                        Sino[g] += TMath::Power(r,w)*TMath::Sin((Float_t)(g)*phi);
                        Ro[g]   += TMath::Power(r,w);

                        } //end for(Int_t i=0; i<NuPart; i++)
```

```
            }//end for(Int_t g=0; g<9; g++)

        } //end if(bGaussianSmearing == kFALSE)

        if(bGaussianSmearing == kTRUE)
        {

        const Int_t SmearingCounter = 100;
        const Float_t kSigma = 0.4; //sigma-parameter in fm
        TF1* Smearing = new TF1("Smearing","x*TMath::Exp(-(x*x/(2.*[1]*[1])))", 0., 5.*kSigma);
        Smearing->SetParameter(1, kSigma);
        Float_t *Smeared_Coordinates = new Float_t[2*NuPart];

                for(Int_t p=0; p<SmearingCounter; p++)
                {
                        Float_t Mean_x = 0.;
                        Float_t Mean_y = 0.;

                        Float_t Mean_x_sqr = 0.;
                        Float_t Mean_y_sqr = 0.;

                        for(Int_t i=0; i<NuPart; i++)
                        {
                                Float_t radius = Smearing->GetRandom();
                                Float_t varphi = gRandom->Uniform(0.,TMath::TwoPi());

                                Smeared_Coordinates[i] = Coordinates_Participants[i] + radius*TMath::Cos(varphi);
                                Smeared_Coordinates[i+NuPart] = Coordinates_Participants[i+NuPart] + radius*TMath::Sin(varphi);

                                Mean_x += Smeared_Coordinates[i];
                                Mean_y += Smeared_Coordinates[i+NuPart];

                        }//for(Int_t i=0; i<NuPart; i++)

                        Mean_x /= NuPart;
                        Mean_y /= NuPart;

                        for(Int_t g=1; g<9; ++g)
                {

                                for(Int_t i=0; i<NuPart; i++)
                                {
                                        Float_t x = Smeared_Coordinates[i] - Mean_x;
                                        Float_t y = Smeared_Coordinates[i+NuPart] - Mean_y;
                                        Float_t r = TMath::Sqrt((x*x)+(y*y));
                                        Float_t phi = TMath::ATan2(y,x);

                                        Float_t w = (Float_t)(g);

                                if (g==1){w = 3.;} // use r^3 weighting for Ecc1/Psi1

                                Coso[g] += TMath::Power(r,w)*TMath::Cos((Float_t)(g)*phi);
                                Sino[g] += TMath::Power(r,w)*TMath::Sin((Float_t)(g)*phi);
                                Ro[g]   += TMath::Power(r,w);

                                } //end for(Int_t i=0; i<NuPart; i++)

                 }//end for(Int_t g=0; g<9; g++)

                } //end for(Int_t p=0; p<SmearingCounter; p++)

                delete [] Smeared_Coordinates;
                delete Smearing;

        } //end if(bGaussianSmearing == kTRUE)


        for(Int_t g=1; g<9; ++g){

                Ecco[g] = TMath::Sqrt(Sino[g]*Sino[g] + Coso[g]*Coso[g]) / Ro[g];
                Symmo[g] = (TMath::ATan2(Sino[g],Coso[g]) + TMath::Pi())/(Float_t)(g);

        }//end for(Int_t g=0; g<9; g++)

} //end void EccentricityAndSymmetryplanes(const Int_t NuPart, Float_t* Coordinates_Participants, Float_t Ecco[9], Float_t Symmo[9]);

//-------------------------------------------------------------------------------------------------------------------------------

void ReFill(const Int_t NuPart, const Int_t Mass_Number, Float_t *Coordinates_Participants, Float_t *Nuc_1, Float_t *Nuc_2, Int_t *Nuc_1_Inter, Int_t *Nuc_2_Inter)
```

```
{

        Int_t Counter=0; //will check if we found all participants

        for(Int_t i=0; i<Mass_Number; i++)
        {
                if(Nuc_1_Inter[i]==1) //take only participants into account
                {
                        Coordinates_Participants[Counter] = Nuc_1[i];
                        Coordinates_Participants[Counter+NuPart] = Nuc_1[i+Mass_Number];

                        ++Counter;

                } //if(Nuc_1_Inter[i]==1)

                if(Nuc_2_Inter[i]==1)
                {
                        Coordinates_Participants[Counter] = Nuc_2[i];
                        Coordinates_Participants[Counter+NuPart] = Nuc_2[i+Mass_Number];

                        ++Counter;

                } //if(Nuc_2_Inter[i]==1)

        } //end for(Int_t i=0; i<Mass_Number; i++)

        if(Counter!=NuPart)
        {
                cout<<"Error␣with␣refilling!"<<endl; exit(0);
        }

} //end void ReFill(const Int_t NuPart, const Int_t Mass_Number, Float_t* Coordinates_Participants, Float_t* Nuc_1, Float_t* Nuc2)

//-----------------------------------------------------------------------------------------------------------------------

void PlotNucleus(const Int_t Mass_Number, Float_t* Nuc_1, Float_t* Nuc_2, Int_t* Nuc_1_Inter, Int_t* Nuc_2_Inter, Int_t* Coll_Para)
{
        const Int_t Part_1 = Coll_Para[2];
        const Int_t Part_2 = Coll_Para[3];

        if(Part_1 != 0) //if part_1 is not 0, then part_2 is not as well
        {

        TCanvas *c1 = new TCanvas("c1","Glauber",800,800);

        Float_t *dx = new Float_t[Mass_Number]; //no errors
        Float_t *dy = new Float_t[Mass_Number]; //no errors

        Float_t *x_1_Part = new Float_t[Part_1]; //x coordinates of participants of nucleus 1
        Float_t *y_1_Part = new Float_t[Part_1]; //y coordinates of participants of nucleus 1

        Float_t *x_2_Part = new Float_t[Part_2];
        Float_t *y_2_Part = new Float_t[Part_2];

        const Int_t No_Part_1 = Mass_Number - Part_1;
        const Int_t No_Part_2 = Mass_Number - Part_2;

        Float_t *x_1_No_Part = new Float_t[No_Part_1]; //x coordinates nucleons from nucleus 1 which did not interact
        Float_t *y_1_No_Part = new Float_t[No_Part_1]; //y coordinates nucleons from nucleus 1 which did not interact

        Float_t *x_2_No_Part = new Float_t[No_Part_2];
        Float_t *y_2_No_Part = new Float_t[No_Part_2];

        Int_t Counter_1_Part = 0; //counter for participants of nucleus 1
        Int_t Counter_1_No_Part = 0; //counter for nucleons without interaction of nucleus 1
        Int_t Counter_2_Part = 0;
        Int_t Counter_2_No_Part =0;

        for(Int_t i=0; i<Mass_Number; i++)
        {
                dx[i] = 0.;
                dy[i] = 0.;

                if(Part_1 != 0) {

                if(Nuc_1_Inter[i]==1)
                {
                x_1_Part[Counter_1_Part] = Nuc_1[i];
                y_1_Part[Counter_1_Part] = Nuc_1[i+Mass_Number];
                Counter_1_Part+=1;
```

```
        }

        if(Nuc_2_Inter[i]==1)
        {
        x_2_Part[Counter_2_Part] = Nuc_2[i];
        y_2_Part[Counter_2_Part] = Nuc_2[i+Mass_Number];
        Counter_2_Part+=1;
        }

        }

        if(Nuc_1_Inter[i]==0)
        {
        x_1_No_Part[Counter_1_No_Part] = Nuc_1[i];
        y_1_No_Part[Counter_1_No_Part] = Nuc_1[i+Mass_Number];
        Counter_1_No_Part++;
        }

        if(Nuc_2_Inter[i]==0)
        {
        x_2_No_Part[Counter_2_No_Part] = Nuc_2[i];
        y_2_No_Part[Counter_2_No_Part] = Nuc_2[i+Mass_Number];
        Counter_2_No_Part++;
        }

} //end for(Int_t i=0; i<Mass_Number; i++)

TGraphErrors *Nuc_1_Part = new TGraphErrors(Part_1,x_1_Part,y_1_Part, dx, dy);
TGraphErrors *Nuc_2_Part = new TGraphErrors(Part_2,x_2_Part,y_2_Part, dx, dy);
TGraphErrors *Nuc_1_No_Part = new TGraphErrors(No_Part_1,x_1_No_Part,y_1_No_Part, dx, dy);
TGraphErrors *Nuc_2_No_Part = new TGraphErrors(No_Part_2,x_2_No_Part,y_2_No_Part, dx, dy);

Nuc_1_Part->SetMarkerStyle(kFullCircle);
Nuc_1_Part->SetMarkerColor(kRed);
Nuc_1_Part->SetMarkerSize(2.7);

Nuc_2_Part->SetMarkerStyle(kFullCircle);
Nuc_2_Part->SetMarkerColor(kBlue);
Nuc_2_Part->SetMarkerSize(2.7);

Nuc_1_No_Part->SetMarkerStyle(kFullCircle);
Nuc_1_No_Part->SetMarkerColor(46);
Nuc_1_No_Part->SetMarkerSize(2.7);

Nuc_2_No_Part->SetMarkerStyle(kFullCircle);
Nuc_2_No_Part->SetMarkerColor(38);
Nuc_2_No_Part->SetMarkerSize(2.7);

TMultiGraph *Collision = new TMultiGraph(); //creating a multigraph for all the particular graphs

Collision->Add(Nuc_1_No_Part);
Collision->Add(Nuc_2_No_Part);
Collision->Add(Nuc_1_Part);
Collision->Add(Nuc_2_Part);

Collision->Draw("ap");
Collision->GetXaxis()->SetLimits(-15.,15.);
Collision->GetYaxis()->SetRangeUser(-15.,15.);
Collision->Draw("ap");

// IMPORTANT: release back the allocated memory. Without this line, you have a memory leak, which is usually very difficult to debug.
delete [] dx;
delete [] dy;
delete [] x_1_Part;
delete [] y_1_Part;
delete [] x_2_Part;
delete [] y_2_Part;
delete [] x_1_No_Part;
delete [] y_1_No_Part;
delete [] x_2_No_Part;
delete [] y_2_No_Part;
} //end if(Part_1 != 0) //if part_1 is not 0, then part_2 is not as well

//,,,,,,,,,,,,,,,,,,,,,,,,,,,,,,,,,,,,,,,,,,,,,,,,,,,,,,,,,,,,,,#

if(Part_1 == 0){

TCanvas *c1 = new TCanvas("c1","Glauber",800,800);

Float_t *dx = new Float_t[Mass_Number]; //no errors
```

```
        Float_t *dy = new Float_t[Mass_Number]; //no errors

        Float_t *x_1 = new Float_t[Mass_Number]; //x coordinates of participants of nucleus 1
        Float_t *y_1 = new Float_t[Mass_Number]; //y coordinates of participants of nucleus 1

        Float_t *x_2 = new Float_t[Mass_Number];
        Float_t *y_2 = new Float_t[Mass_Number];

        for(Int_t i=0; i<Mass_Number; i++)
        {

                x_1[i]=Nuc_1[i];
                y_1[i]=Nuc_1[i+Mass_Number];

                x_2[i]=Nuc_2[i];
                y_2[i]=Nuc_2[i+Mass_Number];
        }

        TGraphErrors *Nuc_1_All = new TGraphErrors(Mass_Number,x_1,y_1, dx, dy);
        TGraphErrors *Nuc_2_All = new TGraphErrors(Mass_Number,x_2,y_2, dx, dy);

        Nuc_1_All->SetMarkerStyle(kFullCircle);
        Nuc_1_All->SetMarkerColor(46);
        Nuc_1_All->SetMarkerSize(2.7);

        Nuc_2_All->SetMarkerStyle(kFullCircle);
        Nuc_2_All->SetMarkerColor(38);
        Nuc_2_All->SetMarkerSize(2.7);

        TMultiGraph *Collision = new TMultiGraph(); //creating a multigraph for all the particular graphs
        Collision->Add(Nuc_1_All);
        Collision->Add(Nuc_2_All);


        Collision->Draw("ap");

        Collision->GetXaxis()->SetLimits(-15.,15.);
        Collision->GetYaxis()->SetRangeUser(-15.,15.);
        Collision->Draw("ap");

        delete [] dx;
        delete [] dy;
        delete [] x_1;
        delete [] y_1;
        delete [] x_2;
        delete [] y_2;

        } //end if(Part_1 == 0)

} //end void PlotNucleus(const Int_t Mass_Number, Float_t* Nuc)
```

Bibliography

[1] ALICE Collaboration. *Correlated event-by-event fluctuations of flow harmonics in Pb-Pb collisions at* $\sqrt{s_{NN}} = 2.76$ *TeV*. Phys. Rev. Lett. 117, 182301 (2016), 2016.

[2] Ante Bilandzic. *Anisotropic Flow Measurements in ALICE at the Large Hadron Collider*. Utrecht Univerity, 2012.

[3] Antonin Maire. found at: https://compstar.uni-frankfurt.de/outreach/short-articles/the-qcd-phase-diagram-and-the-critical-end-point/, 2011 CERN.

[4] E. V. Shuryak. Zh. Eksp. Teor. Fiz. 74 (1978) 408.

[5] K. H. Ackermann et al. [STAR Collaboration]. *Elliptic Flow in Au+Au Collisions at* $\sqrt{s_{NN}} = 130$ *GeV*. Phys. Rev. Lett. 86 (2001) 402-407.

[6] The ALICE Collaboration. *Elliptic flow of charged particles in Pb-Pb collisions at* $\sqrt{s_{NN}} = 2.76$ *TeV*. arXiv:1011.3914 [nucl-ex], 2011.

[7] Edward Shuryak. *Viewpoint: A "Little Bang" arrives at the LHC*. Physics 3, 105, 2010.

[8] D. T. Son P. K. Kovtun and A. O. Starinets. *Viscosity in strongly interacting quantum field theories from black hole physics*. Phys. Rev. Lett. 94.11 (Mar. 2005), p. 111601. arXiv: 0405231v2 [arXiv:hep-th].

[9] Gordon Baym, Tetsuo Hatsuda, Toru Kojo, Philip D. Powell, Yifan Song, and Tatsuyuki Takatsuka. *From hadrons to quarks in neutron stars: a review*. Reports on Progress in Physics 81 (2018) 056902.

[10] Chun Shen. *Sketch of relativistic heavy-ion collisions (2014)*. https://u.osu.edu/vishnu/2014/08/06/sketch-of-relativistic-heavy-ion-collisions/.

[11] Rajeev S. Bhalerao. *Relativistic heavy-ion collisions*. arXiv: 1404.3294, 2014.

[12] J. Jalilian-Marian F. Gelis, E. Iancu and R. Venugopalan. *The Color Glass Condensate*. Ann. Rev. Nucl. Part. Sci. 60 (2010) 463.

[13] Matthew Luzum. *Flow fluctuations and long-range correlations: elliptic flow and beyond*. J. Phys. G: Nucl. Part. Phys. 38 (2011) 124026.

[14] A. K. Chaudhuri. *A short course on Relativistic Heavy Ion Collisions*. arXiv: 1207.7028 [nucl-th], 2012.

[15] Arthur M Poskanzer Sergei A. Voloshin and Raimond Snellings. *Collective phenomena in non-central nuclear collisions*. arXiv: 0809.2949 [nucl-ex]., 2008.

[16] S. Voloshin and Y. Zhang. Z. Phys. C 70 (1996) 665.

[17] Ante Bilandzic, Christian Holm Christensen, Kristjan Gulbrandsen, Alexander Hansen, and You Zhou. *Generic framework for anisotropic flow analyses with multiparticle azimuthal correlations.* Physical Review, 2014.

[18] M. Luzum R. S. Bhalerao and J. Y. Ollitrault. *Determining initial-state fluctuations from flow measurements in heavy-ion collisions.* Phys. Rev. C 84 (2011) 034910 [arXiv:1104.4740 [nucl-th]].

[19] "ROOT System". *https://root.cern.ch.*

[20] S.J. Sanders M.L. Miller, K. Reygers and P. Steinberg. *Glauber Modeling in High-Energy Nuclear Collisions.* Ann. Rev. Nucl. Part. Sci. 57, 205, 2007.

[21] K. A. Bugaev, A. I. Ivanytskyi, V. V. Sagun, B. E. Grinyuk, D. O. Savchenko, G. M. Zinovjev, E. G. Nikonov, L. V. Bravina, E. E. Zabrodin, D. B. Blaschke, A. V. Taranenko, and L. Turko. *Hard-core Radius of Nucleons within the Induced Surface Tension Approach.* arXiv:1810.00486, 2018.

[22] C. Loizides B. Alver, M. Baker and P. Steinberg. *The PHOBOS Glauber Monte Carlo.* arXiv:0805.4411, 2008.

[23] H. Pi. *An Event Generator for Interactions between Hadrons and Nuclei FRITIOF Version 7.0.* 1992.

[24] Steffen A. Bass Hannah Petersen, Guang-You Qin and Berndt Müller. *Triangular flow in event-by-event ideal hydrodynamics in Au+Au collisions at* $\sqrt{s_{NN}} = 200$ *AGeV.* PHYSICAL REVIEW C 82, 041901(R), 2010.

[25] Roy A. Lacey, Rui Wei, J. Jia, N. N. Ajitanand, and A. Taranenko. *Initial eccentricity fluctuations and their relation to higher-order flow harmonics.* Phys.Rev.C83:044902, 2010.

[26] *LHC Season 2: A stronger machine.* https://home.cern/sites/home.web.cern.ch/files/2018-07/CERN-Brochure-2015-003-Eng.pdf.

[27] *The High-Luminosity LHC: a new horizon for science and technology.* https://home.cern/sites/home.web.cern.ch/files/2018-10/flyer_hilumi_eng.pdf.

[28] *LHC: the guide.* http://cdsweb.cern.ch/record/1165534/files/CERN-Brochure-2009-003-Eng.pdf.

[29] The ALICE Collaboration. *Technical Design Report for the Upgrade of the ALICE Time Projection Chamber.* 2014.

[30] The ATLAS Collaboration. *Observation of a new particle in the search for the Standard Model Higgs boson with the ATLAS detector at the LHC.* Phys.Lett. B716 (2012) 1-29.

[31] The CMS Collaboration. *Observation of a new boson at a mass of 125 GeV with the CMS experiment at the LHC.* Phys. Lett. B 716 (2012) 30.

[32] K. Aamodt et al. *The ALICE experiment at the CERN LHC. A Large Ion Collider Experiment.* J. Instrum. 3 S08002, 2008.

[33] G. Dellacasa et al. *ALICE time projection chamber: Technical Design Report.* Technical Design Report ALICE. Geneva: CERN, 2000.

[34] Alberica Toia. *Bulk Properties of Pb-Pb collisions at* $\sqrt{s_{NN}} = 2.76$ *TeV measuredby ALICE.* J. Phys. G38 (2011), p. 124007. arXiv: 1107.1973 [nucl-ex].

[35] *ALICE Inner Tracking System (ITS): Technical Design Report.* Technical Design Report ALICE. Geneva: CERN, 1999.

[36] (Ed.) et al. [ALICE Collaboration] F. Carminati. *ALICE Physics Performance Report Volume II Part 2.* J. Phys. G G30 (2004) 15171763.

[37] G. Aad et al. (ATLAS Collaboration). *Measurement of event-plane correlations in* $\sqrt{s_{NN}} = 2.76$ *TeV lead-lead collisionswith the ATLAS detector.* Phys.Rev.C 90, 024905, 2014.

[38] Alexander Frank. *Analyses of Anisotropic Flow and Symmetry Planes Using Mulit-particle Correlation Techniques in ALICE at the Large Hadron Collider.* Bachelor Thesis, Technichal University Munich, 2016.

[39] *http://www.stat.cmu.edu/ hseltman/files/ratio.pdf and references therein.*

[40] ALICE Collaboration. *Centrality determination of Pb-Pb collisions at* $\sqrt{s_{\mathrm{NN}}} = 2.76$ *TeV with ALICE.* Phys. Rev. C 88 (2013) 044909.

[41] K. Reygers. *Glauber Monte-Carlo Calculations for Au+Au Collisions at* $\sqrt{s_{\mathrm{NN}}} = 200$ *GeV.* 2003.

Acknowledgements

I want to thank Cindy Mordasini for providing the procedure of removing the high multiplicity outliers as well as the correlation plots in the corresponding Sec. F.2.

I especially want to thank my supervisor Ante Bilandzic for teaching me the skills about multi-particle correlation techniques and data analysis that were necessary to accomplish this thesis. Furthermore, I want to thank him for his always very helpful advices and in particular for helping to "kill" one or another very nasty bug.